2022

RECOVERING AND UPGRADING KRAFT LIGNIN FOR APPLICATION IN FLEXIBLE POLYURETHANE FOAM

Peng Quan
Michigan Technological University, pengq@mtu.edu

RECOVERING AND UPGRADING KRAFT LIGNIN FOR APPLICATION IN FLEXIBLE POLYURETHANE FOAM

By

Peng Quan

A DISSERTATION

Submitted in partial fulfillment of the requirements for the degree of

DOCTOR OF PHILOSOPHY

In Forest Science

MICHIGAN TECHNOLOGICAL UNIVERSITY

2022

This dissertation has been approved in partial fulfillment of the requirements for the Degree of DOCTOR OF PHILOSOPHY in Forest Science.

College of Forest Resources and Environmental Science

Dissertation Advisor:	*Dr. Xinfeng Xie*
Committee Member:	*Dr. Alper Kiziltas*
Committee Member:	*Dr. David R. Shonnard*
Committee Member:	*Dr. David DeVallance*
Committee Member:	*Dr. Rebecca G. Ong*
College Dean:	*Dr. David J. Flaspohler*

Table of Contents

List of Figures

List of Tables

List of Models

Author Contribution Statement

This dissertation is submitted for the partial fulfillment for the Doctoral Degree in Forest Science at Michigan Technological University. In this dissertation, two main aspects were investigated: (1) Recovering and upgrading Kraft lignin from black liquor and synthesis of lignin-based polyurethane foams; (2) life cycle assessment of the lignin recovery processes. This research was conducted from 2020 to 2022 under the supervision of Dr. Xinfeng Xie, Dr. Alper Kiziltas, Dr. David R. Shonnard, Dr. David DeVallance, and Dr. Rebecca G. Ong. This work was funded by Ford Motor company and partially funded by Ecosystem Science Center of Michigan Technological University.

Part of this work has been published or is under review: "***Chapter 2- Recovering Kraft Lignin from Black Liquor and Synthesis of Lignin-based Flexible Polyurethane Foam***" have been published in ***ACS omega*** (Reprinted with permission from [ACS Omega 2022, 7, 19, 16705-16715]. Copyright [2022] American Chemical Society. https://pubs.acs.org/doi/10.1021/acsomega.2c01206); this publication was cooperated with Dr. Mojgan Nejad, Akash Gondaliya, and Mohsen Siahkamari from Michigan State University, and Dr. Xinfeng Xie and Dr. Alper Kiziltas provided their valuable comments for this publication; "***Chapter 3-Lignin with Tunable and Predictable Yield and Molecular Properties***" is under review by ***ACS Sustainable Chemistry & Engineering***; Dr. Xinfeng Xie, Dr. Alper Kiziltas, Dr. Rebecca G. Ong, Dr. David DeVallance, and Dr. Junming Xu provided feedback for this manuscript; Dr. Mojgan Nejad and Mohsen Siahkamari provided the GPC tests for the lignin samples.

Part of this work is ready for submission to journals: "***Chapter 4-The Iron-based Desulfurization Process of Lignin***" will be submitted to ***ACS Sustainable Chemistry & Engineering***; Dr. Xinfeng Xie, Dr. Alper Kiziltas, Dr. Rebecca G. Ong, and Dr. David DeVallance provided their comments for this chapter; "***Appendix B-Life Cycle Assessment of the Lignin Recovery Processes***" will be also submitted to ***ACS Sustainable Chemistry & Engineering***; Dr. Xinfeng Xie, Dr. Alper Kiziltas, Dr. David R. Shonnard, Dr. David DeVallance, Dr. Rebecca G. Ong, and Dr. Robert Handler provided their valuable comments for the LCA part.

Abstract

Lignin is the second abundant natural polymer and has been highlighted as a potential substitute for fossil-based raw materials. However, the inherent molecular heterogeneity and the complex recovery processes result in the challenge of controlling the molecular properties and value-added applications of lignin in large scale. To address those issues, a novel acid-liquefaction process was developed in this study to recover Kraft lignin with improved molecular homogeneity directly from black liquor.

In the first study, the liquefaction parameters were screened based on yield and molecular weight properties of the recovered lignin. Then, the recovered lignin samples were used to replace 20 wt% of the fossil-based polyols to prepare flexible polyurethane foams. It was found that most of the recovered lignin had improved molecular uniformity (polydispersity (PDI) value < 2) than the traditional acid-precipitated lignin (PDI = 2.2~5.4). Also, the recovered lignin with the Mw value of 1600 Da and the PDI value of 1.8 could maintain the major properties of the flexible PU foams.

In the second study, the Box-Behnken response surface methodology (RSM) was employed to investigate the effects of the liquefaction parameters (pH, reaction temperature, and reaction time) on the yield, molecular weights, polydispersity, and quantities of different types of hydroxyl groups of the lignin. Computational models were developed and refined to establish the relationships between the liquefaction parameters and the lignin properties. The yield, molecular weight, and polydispersity of the lignin could be predicted by the optimized models with high $R^2_{(pred)}$ values of 87.5-91.5%.

An iron-based desulfurization process was developed in third study to remove covalently bonded sulfur in the lignin. The effects of the desulfurization parameters, including reaction temperature, time, and amount of iron, on the sulfur content and desulfurization rate of the lignin were studied. It was found that the highest desulfurization rate was 39.3% at 90 ℃, 16 h, and 0.3 g iron.

A life cycle assessment on the lignin production processes and its comparison to the fossil-based polyols were demonstrated in the last study. The lignin produced from the liquefaction process with 140 ℃, pH = 7, and 9 min was more suitable for replacing the fossil-based polyols due to lower CO_2 emissions and energy consumptions.

Keywords: Lignin, Polyurethane Foam, Molecular Structure, Prediction, Desulfurization, Life Cycle Assessment

1 Literature Review

1.1 Introduction

Polyurethane (PU) foam is one of the polymeric foams that are composed of a solid phase and a gas phase.[1] PU foams are of light weight originating from the porous or cellular micro-morphology property. In the meantime, low thermal conductivity and good acoustic insulation performance are also the advantages of PU foams due to the gas phase inside the cellular structure. Besides that, the solid network structure endows PU foams with unique mechanical properties (e.g., elasticity).[2]

There are three types of PU foam based on the differences of microstructure and mechanical properties: rigid, semi-rigid, and flexible foams.[3] The rigid PU foam (RPU) exhibits a highly cross-linked and closed-cell structure with outstanding insulation and good mechanical performance. Thus, they can be used as thermal and sound insulators in construction, automotive vehicles, freeze equipment, aeronautics, and astronautics fields.[4] In contrast, semi-rigid PU foam possesses a better load bearing capacity than rigid PU foam due to the exhibition of partial open cellular structures. This type of PU foam can be applied as cushion materials in automotive vehicles or furniture that require a great shock absorption ability.[5-7] The last is the flexible PU foam with a higher rate of open cellular structures, and it can be used as liquid absorbers, filters, and wipes.[8] In particular, the application of PU foam in the building insulation materials has been considered as an approach beneficial for energy conservation. It can effectively maintain the temperature inside the buildings during the cold season and reduce heat loss.[9] Besides that, after incorporating electrically conductive and magnetic matters, the PU foams can also be used

in electromagnetic shielding or microwave absorption to prevent electronic devices and buildings from electromagnetic pollution.[10,11]

However, such wide applications of PU foams in industry and daily life of people lead to serious environmental concerns. The major raw materials of PU foams were polyols and isocyanate, which mainly originate from the petrochemical industry. As such, globally high demands of PU foams may accelerate the depletion of fossil fuel resources. On the other hand, as artificial materials, PU foams are not biodegradable, which may be harmful for the ecosystem health after landfill disposal at the end of life. These concerns expedite the sustainable development of PU foams. One of the promising ways is seeking an alternative for the raw materials (polyols and isocyanate) of PU foams. Among all the candidates, lignin is attractive since it possesses hydroxyl groups and mainly originates from agricultural and paper production wastes without impacting food supply. So far, although some reviews on the lignin-based polyurethanes have been published, none of them are specific to the PU foams. In this review, the recent advances, existing technical and scientific issues, and life cycle assessment of lignin and lignin-based PU foams were discussed.

1.2 Polyurethane foams

The major component of PU foams is polyurethane (PU). The first PU was synthesized by Otto Bayer in 1937 after the discovery of first urethane from Wurtz in 1849.[12-15] Typically, PU is formed by polyaddition reactions between the hydroxyl groups (OH) of polyols and the isocyanate functional groups (NCO) of isocyanates, resulting in urethane linkages (Figure 1.1). [12] To prepare a PU foam, an expansion reaction will occur along with the

polyaddition reaction (Figure 1.2).[12] The carbon dioxide (CO_2) produced during the expansion reaction is a key for the cellular structure formation of PU foams.

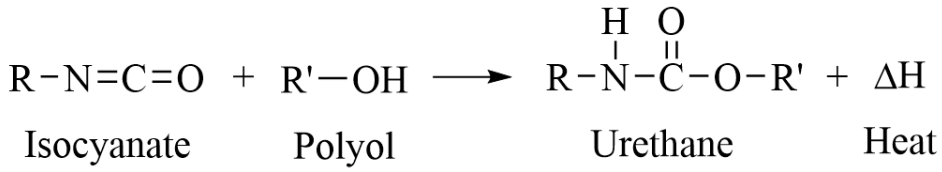

Figure 1.1 Schematic for the reaction of urethane production [12]

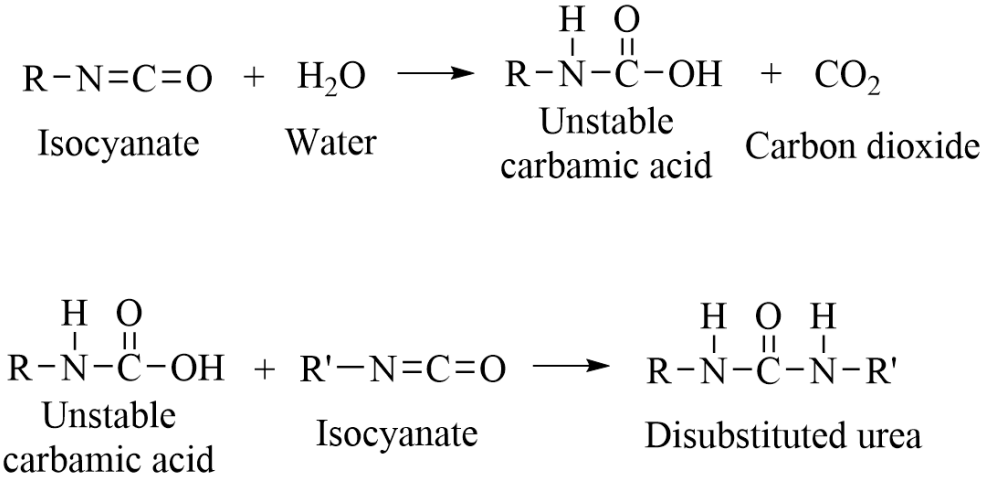

Figure 1.2 Schematic for the reaction between isocyanate and water [12]

Polyols refer to organic compounds with multiple hydroxyl groups, and commercial polyols used in the formula of PU foams can be either polyether polyols or polyester polyols.[16,17] The molecular weight and number of hydroxyl groups are two key parameters that determine the physical and chemical properties of polyols.[8] Generally, the polyols with

high molecular weight (2000-10000) and long carbon chains have better structural flexibility, and they are widely used to prepare flexible PU foams. In contrast, the polyols with lower molecular weight and shorter carbon chains are preferable to the production of rigid PU foams due to the weaker structural flexibility. Moreover, less hydroxyl groups can make polyols more suitable for the preparation of flexible PU foams. For example, dipropylene glycol and polyethylene glycol have two hydroxyl groups, while glycerin has three. Polyols that contain higher number of hydroxyl groups, such as sorbitol (six hydroxyl groups) and sucrose (eight hydroxyl groups) (Figure 1.3), are good precursors to produce rigid PU foams.[17] This is because higher number of hydroxyl groups can increase the amount of urethane linkages which are responsible for the rigidness of PU foams.[2]

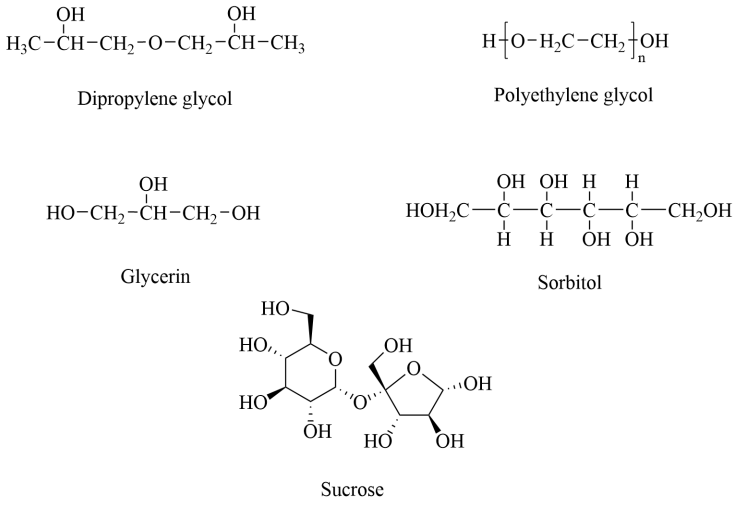

Figure 1.3 Molecular formula of polyols [17]

Another major raw material of PU foams is isocyanate that devotes isocyanate functional groups (NCO) for the polyaddition reaction. The most used isocyanates are aromatic diisocyanates, such as methylene diphenyl diisocyanate (MDI) (Figure 1.4) and toluene

diisocyanate (TDI) (Figure 1.4).[2] The hard segments of PU foams are associated with the urethane and urea parts which mainly originate from isocyanates, and higher consumption of isocyanates in the formula of PU foams is believed to cause higher rigidness of the PU foams.[8]

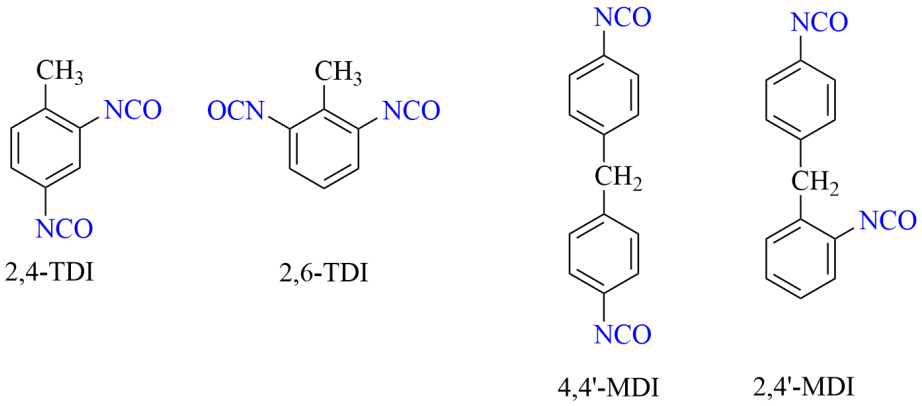

Figure 1.4 Molecular structures of 2,4-TDI, 2,6-TDI, 4,4'-MDI, and 2,4'-MDI [17]

In addition to polyols and isocyanates, the blowing agent, surfactant, catalyst, and additives are smaller proportion of ingredients to synthesize a PU foam successfully.[2] Blowing agents are to generate cellular structures of PU foams through the expansion reactions. In present, two categories of blowing agents have been reported frequently: (1) chemical blowing agents, such as water, can produce carbon dioxide (CO_2) to generate porous structures of PU foams; (2) physical blowing agents with a low boiling point, such as acetone, pentane or hexane, can realize expansion of polymer by vaporization.[18] Additionally, blowing time and temperature are also important factors to adjust the rigidity of foams. Generally, the range of blowing time should be 5 min, and the blowing temperature could be 60-70 °C that is variable according to the properties of blowing agents. The surfactant plays a role in controlling the cell size and foam air permeability by lowering

down the surface tension. Also, the open cell content of the foams is determined by the surfactant.[2] Regarding the catalyst, its function is to improve the reaction rate between polyols, isocyanates and other ingredients, and the property and quantity of catalysts have significant influences on the expansion of PU foams.[2] In addition to the components, processing technology plays a crucial role in the quality of PU foams, and it depends on the formula and application situations. Common processing technologies are molding, slab stock and spraying.[2]

1.3 Lignin

Lignin is a naturally abundant aromatic polymer that is massively found in plant cell walls.[19] The native lignin in plant cell walls is believed to be complex three-dimensional macromolecules which are synthesized by an enzyme-mediated dehydrogenation process of the lignin monomers (Figure 1.5), and it is crosslinked tightly with cellulose and hemicellulose by covalent bonds.[20] The extracted lignin was found to have different types of hydroxyl groups that can be a potential replacement of polyols.[21]

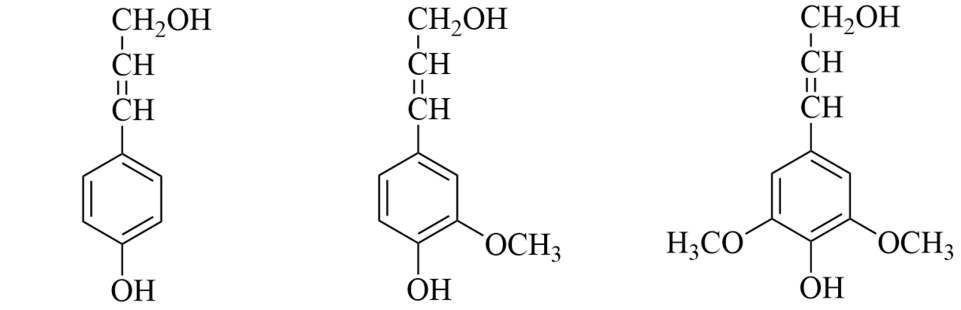

p-coumaryl alcohol coniferyl alcohol sinapyl alcohol

Figure 1.5 The molecular structures of three types of lignin monomers

Generally, there are three major molecular properties of lignin including molecular weight, polydispersity (PDI), and hydroxyl groups. The molecular weight can be classified as number average molecular weight (Mn) and weight average molecular weight (Mw), and they can be characterized by a gel permeation chromatography (GPC) system.[22] The polydispersity (PDI) represents the molecular weight distribution of lignin, which is defined as following:

$$PDI = \frac{M_w}{M_n} \quad (1.1)$$

As for the hydroxyl groups, aliphatic, phenolic, and carboxyl hydroxyl groups have been found in the extracted lignin molecules, and they can be quantitatively determined by ^{31}P nuclear magnetic resonance (NMR).[23] These molecular properties are crucial for the applications of lignin, which will be discussed later.

To utilize lignin, the first step is separating it from lignocellulosic biomass. Four major techniques have been commercialized to realize the separation of lignin. The first technique is using organic solvents or organic solvent/water mixtures to dissolve lignin in biomass, and the resultant lignin is named as organsolv lignin.[24] The most used solvent is ethanol, and the organic dissolution process should be conducted in the presence of acid as a catalyst, such as sulfuric acid, acetic acid, and formic acid.[25, 26] The orgnansolv lignin is with high purity because of the use of solvents and without the use of alkaline chemicals. For example, Christos Nitsos et al. employed 60% ethanol-water solution along with 1% sulfuric acid to dissolve lignin from hardwood and softwood at 180 ℃ for 1h.[27] The dissolution efficiency of lignin from spruce and birch was up to 62% and 69%, respectively, and the lignin purity

reached 93%. Another benefit of this method is that the involved solvents are relatively environmentally friendly. However, the high recovery cost of the solvent is a disadvantage of this method.[28]

The second method is sulfite cooking that treats biomass with HSO_3^- and SO_3^{2-} ions and produce pulp and a bioproduct named as lignosulphonate.[29, 30] The sulfite cooking once was a major technique to separate lignin from biomass, and approximately 1 million tons dry solid per year can be produced by this technique.[31, 32] The lignosulphonate not only contains the molecular structure of lignin but also a large amount of charged groups, leading to its great solubility in the aqueous solution. Owing to the use of sulfite cooking chemicals, there is ash residual in lignosulphonate.[28]

The third delignification method is soda-anthraquinone pulping process, and the major feedstock treated by this method is annual crops such as bagasse, flax, and straws.[33, 34] The function of soda (sodium hydroxide) is to digest the feedstock, and the existence of anthraquinone can prevent carbohydrates from chemically structural damages, promote the delignification efficiency, and make the cooking process milder. This method is a sulfur-free process, while the resultant soda lignin shows a high ash content due to the addition of soda.[28]

The last but not least is Kraft pulping process which occupies about 85% of total lignin production in our world.[35] In the Kraft pulping process, the sodium hydroxide (NaOH) and sodium sulfite (Na_2S) are used as the cooking media for biomass. This process can remove approximately 85-90% of the lignin in biomass and forms a byproduct named as black liquor.[36] The ingredients of black liquor mainly include lignin, sugars, cooking chemicals,

and water.[37] Although the black liquor has been recognized as the major source of lignin, the high sulfur and ash content as well as strongly alkaline property make it difficult to use directly.[38] Therefore, subsequent recovery techniques are required to further utilize lignin in the black liquor.

LignoBoost and LignoForce are two well-known commercial processes for recovering Kraft lignin from the black liquor.[39,40] As shown in Figure 1.6, the primary step in those processes is acidification in which carbon dioxide is used to precipitate lignin out of the black liquor. Afterwards, the precipitated lignin is filtered and washed a few times with sulfuric acid aqueous solution. The mechanism of the acid precipitation of Kraft lignin can be explained by the theory of repulsive forces.[37,41] Theoretically, lignin molecules have colloidal structure with negative surface charges in the alkaline black liquor.[37,42] The negative surface charges induce repulsive forces between lignin molecules, enabling the steady dissolution of lignin in the solution.[37] With the addition of acid, more hydrogen ions can be provided to neutralize the negative charges of lignin molecules. Consequently, the repulsive forces between lignin molecules are reduced, and lignin molecules start to precipitate from the black liquor.[36] Moreover, the acid may catalyze the polymerization reactions of lignin molecules and generate lignin macromolecules, which might be beneficial for the precipitation of lignin as well.[43] Nevertheless, the recovered lignin has high molecular heterogeneity due to the violent conditions of separation and recovery processes, which prevent it from high-value applications.

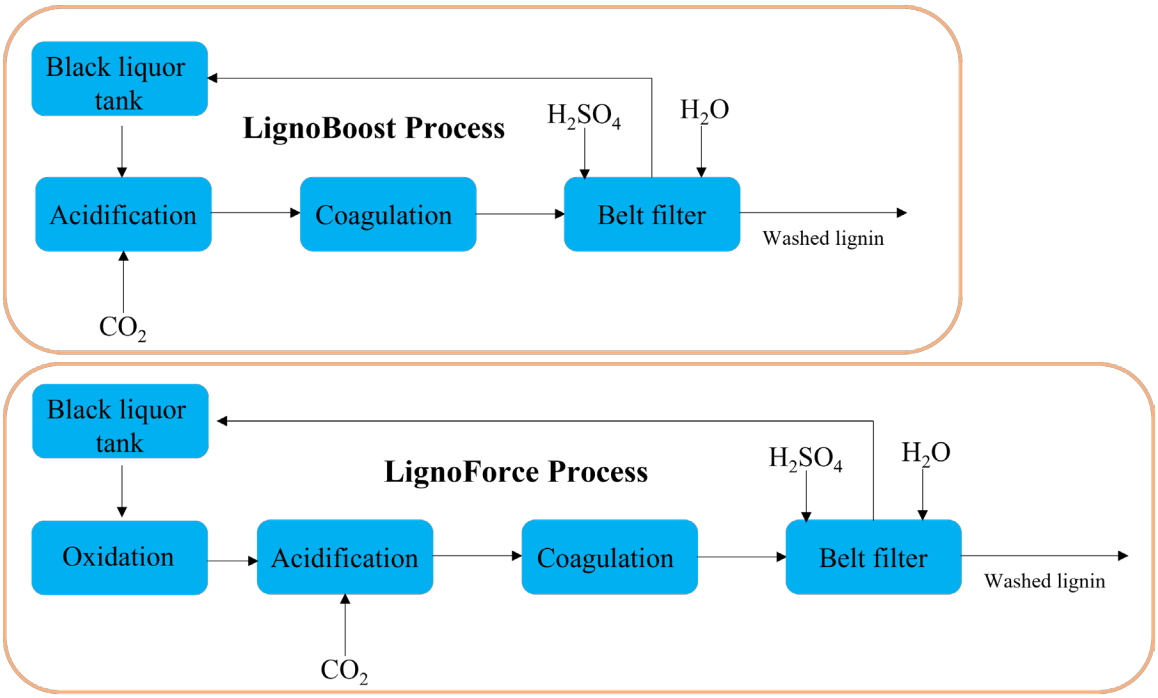

Figure 1.6 Schematic for the comparison between LignoBoost process (Upper) and LignoForce process (Lower).[40]

Fractionation has been considered as an effective method to address this issue. Generally, there are three types of fractionation methods: (1) pH adjustment method; (2) solvent extraction method; (3) ultrafiltration membrane method.[37] For the first method, the pH value of feedstock is adjusted by adding acid to separate different lignin portions. For example, Lourençon et al. used hydrochloric acid to successively adjust the pH of *Eucalyptus sp.* (hardwood) and *Pinus sp.* (softwood) Kraft black liquors to 9, 7, 5, 3, and 1, then the lignin precipitated at different pH values were separated.[44] It was observed that both Mn and Mw values of the lignin fractions tended to be lower with the decreasing pH value, while the polydispersity (PDI) values were very high (5-16), indicating the wide molecular weight distribution of the resulting lignin. In contrast, Marina et al. demonstrated

that using sulfuric acid to decrease the pH of pine Kraft black liquor to 10.5, 5, and 2.5 could obtain the precipitated lignin with lower Mn and Mw values, and the lowest PDI value existed at pH = 5.[43] Besides that, the different lignin factions dissolved in the supernatant after the sequential pH adjustment (12-2) in alkaline lignin solution was also investigated, and they showed variable Mn, Mw, and PDI values.[45]

The second method is based on the solubility distinction of different lignin fragments in solvents. There are two classical equations that can be used to predict the lignin solubility in solvents. The first was reported by Hildebrand, and it is shown as following: [46]

$$\delta = \sqrt{\left(\frac{E}{V_m}\right)}, (cal/cm^3)^{1/2} \qquad (1.5)$$

Where E is the solvent energy of vaporization, and V_m is the molar volume. According to this equation, a substance can be dissolved in a solvent with similar δ values. This indicator was only suitable for nonpolar solvent systems. For the solubility of polar solvent systems, Hansen solubility parameter (HSP) was defined as below:[47]

$$\delta^2 = \delta^2{}_D + \delta^2{}_P + \delta^2{}_H \qquad (1.6)$$

Where δ_D represents dispersion forces, δ_P is polar interactions, and δ_P is related to hydrogen bonding. The HSP indicates that the solubility of lignin in the polar system is associated with the synergic effect of dispersion forces, polar interactions, and hydrogen bonding.

The organic solvents/water system is commonly used to fractionate lignin. In this system, water plays an important role in controlling the polarity, hydrogen bonding, and other parameters of the system, and it endows the system with great solubility for the lignin with

a specific range of molecular weight.[37] Usually, such solvent systems with the gradients of the ratio of organic solvent to water were used to successively fractionate soluble lignin fragments from a feedstock. Among the organic solvents, alcohol was adopted frequently due to its environmentally friendly feature. For example, Alcell lignin was fractionated by an ethanol/water system in which the water percentage ranged from 5% to 90.5%.[48] The experimental results indicated that the solvent system with 29.7% water could achieve the best solubility of lignin. As another example of ethanol/water system, two solutions with 5% and 20% water were employed to conduct sequential fractionation on steam-exploded corn stalk lignin, respectively.[49] It was observed that the lignin fractionated by the solution with 20% water had higher molecular weight values than that fractionated by the solution with 5% water.

Acetone/water system is also a representative organic solvents/water system. For instance, organosolv lignin from pine and switchgrass, respectively, was fractionated sequentially by acetone-water solution with water in the range of 40-70%.[50] The results revealed that increasing the water percentage in the acetone/water solution was able to fractionate the insoluble lignin with lower molecular weight and polydispersity values. Another study on softwood Kraft lignin fractionation with acetone-water solution has been reported as well.[51] The initial concentration of acetone in the solution was 60%, and then it was diluted to 50%, 40%, 30%, 20%, and 10% by gradually adding water. Then, the insoluble lignin portions were separated and investigated. It was found that the molecular weight and polydispersity of the insoluble lignin tended to decrease with the lower concentrations of acetone.

Recently, an acetic acid/water solvent system was developed to control the molecular weight of Kraft lignin.[52] The percentage of acetic acid in the solvent systems varied from 0 to 100%. The Kraft lignin was mixed with the acetic acid/water solution and then heated, generating a lignin-rich phase and a liquid phase. The results showed that the number average molecular weight (Mn) of the Kraft lignin from the lignin-rich phase was higher than that of the lignin from the liquid phase, and the increase in water content of the solvent system tended to reduce the Mn values of lignin from the lignin-rich phase.

In addition to the organic solvent/water system, water-free organic solvent systems have been used for the fractionation of lignin as well. The theoretical basis of choosing the solvents is the hydrogen-bonding ability and cohesive energy of the solvent molecules.[37] An operation unit of this method is that the lignin is mixed with an organic solvent, then the insoluble and soluble parts are separated. This procedure can be repeated by changing the types of organic solvents. Afterward, the lignin fragments with different molecular weights could be obtained.[37] The commonly used organic solvents are alcohol, ketone, ether, and ester. For example, Thring et al. used diethyl ether and methanol to fractionate Alcell hardwood lignin.[53] They observed that the molecular weight and polydispersity of the lignin in ether (M_w = 720, PDI = 1.5) were lower than that in methanol (M_w = 6950, PDI = 2.3). Duval et al. screened different types of solvents for softwood Kraft lignin based on the yield, molecular weight, and polydispersity. Then, ethyl acetate, ethanol, methanol, and acetone were chosen to conduct sequential fractionation of the lignin.[54] The lignin extracted by ethyl acetate had the lowest values of Mn (350 g/mol) and Mw (750 g/mol), while those values of the lignin extracted by acetone were the highest (Mn = 2990 g/mol and Mw = 5150 g/mol).

Membrane fractionation technology was also considered a promising method for the fractionation of lignin. In general, the membrane technology can be classified into three types: microfiltration, ultrafiltration, and nanofiltration.[55] The mechanism of such technology is the cross flow produced by the tubular microstructures in membranes, and the molecular weight cutoff (MWCO) is an indicator for the filtration ability of membranes.[37] The Figure 1.7 is a typical schematic of the membrane technology, in which a series of membranes with MWCO gradients are integrated to treat the fluid containing lignin fractions under elevated temperatures and pressures.[56,57] The membranes are usually made of ceramics (e.g., TiO_2 and ZrO_2) or polymers (e.g., cellulose and polyethersulfone). Among them, ceramic membranes are ideal for the fractionation of the lignin in black liquor because of its great tolerance ability to extreme pH and temperature conditions.[55]

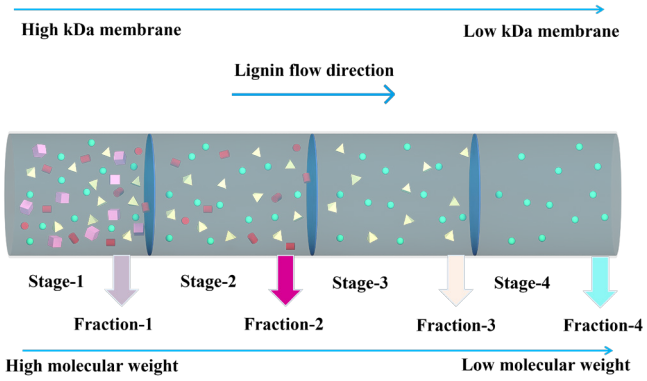

Figure 1.7 Schematic for a fractionation system with multiple membranes[36]

Tremendous efforts have been made on the membrane technology for the fractionation of lignin. A pilot-scale case using a cutoff 1 kDa membrane indicated that changing temperature could affect the behavior of lignin, and higher ionic concentration was required to obtain better fractionation performance.[58] This study also demonstrated that there were

sulfur and salt content residual in the recovered lignin fractions after the ultrafiltration process. A sequential ultrafiltration was conducted using 5 kDa and 30 kDa membranes to treat bamboo Kraft lignin.[59] After the ultrafiltration, three lignin fractions with molecular weights of 7010 g/mol, 3540g/mol, and 1890 g/mol, respectively, were recovered, and their polydispersity was lower than the feedstock. However, the recovery efficiency of this process was lower than that of the pH adjustment methods and solvents extraction methods.[37,55] The fouling is another issue of membranes after long-time operation, and it will decline the flux of membranes.[55] Although it can be solved by the wash of sodium hydroxide solution, the cost will be increased accordingly.

The residual sulfur content in Kraft lignin is one of the main issues that prevent lignin from further valorization. It may weaken the performance of lignin-based products and cause environmental impacts. For example, the sulfur content in lignin can cause unpleasant odor during the application of lignin-based products.[60] The residual sulfur content in Kraft lignin or Kraft black liquor originates from the sodium sulfide as a cooking medium in the Kraft pulping processes.[35] Although the LignoBoost and LignoForce technologies can produce pretreated lignin, the use of sulfuric acid at the step of wash introduces external sulfur elements into the resultant lignin.[39, 40] In general, the sulfur content in the lignin was in the range of 1.5-8%, but it usually varies depending on the processes of delignification.[60] Regarding the positions and forms of sulfur elements in the lignin, they are so complex that it is still controversial recently. It was supposed that the sulfur is present in the lignin as: inorganic sulfur (mainly SO_4^{2-}), elemental sulfur, adsorbed polysulfide (S_nS^{2-}), and covalently bonded sulfur.[61] As shown in Figure 1.8, the estimated structures of covalently bonded sulfur include thiol (-SH), sulfide (-S-), and disulfide bonds (-S-S-).

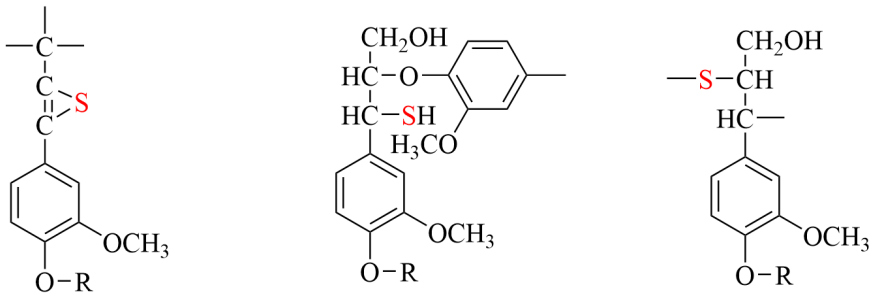

Figure 1.8 The estimated structures of covalently bonded sulfur in Kraft lignin [60]

To reduce sulfur content in the lignin, several desulfurization methods were proposed. The oxidation step was introduced in the LignoForce process to solve this problem (Figure 1.6). Possible chemical reactions are shown as below:[62]

$$2NaHS + 2O_2 \rightarrow Na_2S_2O_3 + H_2O \quad (1.2)$$

$$Na_2S_2O_3 + 2O_2 + 2NaOH \rightarrow 2Na_2SO_4 + H_2O \quad (1.3)$$

$$Organic\ reduced\ sulfur\ compounds\ + O_2 \rightarrow non - volatile\ sulphur\ compounds \quad (1.4)$$

Experimental results have verified that, after the LignoForce process, the sulfur content of lignin could be reduced approximately 60%.

Sara Svensson systematically demonstrated a combined method and realized efficient reduction of sulfur content in Kraft lignin.[61] First, the Kraft lignin was washed with hydrochloric aqueous solution at pH = 6 and pH = 2, respectively. The purpose of this step was to remove the inorganic sulfur content in the lignin. After four times washes, the inorganic sulfur could be reduced to 0.01 mg S/g lignin at pH = 6 and 0.0003 mg S/g lignin at pH = 2, respectively. Second, Soxhlet extraction was used to remove the elemental sulfur

in the lignin, and the solvent was n-pentane. A sulfur content of 0.16 mg S/g lignin could be removed by this step. Third step is the oxidation for covalently bonded sulfur in the lignin. The lignin samples were first dissolved in 50 mM NaOH solution, then heated to a target temperature followed by the addition of oxygen. Interestingly, the sulfur content in the lignin was not reduced significantly after this procedure, which is opposite to the results from the LignoForce process.[62] Finally, Raney nickel was used as a catalyst for the reduction reaction of covalently bonded sulfur in the lignin. It was observed that the reduction of covalently bonded sulfur in the lignin exceeded 65% after the reduction reaction.

Huang et al. employed formic acid as an in-situ hydrogen source and an ethanol/water mixture as a solvent system to depolymerize Kraft lignin.[63] Multiple operation parameters were optimized systematically, including feedstock mass ratio, reaction temperature and time, solvent composition, and substrate concentration. Experimental results showed that the Kraft lignin with a M_w value of approximately 10000 could be depolymerized into the lignin fraction with a M_w value of approximately 1270 under the optimal conditions (300 ℃, 1h, ethanol/water (50/50 v/v), and mass ratios of formic acid to lignin = 0.7-2.4). Along with the depolymerization processes, the sulfur content of the lignin was also significantly reduced from 1.5 wt.% to 0.6 wt%. This study indicated that the depolymerization process with hydrogenation may be an effective approach to the effective desulfurization of Kraft lignin.

Evdokimov et al. established a sequential process for the desulfurization of sulfate lignin involving benzene extraction, silver catalysis in dimethylformamide, aqueous sodium

sulfide solution treatment, and perchloric acid + acetic anhydride mixture treatment.[60] Consequently, the total sulfur content in sulfate lignin was reduced from 23800~27800 pm to 235~855 pm.

Overall, the inorganic sulfur impurities in the Kraft lignin can be removed by dilute acid washes, and the elemental sulfur in the lignin could be reduced by the extraction of organic solvents. However, it is still challenging to realize an effective removal of covalently bonded sulfur in the lignin through a relatively moderate and simple method.

1.4 Life Cycle Assessment

Climate Change (IPCC) Working Group I Fifth Assessment Report states that "Human influence on the climate system is clear. This is evident from the increasing greenhouse gas concentrations in the atmosphere, positive radiative forcing, observed warming, and understanding of the climate system".[19] A consensus is that the continuous petroleum consumption for energy generation and fabrication of products offers a chance for the accumulation of green-house gas in the atmosphere.[64] As discussed earlier, lignin has been considered a potential sustainable substitute for fossil-based materials. A variety of products have been developed based on the processing technologies for lignin such as low-cost carbon fibers, PU foams, engineering plastics, and adhesives.[19]

Life cycle assessment (LCA) is an effective tool to evaluate the environmental impacts caused by the products from raw materials to its end of life.[65,66] The first conception of life cycle thought was proposed by Harold Smith in 1963, and after four decades, it has been developed as an international standard evaluation method for the environmental impacts of products.[65,66] International Standards Organization (ISO) published the ISO 14040 series

of standards for LCA. ISO 14040 describes the basic methodology for the operation of LCA investigation including goal and scope definition, life cycle inventory analysis, impact assessment, and results interpretation (Figure 1.9).[67]

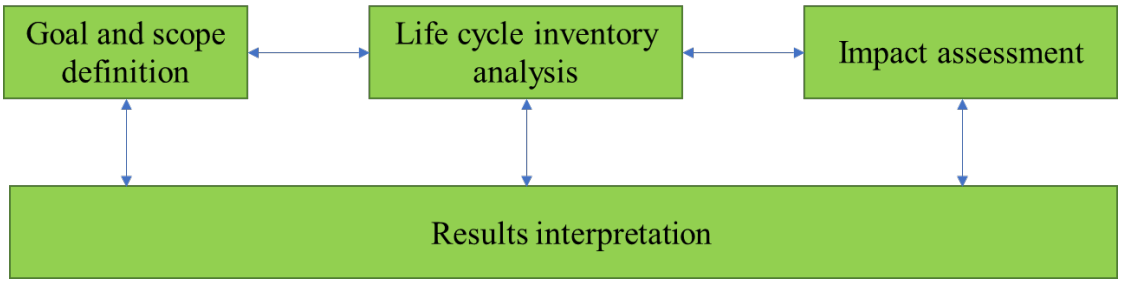

Figure 1.9 Schematic for the methodology of LCA

The goal and scope definition illustrates the key objectives of an LCA study, target application and audience, and whether the results will be publicized for comparison purposes. In this stage, the product system and functions of the study should be defined, and the function unit, the system boundaries, the data requirements, the methodology of environmental impact assessment as well as any limitations or assumptions are supposed to be taken into consideration.[68] In particular, function unit is very important because it provides a reference for the input of involving product systems to realize the same function or goal. System boundaries define the limitations of studied systems, and there are two types of strategies of definition for the system boundaries. One is known as "cradle-to-gate" which stretches system boundaries from raw materials suppliers to final products. The "cradle-to-grave" is another strategy including from raw materials suppliers to waste disposal.[65]

Life cycle inventory analysis involves the collection of the data of appropriate inputs and outputs in the investigated products systems.[68] The inputs usually include energy resources and raw materials, and gas emissions, waste, and land use are common outputs. The data can be obtained from database, such as ecoinvent ™ and SimaPro software, company reports, survey or second literature. In this stage, when there are multiple products, allocation methods for the inputs and the outputs are crucial as they affect the allocation of environmental burdens.

Impact assessment connects input and output with environmental impacts. Human health, ecosystem quality, and resources are major environmental elements considered in the impact assessment, but it is variable according to the targets of investigations.[69]

Results interpretation is to quantitatively demonstrate the environmental impacts caused by each step in the life cycle of products. In this stage, preliminary conclusions can be made based on the environmental performance of products and provide suggestions in response to the study objectives. The ideal interpretation should provide a comprehensive picture of the studied products.[70]

Recently, LCA has been used to predict environmental impacts of lignin products. For instance, Charles Culbertson and the authors conducted LCA on the production of southern bleached softwood Kraft (SBSK) pulp from southern loblolly pine with and without a lignin extraction process.[71] The strategy of cradle-to-gate was used in the definition of system boundaries, and the functional unit was 1 air dry metric tonne (ADmt) softwood Kraft pulp. Additionally, mass and energy allocation methods were involved in this study. It was observed that the softwood Kraft pulp with the lignin extraction process emitted 602

kg CO_2eq per ADmt SBSK pulp, which was lower than the 722 kg CO_2eq per ADmt SBSK pulp produced by the pulp process without the lignin extraction process. It was also found that sodium chlorate and natural gas were major contributions to the environmental impacts of mill.

Frida Hermansson et al. explored the effects of different allocation methods on the final climate impact caused by the LignoBoost process for lignin extraction from Kraft pulp mill.[72] This study involved twelve allocation methods including changes made to the mill, marginal approach, main product bears all burden, system expansion by substitution, mass-based allocation, energy-based allocation, exergy-based allocation, energy- and mass-based allocation, mass- and energy-based allocation, economic allocation, allocation based on substituted impact, and allocation based on inversed substituted impact. The results indicated that the influence of choice of allocation was significant on the cradle-to-grave climate impact of the final products.

Alessandro Manzardo et al. designed a life cycle assessment framework for biobased rigid PU foams.[73] Three types of foams are partially made of lignin. This study comprehensively investigated a set of impact assessment categories. It was proved that the introduction of lignin in the formulations of PU foams resulted in lower greenhouse gas emissions and consumption of fossil-based resources.

1.5 References

1. Lee, S.-T., Introduction: polymeric foams, mechanisms, and materials. In *Polymeric foams*, CRC press: 2004; pp 15-29.

2. Gama, N. V.; Ferreira, A.; Barros-Timmons, A., Polyurethane foams: Past, present, and

future. *Materials* **2018,** *11* (10), 1841.

3. Zhang, Q.; Zhang, G.; Xu, J.; Gao, C.; Wu, Y. Recent advances on lignin-derived polyurethane polymers. *Reviews on advanced materials science* **2015**, *40* (2), 146-154.

4. Amaral, J. S.; Sepúlveda, M.; Cateto, C. A.; Fernandes, I. P.; Rodrigues, A. E.; Belgacem, M. N.; Barreiro, M. F., Fungal degradation of lignin-based rigid polyurethane foams. *Polymer degradation and stability* **2012,** *97* (10), 2069-2076.

5. Sakai, M.; Ishikawa, A.; Morii, M., Semi-rigid polyurethane foam. Google Patents: 2001.

6. Lindewall, F. W., Process for the preparation of semi-rigid polyurethane foam having exceptional shock-absorbing properties and vehicle bumpers thereof. Google Patents: 1979.

7. Mascioli, R. L., Method for the preparation of semi-rigid polyurethane modified polyurea foam compositions. Google Patents: 1986.

8. Cinelli, P.; Anguillesi, I.; Lazzeri, A. Green synthesis of flexible polyurethane foams from liquefied lignin. *European Polymer Journal* **2013**, *49* (6), 1174-1184.

9. Huang, K.; Chen, M.; He, G.; Hu, X.; He, W.; Zhou, X.; Huang, Y.; Liu, Z. Stretchable microwave absorbing and electromagnetic interference shielding foam with hierarchical buckling induced by solvent swelling. *Carbon* **2020**, *157*, 466-477.

10. Sun, Z.; Chen, Y.; Zheng, J.; Jiang, S.; Dong, W.; Li, X.; Li, Y.; E, S. Temperature-Dependent Electromagnetic Microwave Absorbing Characteristics of Stretchable Polyurethane Composite Foams with Ultrawide Bandwidth. *Advanced Engineering Materials* **2022**, *24* (7), 2101489.

11. Ashida, K. *Polyurethane and related foams: chemistry and technology*; CRC press,

2006.

12. Ionescu, M. *Chemistry and technology of polyols for polyurethanes*; iSmithers Rapra Publishing, 2005.

13. Oertel, G. handbook of polyurethanes. CRC press: 1999.

14. Prisacariu, C. *Polyurethane elastomers: from morphology to mechanical aspects*; Springer Science & Business Media, 2011.

15. Sharmin, E.; Zafar, F. Polyurethane: an introduction. *Polyurethane* **2012**, 3-16.

16. Sivertsen, K. Polymer foams. *Polymer Physics, Spring, Massachusetts Institute of Technology, USA* **2007**.

17. Dutta, A. S. Polyurethane foam chemistry. In *Recycling of polyurethane foams*, Elsevier, 2018; pp 17-27.

18. Singh, S. N. *Blowing agents for polyurethane foams*; iSmithers Rapra Publishing, 2001.

19. Ragauskas, A. J.; Beckham, G. T.; Biddy, M. J.; Chandra, R.; Chen, F.; Davis, M. F.; Davison, B. H.; Dixon, R. A.; Gilna, P.; Keller, M. Lignin valorization: improving lignin processing in the biorefinery. *science* **2014**, *344* (6185), 1246843.

20. Vanholme, R.; Demedts, B.; Morreel, K.; Ralph, J.; Boerjan, W. Lignin biosynthesis and structure. *Plant physiology* **2010**, *153* (3), 895-905.

21. Ma, X.; Chen, J.; Zhu, J.; Yan, N. Lignin-Based Polyurethane: Recent Advances and Future Perspectives. *Macromolecular Rapid Communications* **2021**, *42* (3), 2000492.

22. Tolbert, A.; Akinosho, H.; Khunsupat, R.; Naskar, A. K.; Ragauskas, A. J.

Characterization and analysis of the molecular weight of lignin for biorefining studies. *Biofuels, Bioproducts and Biorefining* **2014**, *8* (6), 836-856.

23. Capanema, E. A.; Balakshin, M. Y.; Kadla, J. F. A comprehensive approach for quantitative lignin characterization by NMR spectroscopy. *Journal of agricultural and food chemistry* **2004**, *52* (7), 1850-1860.

24. Gullichsen, J.; Paulapuro, H.; Fogelholm, C.-J. Papermaking Science and Technology, Book 6B. Chemical Pulping. **2000**.

25. Laskar, D. D.; Yang, B.; Wang, H.; Lee, J. Pathways for biomass-derived lignin to hydrocarbon fuels. *Biofuels, Bioproducts and Biorefining* **2013**, *7* (5), 602-626.

26. Xu, F.; Sun, J.-X.; Sun, R.; Fowler, P.; Baird, M. S. Comparative study of organosolv lignins from wheat straw. *Industrial crops and products* **2006**, *23* (2), 180-193.

27. Nitsos, C.; Stoklosa, R.; Karnaouri, A.; Voros, D.; Lange, H.; Hodge, D.; Crestini, C.; Rova, U.; Christakopoulos, P. Isolation and characterization of organosolv and alkaline lignins from hardwood and softwood biomass. *ACS Sustainable Chemistry & Engineering* **2016**, *4* (10), 5181-5193.

28. Gillet, S.; Aguedo, M.; Petitjean, L.; Morais, A.; da Costa Lopes, A.; Łukasik, R.; Anastas, P. Lignin transformations for high value applications: towards targeted modifications using green chemistry. *Green Chemistry* **2017**, *19* (18), 4200-4233.

29. Juan, F.; Huaiyu, Z. Optimization of synthesis of spherical lignosulphonate resin and its structure characterization. *Chinese Journal of Chemical Engineering* **2008**, *16* (3), 407-410.

30. Belgacem, M. N.; Gandini, A., *Monomers, polymers and composites from renewable resources*. Elsevier: 2011.

31. Mansouri, N.; Salvadó, J. Structural characterization of technical lignins for the production of adhesives: Application to lignosulfonate, kraft, soda-anthraquinone, organosolv and ethanol process lignins. *Industrial Crops & Products* **2006**, *24* (1), 8-16.

32. González-García, S.; Moreira, M. T.; Artal, G.; Maldonado, L.; Feijoo, G., Environmental impact assessment of non-wood based pulp production by soda-anthraquinone pulping process. *Journal of Cleaner Production* **2010,** *18* (2), 137-145.

33. Rodríguez, A.; Sánchez, R.; Requejo, A.; Ferrer, A. Feasibility of rice straw as a raw material for the production of soda cellulose pulp. *Journal of Cleaner Production* **2010**, *18* (10), 1084-1091.

34. Tejado, A.; Pea, C.; Labidi, J.; Echeverria, J. M.; Mondragon, I. Physico-chemical characterization of lignins from different sources for use in phenol–formaldehyde resin synthesis. *Bioresource Technology* **2007**, (8).

35. Chakar, F. S.; Ragauskas, A. J. Review of current and future softwood kraft lignin process chemistry. *Industrial crops and products* **2004**, *20* (2), 131-141.

36. Andeme Ela, R. C.; Spahn, L.; Safaie, N.; Ferrier Jr, R. C.; Ong, R. G. Understanding the effect of precipitation process variables on hardwood lignin characteristics and recovery from black liquor. *ACS Sustainable Chemistry & Engineering* **2020**, *8* (37), 13997-14005.

37. Sadeghifar, H.; Ragauskas, A. Perspective on technical lignin fractionation. *ACS*

Sustainable Chemistry & Engineering **2020**, *8* (22), 8086-8101.

38. Fengel, D.; Wegener, G. *Wood: chemistry, ultrastructure, reactions*; Walter de Gruyter, 2011.

39. Tomani, P. The lignoboost process. *Cellulose Chemistry & Technology* **2010**, *44* (1), 53.

40. Norgren, M.; Lindström, B., Dissociation of Phenolic Groups in Kraft Lignin at Elevated Temperatures. **2000,** *54* (5), 519-527.

41. Zhao, W.; Simmons, B.; Singh, S.; Ragauskas, A.; Cheng, G. From lignin association to nano-/micro-particle preparation: extracting higher value of lignin. *Green Chemistry* **2016**, *18* (21), 5693-5700.

42. Alekhina, M.; Ershova, O.; Ebert, A.; Heikkinen, S.; Sixta, H. Softwood kraft lignin for value-added applications: Fractionation and structural characterization. *Industrial Crops and Products* **2015**, *66*, 220-228.

43. Lourençon, T. V.; Hansel, F. A.; Da Silva, T. A.; Ramos, L. P.; De Muniz, G. I.; Magalhães, W. L. Hardwood and softwood kraft lignins fractionation by simple sequential acid precipitation. *Separation and purification technology* **2015**, *154*, 82-88.

44. Alekhina, M.; Ershova, O.; Ebert, A.; Heikkinen, S.; Sixta, H. Softwood kraft lignin for value-added applications: Fractionation and structural characterization. *Industrial Crops & Products* **2015**, *66*, 220-228.

45. Brenelli, L. B. M., F.; Mercadante, A. Z.; de Moraes Rocha, G. J.; Rocco, S. A.; Craievich, A. F.; Goncalves, A. R.; da Cruz Centeno, D.; de Oliveira Neto, M.; Squina,

F. M. Acidification treatment of lignin from sugarcane bagasse results in fractions of reduced polydispersity and high free-radical scavenging capacity. *Industrial Crops & Products* **2016**, *83*, 94-103.

46. Hildebrand, J. H.; Scott, R. L.. *The Solubility of Nonelectrolytes*; Reinhold Pub. Corp.: New York, 1950.

47. Hansen, C. M. *Hansen Solubility Parameters: A User's Handbook*; CRC Press: Boca Raton, 2007.

48. Ni, Y.; Hu, Q. Alcell® lignin solubility in ethanol-water mixtures. *Journal of Applied Polymer Science* **1995**, *57* (12), 1441-1446.

49. Wang, G.; Chen, H. Fractionation and characterization of lignin from steam-exploded corn stalk by sequential dissolution in ethanol–water solvent. *Separation & Purification Technology* **2013**, *120*, 402-409.

50. Sadeghifar, H.; Wells, T.; Le, R. K.; Sadeghifar, F.; Yuan, J. S.; Jonas Ragauskas, A., Fractionation of organosolv lignin using acetone: water and properties of the obtained fractions. *ACS Sustainable Chemistry & Engineering* **2017,** *5* (1), 580-587.

51. Jääskeläinen, A.-S. L., T.; Mikkelson, A.; Tamminen, T. Aqueous organic solvent fractionation as means to improve lignin homogeneity and purity. *Industrial Crops and Products* **2017**, *103*, 51-58.

52. Klett, A. S.; Chappell, P. V.; Thies, M. C. Recovering ultraclean lignins of controlled molecular weight from Kraft black-liquor lignins. *Chemical Communications* **2015**, *51* (64), 12855-12858.

53. Thring, R. W.; Vanderlaan, M. N.; Griffin, S. L., Fractionation Of Alcell® Lignin By Sequential Solvent Extraction. *Journal of Wood Chemistry and Technology* **1996,** *16* (2), 139-154.

54. Duval, A.; Vilaplana, F.; Crestini, C.; Lawoko, M., Solvent screening for the fractionation of industrial kraft lignin. *Holzforschung* **2016,** *70* (1), 11-20.

55. Suárez, L.; Díez, M. A.; García, R.; Riera, F. A., Membrane technology for the recovery of detergent compounds: A review. *Journal of Industrial and Engineering Chemistry* **2012,** *18* (6), 1859-1873.

56. Sultan, Z.; Graça, I.; Li, Y.; Lima, S.; Peeva, L. G.; Kim, D.; Ebrahim, M. A.; Rinaldi, R.; Livingston, A. G., Membrane Fractionation of Liquors from Lignin-First Biorefining. *ChemSusChem* **2019,** *12* (6), 1203-1212.

57. Arkell, A.; Olsson, J.; Wallberg, O., Process performance in lignin separation from softwood black liquor by membrane filtration. *Chemical Engineering Research and Design* **2014,** *92* (9), 1792-1800.

58. Helander, M.; Theliander, H.; Lawoko, M.; Henriksson, G.; Zhang, L.; Lindström, M. E. Fractionation of technical lignin: Molecular mass and pH effects. *BioResources* **2013**, *8* (2), 2270-2282.

59. Huang, C.; He, J.; Narron, R.; Wang, Y.; Yong, Q. Characterization of kraft lignin fractions obtained by sequential ultrafiltration and their potential application as a biobased component in blends with polyethylene. *ACS Sustainable Chemistry & Engineering* **2017**, *5* (12), 11770-11779.

60. Evdokimov, A. N.; Kurzin, A. V.; Fedorova, O. V.; Lukanin, P. V.; Kazakov, V. G.; Trifonova, A. D. Desulfurization of kraft lignin. *Wood Science and Technology* **2018**, *52* (4), 1165-1174.

61. Svensson, S. Minimizing the sulphur content in Kraft lignin. 2008.

62. Kouisni, L.; Gagné, A.; Maki, K.; Holt-Hindle, P.; Paleologou, M. LignoForce system for the recovery of lignin from black liquor: feedstock options, odor profile, and product characterization. *ACS Sustainable Chemistry & Engineering* **2016**, *4* (10), 5152-5159.

63. Huang, S.; Mahmood, N.; Tymchyshyn, M.; Yuan, Z.; Xu, C. C. Reductive de-polymerization of kraft lignin for chemicals and fuels using formic acid as an in-situ hydrogen source. *Bioresource technology* **2014**, *171*, 95-102.

64. Ritchie, H.; Roser, M.; Rosado, P. CO_2 and Greenhouse Gas Emissions-Our World in Data. 2021.

65. Kylili, A.; Seduikyte, L.; Fokaides, P. A., Life cycle analysis of polyurethane foam wastes. In *Recycling of polyurethane foams*, Elsevier: 2018; pp 97-113.

66. Guinee, J. B.; Heijungs, R.; Huppes, G.; Zamagni, A.; Masoni, P.; Buonamici, R.; Ekvall, T.; Rydberg, T. Life cycle assessment: past, present, and future. *Environ. Sci. Technol.* 2011, 45, 1, 90–96.

67. Klöpffer, W., Life cycle assessment. *Environmental Science and Pollution Research* **1997,** *4* (4), 223-228.

68. Hellweg, S.; Milà i Canals, L. Emerging approaches, challenges and opportunities in life cycle assessment. *Science* **2014**, *344* (6188), 1109-1113.

69. Pennington, D. W.; Potting, J.; Finnveden, G.; Lindeijer, E.; Jolliet, O.; Rydberg, T.; Rebitzer, G. Life cycle assessment Part 2: Current impact assessment practice. *Environment international* **2004**, *30* (5), 721-739.

70. Scientific Applications International Corporation (SAIC), Curran, M.A., National Risk Management Research Laboratory (US) and Office of Research and Development, Environmental Protection Agency, United States, *Life-cycle assessment: principles and practice*, 2006.

71. Culbertson, C.; Treasure, T.; Venditti, R.; Jameel, H.; Gonzalez, R. Life cycle assessment of lignin extraction in a softwood kraft pulp mill. *Nordic Pulp & Paper Research Journal* **2016**, *31* (1), 30-40.

72. Hermansson, F.; Janssen, M.; Svanström, M. Allocation in life cycle assessment of lignin. *The International Journal of Life Cycle Assessment* **2020**, *25* (8), 1620-1632.

73. Manzardo, A.; Marson, A.; Roso, M.; Boaretti, C.; Modesti, M.; Scipioni, A.; Lorenzetti, A. Life cycle assessment framework to support the design of biobased rigid polyurethane foams. *ACS omega* **2019**, *4* (9), 14114-14123.

2 Recovering Kraft Lignin from Black Liquor and Synthesis of Lignin-based Flexible Polyurethane Foam

2.1 Abstract

An effective method that can produce a large amount of Kraft lignin with improved homogeneity is strongly desired for Kraft lignin's high-value applications and scientific advancements. Herein, a one-pot acid-catalyzed liquefaction method was developed to recover Kraft lignin directly from black liquor. The recovery rate and properties of the recovered lignin were affected by the reaction time, reaction temperature, moisture content (MC), pH, and acid categories. The highest lignin recovery rate of 75% was achieved when the concentrated black liquor (MC=25%) reacted with methanol at pH=7 and 160 ℃ for 10 minutes using acetic acid as the catalyst. Most of the recovered lignin from this method showed a weight average molecular weight (Mw) value less than 2000 Da and a polydispersity (PDI) value less than 2.0. Such a PDI value was lower than that of current acid precipitated lignin (2.2~5.4). The recovered lignin was directly used to replace 20% of the petroleum-based polyol in the formula of a flexible polyurethane (PU) foam, and it was found that the molecular weight characteristics of the lignin affected the physical and mechanical properties of the flexible PU foams. The recovered lignin with the Mw value of 1600 Da and the PDI value of 1.8 was able to maintain the major physical and mechanical properties of the flexible PU foams. This study provided a promising way to recover lignin with improved homogeneity from black liquor with the potential to customize lignin properties to meet the requirements of downstream processes.

2.2 Introduction

Lignin is an attractive renewable substitute for the raw materials of fossil-based products, which has been highlighted as one of the most promising solutions to mitigate global climate change caused by excessive fossil-fuel usage and long-term greenhouse gas emissions.[1-3] Lignin represents a class of aromatic polymers massively found in nature, and it composes around 10~30% of plants.[2] In addition to the benzene rings, isolated lignin also contains plenty of hydroxyl groups and aliphatic carbons.[4,5] As a result, lignin holds a great potential as a raw material to make bio-materials, fuels and chemicals.[6-8]

Globally, the technical lignin is still an underutilized byproduct from the pulping process.[9] Kraft pulping process is one of the main pulping processes in the world, and this process uses strong alkali aqueous solution (H_2O, Na_2S and NaOH) to dissolve and isolate lignin from the cell walls of biomass at elevated temperatures, resulting in the black liquor containing Kraft lignin.[10] Most isolated Kraft lignin is in an ionized form and dissolved in the strong alkali black liquor.[11] To recover the Kraft lignin, acid precipitation methods are commonly employed in commercial techniques, such as LignoBoost, LignoForce and sequential liquid-lignin recovery and purification (SLRP).[12-14] Although those methods are able to recover lignin from black liquor, the precipitated lignin usually displays a wide range of molecular weight, which hinders the value-added applications of the lignin.[13,15,16,17] This issue has been further shown in a recent study in which the precipitated hardwood lignin possessed Mw values ranging from 15060 Da to 77450 Da and PDI values in the range of 2.24~5.36.[18] Such a situation necessitates developing a process to improve the molecular homogeneity of Kraft lignin.

Currently, fractionation is the major approach to narrow down the molecular weight distribution of lignin, including sequential acid precipitation, solvent extraction, and ultrafiltration technologies.[17, 19] These methods aim at separating different lignin fractions from one feedstock (lignin or black liquor). To achieve this goal, the first method requires multiple pH adjustments; the second method usually involves different solvents with variable components and ratios; the third method needs an ultrafiltration system integrated by a few of membranes with specific cutoff values.[17, 19] Although some of the fractionated lignin portions presented relatively narrowed molecular weight distributions, they entail either time-consuming operations or expensive devices, which limit their practical applications.[20] Thus, it is desirable to develop a simple and efficient technique to recover lignin with improved homogeneity directly from Kraft black liquor.

Liquefaction is a facile thermochemical conversion technique that has been widely employed to convert biomass to chemicals and bio-fuels.[21,22] For instance, Asim et al.[23] conducted liquefaction processes on two types of extracted lignin in supercritical ethanol/formic acid mixtures to produce bio-oil. Moreover, Xu et al.[24] developed a directional liquefaction coupling fractionation method to obtain platform chemicals from lignocellulosic biomass. However, there is no study of developing a liquefaction process suitable for recovering lignin directly from Kraft black liquor.

As one of the potential applications of lignin, polyurethane (PU) foams have been investigated frequently by replacing petroleum-based polyols with technical or modified lignin. [25,26] For instance, Pan and Saddler[27] developed rigid PU foams by replacing petrochemical polyols with organosolv or hardwood Kraft lignin. The cellular structure,

density, and compressive strength of the synthesized lignin-based PU foams exhibited high dependence on the lignin replacement ratio. Moreover, Bernardini et al.[28] successfully prepared lignin-based flexible PU foams with the aid of castor oil and polypropylene glycol triol (PPG triol). This study showed that altering the formulations was able to affect the prepared flexible PU foams' apparent density, compression force deflection, and cellular structures. Recently, a study reported biobased rigid PU foams made of the Kraft lignin recovered from black liquor using the gradient acid precipitation method and related the lignin's molecular structures to the performance of the rigid PU foams.[29] However, the studies on how the Kraft lignin's molecular weight properties affect the performance of lignin-based flexible PU foams are still limited, and it may be due to the lack of an effective method to produce large amount of Kraft lignin with adjustable molecular weight features.

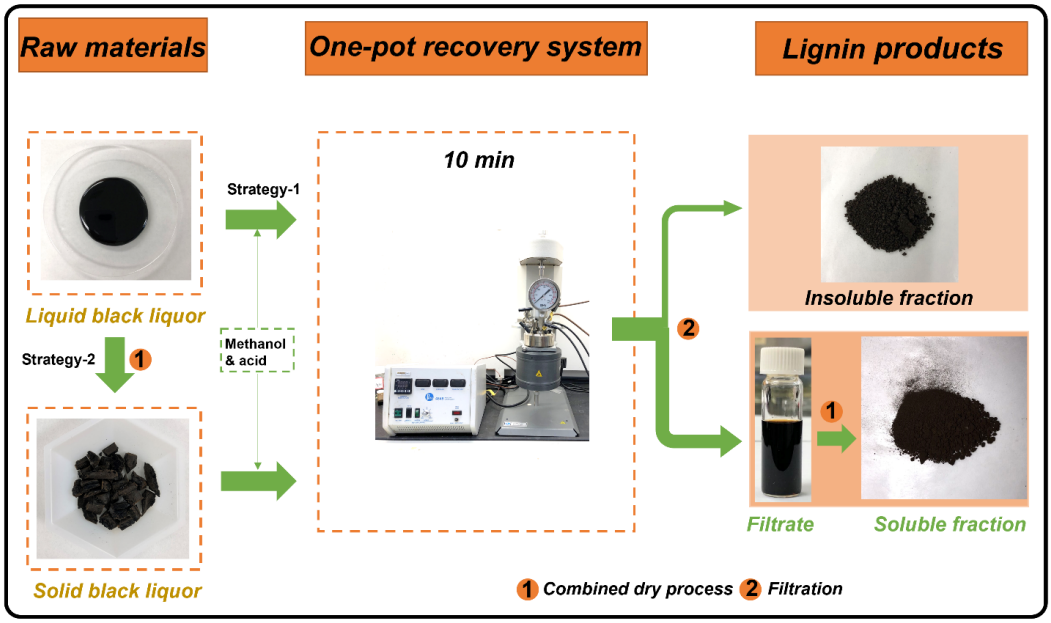

Scheme 2.1 Schematic of technical pathways from raw materials to lignin products.

In this study, a one-pot liquefaction process was developed to recover lignin directly from the Kraft black liquor (Scheme 2.1). The recovery method utilized subcritical methanol and acid as the recovery medium in which the lignin in black liquor was dissolved. Then, the dissolved lignin was obtained after evaporating the recovery medium. The types of acid, the amount of water in black liquor, and the processing temperature and time were explored with respect to the recovery rate and molecular weight of lignin. Afterward, the resultant lignin without further modifications was directly used to replace 20 wt.% fossil-based polyols in the formulation of flexible PU foams, and the relation between the recovered lignin's molecular weight properties and the physical/mechanical properties of the lignin-based flexible PU foams was investigated as well.

2.3 Experimental Section

2.3.1 Materials

As shown in Scheme 2.1, two kinds of Kraft black liquor were used in this study. The first was concentrated liquid black liquor (mixed hardwood) with an approximate 25% moisture content (MC), and it was kindly provided by Verso Corporation (Quinnesec, MI). The second was solid black liquor (MC = 0) derived from the liquid black liquor after a combined drying process in the lab. The combined dry process included oven drying at 80 ℃ for 8 h followed by vacuum drying at 50 ℃ for 24 h. The ash content in the solid of black liquor was measured as 47%. Methanol, sulfuric acid, and glacial acetic acid used in the black liquor liquefaction processing were purchased from Sigma-Aldrich. The reagents used to determine the molecular weight of lignin were tetrahydrofuran (THF), pyridine, acetic anhydride, hydrochloric acid purchased from Sigma-Aldrich, and polystyrene standards purchased from Agilent Technologies.

The chemicals used in the formulation of flexible PU foams included a polyether-based polyol with an OH number of 28 mg KOH/g (OH content of 0.50 mmol/g), an amine-based blowing catalyst, a polymerization catalyst, and a mixture of methylene diphenyl diisocyanate (MDI) and polymeric diphenylmethane diisocyanate (pMDI) with an isocyanate content of 28% (%NCO). Distilled water was used as the chemical blowing agent. Momentive Performance Materials Inc. provided a silicone-based surfactant. All the chemicals were used as received.

2.3.2 Lignin Recovery Processes

Table 2.1 The feedstock, recovery medium, and treatment parameters of lignin recovery processes.

Recovery Process	MC* (%) of black liquor	Recovery medium	pH	Temperature (°C)	Time (min)	Label of lignin
1	0	MeOH	12	25	1440	Lignin-1
2	0	MeOH and AcOH	7	25	1440	Lignin-2
3	0	MeOH and AcOH	7	160	10	Lignin-3
4	25	MeOH and AcOH	7	160	10	Lignin-4
5	25	MeOH and H_2SO_4	7	160	10	Lignin-5

*Moisture Content

The feedstock, recovery medium, and treatment parameters of five kinds of lignin recovery processes are listed in Table 2.1. The purpose of entry-1 and 2 was to study the effect of pH on the molecular weight, recovery rate of lignin, and the physical/mechanical properties of resultant lignin-based PU flexible foams. Entry-2 and 3 were purposed to disclose the effect of processing temperature and time on the same properties of lignin and lignin-based

PU foams. The entry-3 vs. 4 and entry-4 vs. 5 were aimed at exploring the effect of water content and acid categories within the liquefaction system on the investigated properties of lignin and lignin-based PU foams.

As for the operation procedures in entry-1 and 2, the solid black liquor was directly dissolved in methanol with a mass ratio of 1:10 at room temperature. Then, the pH of the mixture in entry-1 was measured as 12 using a pH meter (VWR sympHony, B10P), while that in entry-2 was adjusted to 7 through adding acetic acid. To accelerate the dissolution process of the mixtures, the magnetic stir was conducted on them at 600 rpm for 24 h (1440 min). After that, the filtrate and filter cake were separated from the mixture through vacuum filtration, followed by a 20 mL methanol wash. The soluble fraction was collected after removing the solvent in the filtrate through the combined drying process as mentioned before. The soluble fractions obtained from entry-1 and 2 were labeled as Lignin-1 and Lignin-2 in Table 2.1, respectively. The filter cake was also collected as an insoluble fraction.

As shown in Scheme 2.1, entry-3, 4, and 5 were one-pot liquefaction processes conducted in a mini parr pressure reactor (Model No: 4560 and maximum processing capacity = 300 mL). The formulation of each entry is illustrated in Table 2.1. It should be noted that the mass ratio between the solid of black liquor and methanol was maintained as 1:10 regardless of the types of black liquor. Before the liquefaction processing, the solid or liquid black liquor was mixed with methanol in the reactor, and then the pH of the mixture was adjusted to 7 by adding acid. Afterward, the reactor was heated with a heating rate of 5 ℃/min and then maintained at 160 ℃ for 10 min. At the end of the constant temperature

stage, the reactor was cooled down to room temperature using cooling water. During the entire liquefaction process, the mechanical stir was continuously conducted on the mixture. The resultant products were subsequently filtered, followed by a 20 mL methanol wash. Finally, both soluble and insoluble fractions were collected after the same process as entry-1 and 2. The soluble fractions from entry-3, 4, and 5 were labeled as Lignin-3, 4, and 5 in Table 2.1, respectively.

2.3.3 Determination of Ash Content

The samples' ash content (AC) was determined using a thermogravimetric analyzer (TGAQ500, TA company). All samples were oven-dried before the ash content measurement. During a typical TGA test, a sample (~5.0 mg) was heated under airflow (flow rate = 75 mL/min) directly from room temperature to 800 ℃ with a heating rate of 10 ℃/min and then cooled under the airflow with the same flow rate. The AC (%) was calculated based on the equation as follows:

$$AC\ (\%) = \frac{M_r}{M_o} \times 100 \tag{2.1}$$

Where the M_r is the mass of residue solid after the heating process, and the M_o represents the original mass of a sample.

2.3.4 Determination of Recovery Rate of Lignin

To quantify the recovery efficiency of lignin, the recovery rate (%) is defined as below:

$$Recovery\ rate(\%) = \left[1 - \frac{M_{IF} \times (1 - AC_{IF})}{M_{BL} \times (1 - AC_{BL})}\right] \times 100 \tag{2.2}$$

Where the M_{IF} represents the mass of dry insoluble fraction, and the AC_{IF} refers to the ash content of dry insoluble fraction; The M_{BL} is the mass of dry solid in black liquor; the AC_{BL} is the ash content of dry solid in black liquor. According to the previous study, the amount of carbohydrate in both black liquor and insoluble fractions was ignored in the calculation since it was pretty low.[18]

2.3.5 Characterization for Molecular Weight of Recovered Lignin

The number average (M_n) and weight average (M_w) molecular weights of the recovered lignin were determined by a gel permeation chromatography (GPC) system (Waters Company) equipped with a refractive index detector and three 300 mm×7.8 mm Waters columns including 1-Styragel HR 4, 2-Styragel HR 3 and 3-Ultrastyragel in tandem. THF (tetrahydrofuran) was used as the mobile phase in the GPC system, and its flow rate was 1 mL/min. The preparation and characterization processes were conducted according to a previous report.[31]

2.3.6 Synthesis of PU Foams

Table 2.2 Formulations of lignin-based and control PU foams.

	Copolyol (g)	Lignin (g)	Water (g)	Gelation catalyst (g)	Blowing catalyst (g)	Surfactant (g)	Diisocyanate (g)
Control	25	-	0.63	0.13	0.08	0.20	10.05
Lignin-1	20	5	0.63	0.13	0.08	0.20	10.05
Lignin-2	20	5	0.63	0.13	0.08	0.20	10.05
Lignin-3	20	5	0.63	0.13	0.08	0.20	10.05
Lignin-4	20	5	0.63	0.13	0.08	0.20	10.05
Lignin-5	20	5	0.63	0.13	0.08	0.20	10.05

The components of lignin-based and control PU foams are listed in Table 2.2. In this study, the five types of solid lignin powder, obtained from different recovery processes (Table 2.1), were directly used to replace 20 wt.% petroleum-based polyols to prepare lignin-based flexible PU foams. More specifically, polyol was first added in a 12 oz cup, followed by the sequential addition of water, gelation catalyst, blowing catalyst, and silicone-based surfactant. Afterward, the solid lignin powder was added to the cup. The mixture was blended thoroughly for 2 min at 2000 rpm using a high-speed digital overhead stirrer to ensure homogenous mixing. Then, isocyanate was added to the polyol component, and the solution was mixed vigorously at 2000 rpm for 4-5 s. After that, the mixture was immediately poured into a silicone mold to rise in free expansion at 60 ℃ for an hour and then air-dried at room temperature for 24 h to ensure complete curing before characterizations.

2.3.7 Characterizations of PU Foams

The characterizations of lignin-based and control PU foams in this investigation involved measuring apparent density, compression force deflection, tensile strength, ultimate elongation, tear-resistance test, compression set, and support factor, based on the previous study using ASTM 3574 standard methods.[31]

2.3.8 Statistical Analysis

The physical and mechanical data of PU foams were shown in average values with standard deviations, and one-way ANOVA ($\alpha = 0.05$) for these data was conducted in SPSS software.

2.4 Results and Discussion

2.4.1 Characteristics of Recovered Lignin

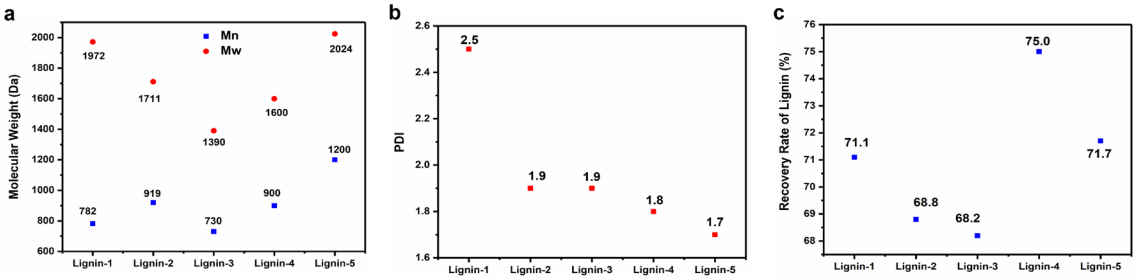

Figure 2.1 Plots of number average molecular weight (Mn), weight average molecular weight (Mw) (a), polydispersity (PDI) (b) and recovery rate (c) of different types of recovered lignin.

The molecular weight properties and recovery rate of lignin are shown in Figure 2.1. The recovered lignin exhibited number average molecular weight (Mn) values in the range of 730~1200 Da and weight average molecular weight (Mw) values ranging from 1390 to 2024 Da (Figure 2.1a). Such Mw values were lower than that of acid precipitated lignin (15000~77000 Da) reported by a previous study employing the same Kraft black liquor source.[18] A possible explanation regarding this difference is that there are condensation reactions of lignin molecules during the acid precipitation process,[18] while such reactions could be reduced due to the existence of subcritical methanol during the lignin recovery processes.[24] Moreover, the highest polydispersity (PDI) of 2.5 was present in Lignin-1 that originated from the alkaline recovery system (pH=12) (Figure 2.1b). In contrast, the lignin samples (Lignin-2, 3, 4, and 5) produced from the neutral recovery system (pH=7) showed a lower PDI value ranging from 1.7 to 1.9 (Figure 2.1b). Such PDI values were lower than those generated by the acid precipitation method (PDI=2.2~5.4).[18] It also suggested that

the recovery system neutralized by acid was able to produce more homogeneous lignin molecules. Moreover, the relatively high Mn and low Mw of Lignin-2 compared with Lignin-1 implied that the molecular weight distribution of soluble lignin could be narrowed by the neutralization using acetic acid (Figure 2.1b). This improved uniformity of soluble lignin might be caused by the transformation of some inhomogeneous lignin fractions dissolved in the methanol to the insoluble fractions after the addition of acid. This explanation can be verified by the slightly decreased recovery rate of Lignin-2 in comparison with Lignin-1 (Figure 2.1c). In contrast to Lignin-2, Lignin-3 presented lower values of both Mn and Mw but the same value of PDI (Figure 2.1a and b), which suggested that the heating in the given lignin recovery process was beneficial to producing smaller lignin molecules. The comparison of Mn and Mw between Lignin-3 and 4 demonstrated that introducing water into the liquefaction process might be able to dissolve lignin fractions with higher molecular weight (Figure 2.1a). Additionally, both Mn and Mw of Lignin-4 were lower than that of Lignin-5, while the PDI of Lignin-4 was similar to that of Lignin-5 (Figure 2.1a and b). This phenomenon indicated that replacing the acetic acid with sulfuric acid could boost the shift of soluble lignin from lower molecular weight to higher molecular weight, and it can be explained by the repolymerization of lignin during the liquefaction process aided by sulfuric acid.[24]

As for the recovery rate (Figure 2.1c), the Lignin-4 possessed the highest value of 75.0%, while the Lignin-3 showed the lowest value of 68.2%. As mentioned before, the slightly reduced recovery rate of Lignin-2 compared to Lignin-1 was due to the partial precipitation of soluble lignin molecules triggered by adding acetic acid. It was noticeable that the recovery rate of Lignin-2 was similar to Lignin-3, which was produced from the water-free

liquefaction process. The limited solubility of lignin in certain amount of methanol may result in the similar recovery rate. Although the heat input in the liquefaction process was unable to improve the recovery rate, the dissolution process of lignin in methanol could be remarkably accelerated. More specifically, obtaining such a recovery rate of Lignin-2 involved a time-consuming dissolution process (1440 min), while the liquefaction process for the Lignin-3 only needed 10 min. Such a short duration enables the liquefaction process to be more compatible with existing industrial pulping processes. Furthermore, the introduction of water into the liquefaction process increased the recovery rate from 68.2% of Lignin-3 to 75.0% of Lignin-4. However, replacing acetic acid with sulfuric acid in the water-containing liquefaction process reduced the amount of recovered lignin (Lignin-4 vs. Lignin-5). According to the previous study, acetic acid is also an organic solvent for lignin besides its deprotonation effect, promoting the recovery rate of Lignin-4.[19]

2.4.2 Apparent Density and Compression Force Deflection of PU Foams

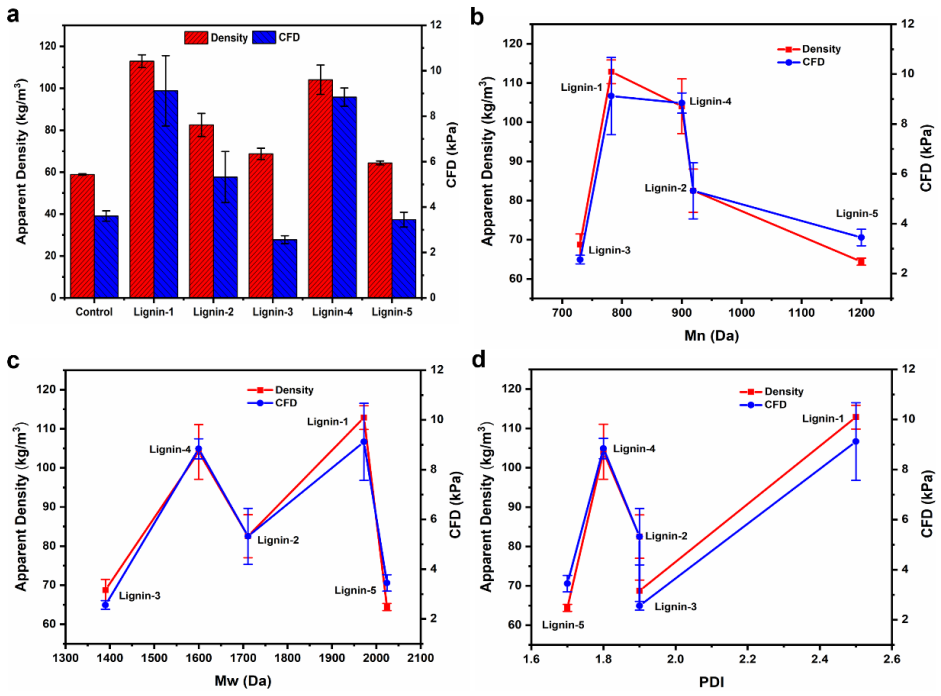

Figure 2.2 The apparent density and compression force deflection (CFD) of control and lignin-based PU foams (a); the lignin-based PU foams' apparent density and compression force deflection (CFD) versus the number average molecular weight (Mn) (b), the weight average molecular weight (Mw) (c), and the polydispersity (PDI) (d) of recovered lignin, respectively.

Apparent density is an essential parameter of PU foams since it significantly affects foams' durability and support ability. Generally, the PU foams with higher density show better durability and support ability.[30] The apparent densities of the lignin-based PU foams and the control are shown in Figure 2.2a. The control PU foam presented an average apparent density value of 59 kg/m^3, while the average apparent density values of the PU foams were higher than that of the control PU foams and varied with the types of lignin in the range of

64~113 kg/m^3. Such a difference between most lignin-based PU foams (except Lignin-5 samples) and control PU foams in apparent density was statistically significant ($P<0.05$). A previous study demonstrated that the lignin macromolecules comprised higher content of hydroxyl groups than the polyether-based polyols.[31] Hence, lignin may react with more diisocyanate to form more urethane linkages, increasing the density of PU foams. The density of Lignin-1 and 2-based PU foams indicated that the Kraft lignin recovered at pH=7 was more suitable than the Kraft lignin recovered at pH=12 to produce the lower-density PU foams. Moreover, the comparison between Lignin-2 and 3 samples suggested that the density of PU foams could be further lowered when the lignin recovered from the water-free liquefaction process was used. However, the PU foams' density was reversely increased by incorporating Lignin-4, which originated from the water-containing liquefaction process. Furthermore, the higher density of Lignin-4 PU foams compared to that of Lignin-5 PU foams was associated with the different types of acid used in the liquefaction processes. The change in the density of lignin-based flexible PU foams may be associated with the molecular weight of the lignin produced from the recovery processes using different parameters since the molecular weight of lignin determines the distance between the crosslinks in PU foams and thus affects the density.[32] The correlation between the lignin-based PU foams' apparent density and the molecular weight properties of recovered lignin was given in Figure 2.2b-d. Statistically, the Mn, Mw, and PDI of recovered lignin showed significant effect on the apparent density of lignin-based PU foams ($P<0.05$). Increasing the Mn of recovered lignin from 730 to 1200 Da, the average apparent density value of lignin-based PU foams increased from 69 to 113 kg/m^3 and then

gradually decreased to 64 kg/m^3 (Figure 2.2b), while it occurred in a fluctuating manner with respect to the Mw and PDI of recovered lignin (Figure 2.2c and d).

The compression force deflection (CFD) of PU foams was also shown in Figure 2.2a. CFD reflects the force needed to compress the foam to 50% of the original thickness. The CFD exhibited a trend similar to the apparent density, suggesting their close correlation. The average CFD value of control PU foams was 4 kPa, while it ranged from 3 to 9 kPa and highly depended on the types of lignin. The CFD values of Lignin-1, 2, and 4 PU foams were statistically different from that of the control ($P<0.05$). Moreover, the CFD of the lignin-based PU foams showed a trend similar to the apparent density with regard to the molecular weight features of the lignin samples (Figure 2.2b-d). The effect of Mn, Mw, and PDI of the recovered lignin on the CFD of the lignin-based PU foams was also statistically significant ($P<0.05$). These results indicated that not only apparent density but also the CFD of lignin-based PU foams could be changed by adjusting the parameters of the recovery processes.

2.4.3 Compression Set of PU Foams

The compression set (CS) is an indicator of the resiliency of PU foams. Generally, a lower CS value means less thickness loss and better resiliency for long-term cushioning applications.[33] As shown in Figure 2.3a, the average CS value of the control PU foams was less than 10%, while the lignin-based PU foams presented higher average CS values in the range of 11~91%. Such a difference in the CS values of between the lignin-based PU foams and the control was statistically significant ($P<0.05$). The results indicated that partially replacing fossil-based polyols with lignin weakened the resiliency of PU foams, which may

be related to an increase in crosslinking density between lignin and isocyante.[34] However, the reduction in the resiliency of lignin-based PU foams varied with the types of lignin.

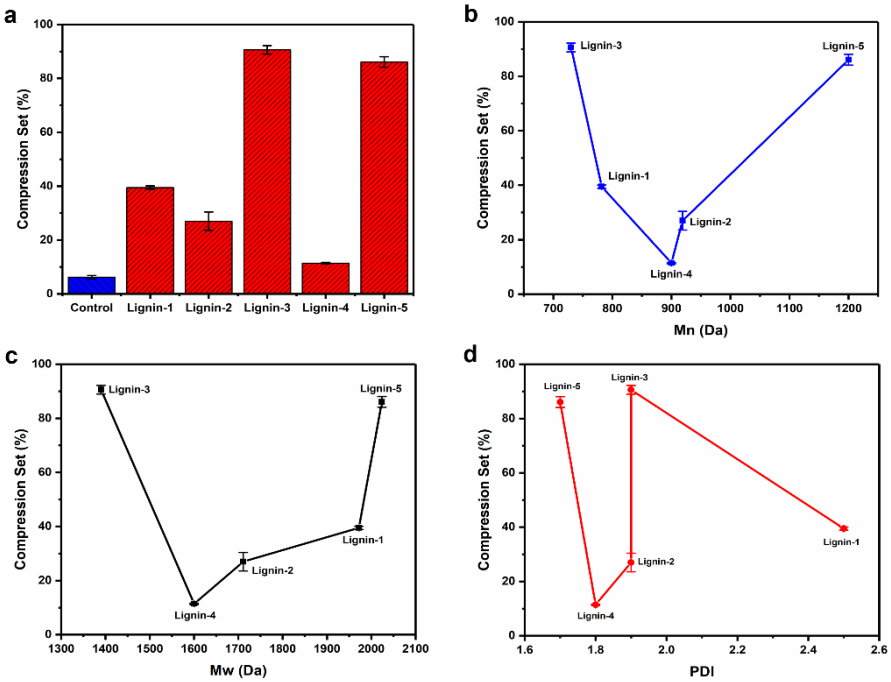

Figure 2.3 The compression set (CS) of control and lignin-based PU foams (a); the lignin-based PU foams' compression set (CS) versus the number average molecular weight (Mn) (b), weight average molecular weight (Mw) (c), and polydispersity (PDI) (d) of recovered lignin, respectively.

Furthermore, the relationship between the molecular weight nature of recovered lignin and relevant lignin-based PU foams' CS values is described in Figure 2.3b, c and d. Statistically, the Mn, Mw, and PDI of recovered lignin displayed statistical effect on the CS value of lignin-based PU foams ($P<0.05$). As shown in Figure 2.3b and c, the CS value of lignin-based PU foams declined first and then increased with the increase in Mn and Mw of recovered lignin, and the lowest CS value (11%) was exhibited at the samples made of

Lignin-4 (Mn=900 and Mw=1600). Such a CS value of Lignin-4-based PU foams was similar to that of the control PU foams, and it indicated that the Lignin-4 recovered from the liquefaction process for liquid black liquor neutralized by acetic acid seems to be best for maintaining the resiliency of PU foams. In Figure 2.3d, it could be found that the PDI value of Lignin-4 was not the lowest, but its derived PU foams had the lowest average CS value, suggesting that the molecular weight of recovered lignin restricted in a moderate range could be preferable to reduce the loss of PU foams' resiliency.

2.4.4 Tensile Strength of PU Foams

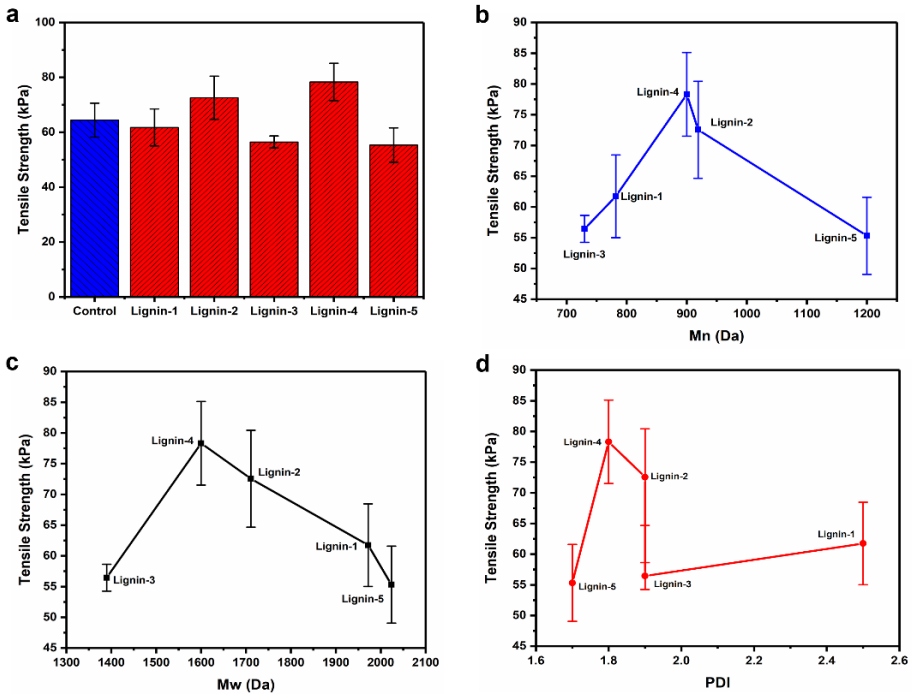

Figure 2.4 The tensile strength of control and lignin-based PU foams (a); the lignin-based PU foams' tensile strength versus the number average molecular weight (Mn) (b), weight average molecular weight (Mw) (c), and polydispersity (PDI) (d) of recovered lignin, respectively.

The tensile strength of a PU foam is an important indicator to its ability to resist a force that tends to pull them apart in situations where the foam needs to be bent or stretched to fit the uneven surface of substrate materials.[35] The tensile strength results of the PU foams are presented in Figure 2.4a. The average tensile strength value of the control PU foams was 64 kPa, and that of the lignin-based PU foams fluctuated in the range of 55~78 kPa. Only the tensile strength of Lignin-4 samples was statistically higher than that of the control samples ($P<0.05$). Figure 2.4b-d showed the relationship between the molecular weight properties of the recovered lignin samples and the tensile strength of lignin-based PU foams. Statistically, the influence of Mn, Mw, and PDI of recovered lignin on the lignin-based PU foams' tensile strength was significant ($P<0.05$). In contrast to the CS, the tensile strength of lignin-based PU foams displayed a reverse trend within the same range of Mn, Mw, and PDI. However, the best tensile strength (78 kPa) still existed in the PU foams made of Lignin-4 (Mn = 900, Mw = 1600 and PDI = 1.8). This result indicated that the molecular weight of recovered lignin may need to be restricted in a suitable range to enhance the tensile strength of PU foams. Moreover, although the tensile strength varied among the lignin-based PU foams, they still met the requirements for some automotive applications such as panel insulators and floor carpets.[36]

2.4.5 Ultimate Elongation of PU Foams

The ultimate elongation is an indicator of the flexibility and elasticity of PU foams.[31] As shown in Figure 2.5a, the control PU foams possessed an average ultimate elongation value of 124%, while the lignin-based PU foams showed relatively lower average ultimate elongation values ranging from 69% to 93%, suggesting that lignin-based PU foams had lower flexibility and elasticity than the control PU foams. Such a difference between the

lignin-based PU foams and control PU foams in the ultimate elongation was statistically significant ($P<0.05$), and it might be related to the rigid aromatic rings in the lignin macromolecules.[31] Moreover, the ultimate elongation of lignin-based PU foams was observed to rely on the lignin categories, indicating that the flexibility and elasticity of lignin-based PU foams were indirectly affected by the lignin recovery processes.

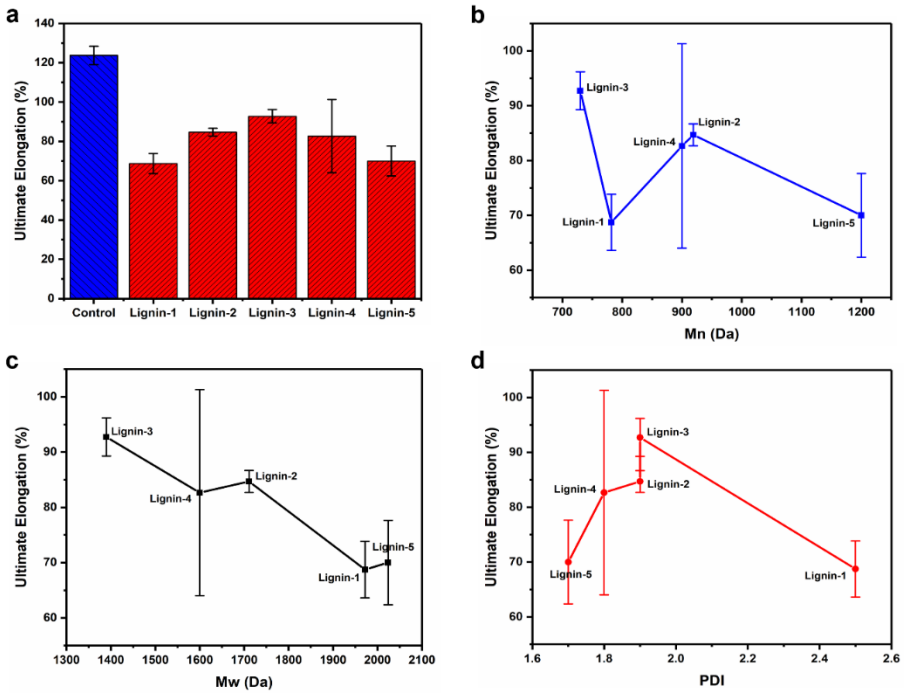

Figure 2.5 The ultimate elongation of control and lignin-based PU foams (a); the lignin-based PU foams' ultimate elongation versus the number average molecular weight (Mn) (b), weight average molecular weight (Mw) (c), and polydispersity (PDI) (d) of recovered lignin, respectively.

Figure 2.5b-d were given to further show the influence of recovered lignin's Mn, Mw, and PDI on the flexibility and elasticity of lignin-based PU foams. Statistically, only the effect of recovered lignin's PDI values on the ultimate elongation of lignin-based PU foams was

significant (P<0.05). The lignin-based PU foams' ultimate elongation fluctuated with increasing the Mn of recovered lignin, yet it trended to decline when increasing the Mw of recovered lignin. The best ultimate elongation (93%) was present in the PU foams modified by Lignin-3 whose Mn (730 Da) and Mw (1390 Da) values were the lowest (Figure 2.5b and c). Moreover, the ultimate elongation first gradually increased and then declined with the growth of PDI values (Figure 2.5d). Above results suggested that the recovered lignin with a narrow distribution in lower molecular weight could be more desirable to produce flexible and elastic lignin-based PU foams.

2.4.6 Tear Strength of PU Foams

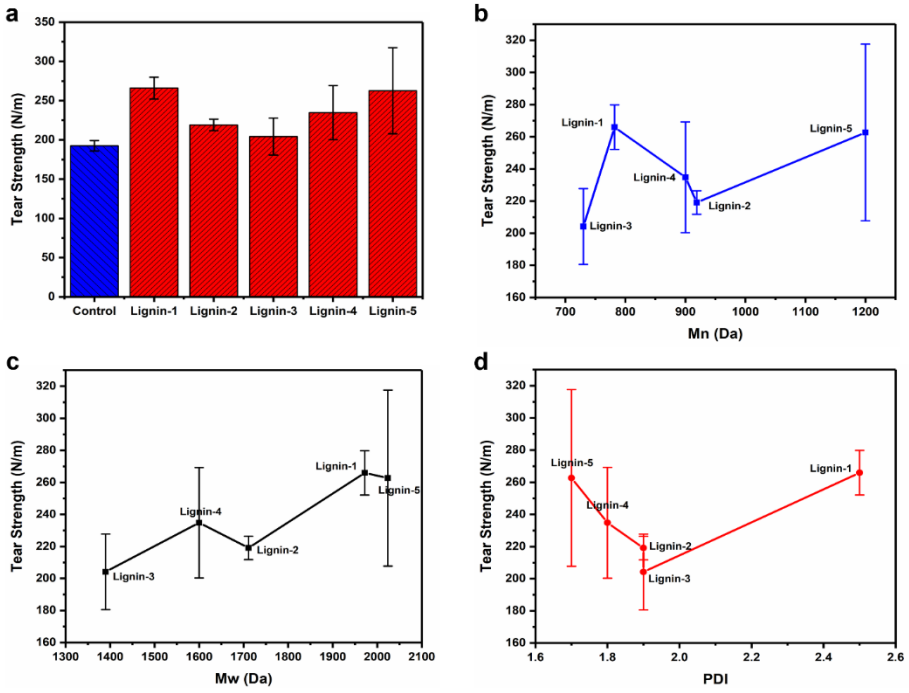

Figure 2.6 The tear strength of control and lignin-based PU foams (a); the lignin-based PU foams' tear strength versus the number average molecular weight (Mn) (b), weight

average molecular weight (Mw) (c), and polydispersity (PDI) (d) of recovered lignin, respectively.

The ability of PU foams to resist the crack propagation can be represented by the tear strength,[33] and the tear strength results of PU foams made in this study are presented in Figure 2.6a. The tear strength of PU foams appeared to follow a reverse trend to that of the ultimate elongation. The lignin-based PU foams had higher average tear strength values (204~266 N/m) compared to the control PU foams (192 N/m), suggesting that the addition of recovered lignin improved the ability of PU foams to resist the crack propagation. Nevertheless, compared to the control samples, only the improvement of Lignin-1 and 5 samples in tear strength was statistically significant ($P<0.05$). Moreover, compared with the ultimate elongation, the tear strength of the lignin-based PU foams also showed an opposite variation within the same range of Mn, Mw, and PDI of recovered lignin (Figure 2.6b-d), while these variations were statistically insignificant ($P>0.05$). Among them, the PU foams made of Lignin-3 with the lowest Mn and Mw exhibited the lowest average tear strength value (204 N/m) (Figure 2.6b and c). Moreover, the tear strength of PU foams made of Lignin-1 with the highest PDI value displayed the highest average tear strength value, and that was followed by the PU foams made of Lignin-5 with the lowest PDI value (Figure 2.6d).

2.4.7 Support Factor of PU Foams

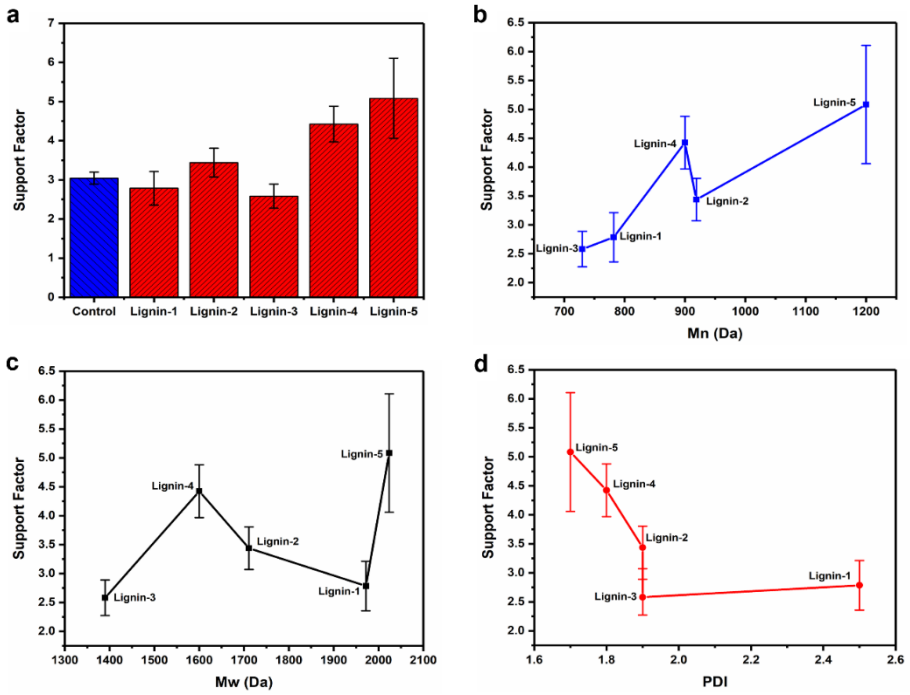

Figure 2.7 The support factor of control and lignin-based PU foams (a); the lignin-based PU foams' support factor versus the number average molecular weight (Mn) (b), weight average molecular weight (Mw) (c), and polydispersity (PDI) (d) of recovered lignin, respectively.

The weight loading capacity of PU foams is often considered in the application of floor carpets, and the effect of adding the lignin into the PU foams on the support factor was evaluated in this study.[31] Generally, a higher value of support factor indicates a better ability of PU foams supporting the weight.[31] As shown in Figure 2.7a, the average support factor value of control PU foams was 3.0, and that of lignin-based PU foams ranged from 2.6 to 5.1. Among the lignin-based PU foams, only the variation of Lignin-4 and 5-based PU foams' support factor was statistically significant ($P<0.05$) compared to the control PU

foams. Furthermore, the relationship between the recovered lignin's molecular properties and the support factor of lignin-based PU foams was shown in Figure 2.7b-d. The influence of Mn, Mw, and PDI of recovered lignin on the support factor of lignin-based PU foams was statistically significant ($P<0.05$). The lignin-based PU foams' support factor tended to grow while increasing the Mn of recovered lignin, but it fluctuated with the increase in Mw. Moreover, the lower PDI value of recovered lignin resulted in the higher support factor value of PU foams. Such results demonstrated that the recovered lignin with higher molecular weight in a narrow distribution may be beneficial to promoting the weight loading ability of PU foams.

2.5 Conclusions

In this study, a novel one-pot acid-catalyzed liquefaction technique was developed to recover Kraft lignin directly from black liquor. Most of the recovered lignin samples had narrower molecular weight distributions (PDI =1.7~1.9) compared to the acid precipitated lignin (PDI = 2.2~5.4). The highest recovery rate of 75% was achieved when reacting the black liquor (MC=25%) with methanol and acetic acid at pH=7 and 160 ℃ for 10 min. Moreover, the physical and mechanical properties of lignin-based flexible PU foams were found to be related to the molecular weight properties of the recovered lignin. Particularly, the recovered lignin with the Mw value of 1600 Da and the PDI value of 1.8 could maintain the major properties of the flexible PU foams. This preliminary study demonstrated that reacting black liquor with organic solvent and acid at elevated temperatures can provide a facial method to recover the Kraft lignin with improved molecular homogeneity, and the recovered lignin can be directly used to partially replace the petroleum-based polyols in flexible PU foam formulations without compromising the major physical and mechanical

properties. Fine tuning of the reaction parameters to optimize the lignin properties and a techno-economic analysis will be needed in the future to qualify the technical and economic advantages of this method.

2.6 References

1. Hu, J.; Zhang, Q.; Lee, D.-J., Kraft lignin biorefinery: A perspective. *Bioresour. Technol.* **2018,** *247*, 1181-1183.

2. Ragauskas, A. J.; Beckham, G. T.; Biddy, M. J.; Chandra, R.; Chen, F.; Davis, M. F.; Davison, B. H.; Dixon, R. A.; Gilna, P.; Keller, M., Lignin valorization: improving lignin processing in the biorefinery. *Science* **2014,** *344* (6185).

3. Cao, Y.; Chen, S. S.; Zhang, S.; Ok, Y. S.; Matsagar, B. M.; Wu, K. C.-W.; Tsang, D. C., Advances in lignin valorization towards bio-based chemicals and fuels: Lignin biorefinery. *Bioresour. Technol.* **2019,** *291*, 121878.

4. Garlapati, V. K.; Chandel, A. K.; Kumar, S. J.; Sharma, S.; Sevda, S.; Ingle, A. P.; Pant, D., Circular economy aspects of lignin: Towards a lignocellulose biorefinery. *Renewable Sustainable Energy Rev.* **2020,** *130*, 109977.

5. Ponnusamy, V. K.; Nguyen, D. D.; Dharmaraja, J.; Shobana, S.; Banu, J. R.; Saratale, R. G.; Chang, S. W.; Kumar, G., A review on lignin structure, pretreatments, fermentation reactions and biorefinery potential. *Bioresour. Technol.* **2019,** *271*, 462-472.

6. Moreno, A.; Sipponen, M. H., Lignin-based smart materials: a roadmap to processing and synthesis for current and future applications. *Mater. Horiz.* **2020,** *7* (9), 2237-2257.

7. Xu, C.; Arancon, R. A. D.; Labidi, J.; Luque, R., Lignin depolymerisation strategies: towards valuable chemicals and fuels. *Chem. Soc. Rev.* **2014,** *43* (22), 7485-7500.

8. Torres, L. A. Z.; Woiciechowski, A. L.; de Andrade Tanobe, V. O.; Karp, S. G.; Lorenci, L. C. G.; Faulds, C.; Soccol, C. R., Lignin as a potential source of high-added value compounds: A review. *J. Cleaner Prod.* **2020,** *263*, 121499.

9. Gigli, M.; Crestini, C., Fractionation of industrial lignins: opportunities and challenges. *Green Chem.* **2020,** *22* (15), 4722-4746.

10. Gierer, J., Chemical aspects of kraft pulping. *Wood Sci. Technol.* **1980,** *14* (4), 241-266.

11. Norgren, M.; Lindström, B., Dissociation of Phenolic Groups in Kraft Lignin at Elevated Temperatures. *Holzforschung* **2000,** *54* (5), 519-527.

12. Tomani, P., The lignoboost process. *Cellul. Chem. Technol.* **2010,** *44* (1), 53.

13. Kouisni, L.; Holt-Hindle, P.; Maki, K.; Paleologou, M., The lignoforce system: a new process for the production of high-quality lignin from black liquor. *J. Sci. Technol. For. Prod. Processes* **2012,** *2* (4), 6-10.

14. Lake, M. A., Blackburn, J. C. Process for recovering lignin. International Patent Application PCT/US2010/049773, 2011.

15. Zhu, W.; Westman, G.; Theliander, H., Investigation and characterization of lignin precipitation in the lignoboost process. *J. Wood Chem. Technol.* **2014,** *34* (2), 77-97.

16. Velez, J.; Thies, M. C., Temperature effects on the molecular properties of liquid lignin recovered from Kraft black liquor. *ACS Sustainable Chem. Eng.* **2015,** *3* (6), 1032-1038.

17. Pang, T.; Wang, G.; Sun, H.; Sui, W.; Si, C., Lignin fractionation: Effective strategy to reduce molecule weight dependent heterogeneity for upgraded lignin valorization. *Ind. Crops Prod.* **2021,** *165*, 113442.

18. Andeme Ela, R. C.; Spahn, L.; Safaie, N.; Ferrier Jr, R. C.; Ong, R. G., Understanding the effect of precipitation process variables on hardwood lignin characteristics and recovery from black liquor. *ACS Sustainable Chem. Eng.* **2020,** *8* (37), 13997-14005.

19. Sadeghifar, H.; Ragauskas, A., Perspective on technical lignin fractionation. *ACS Sustainable Chem. Eng.* **2020,** *8* (22), 8086-8101.

20. Rodrigues, J. S.; Lima, V.; Araújo, L. s. C.; Botaro, V. R., Lignin Fractionation Methods: Can Lignin Fractions Be Separated in a True Industrial Process? *Ind. Eng. Chem. Res.* **2021,** *60* (30), 10863-10881.

21.Kozliak, E. I.; Kubátová, A.; Artemyeva, A. A.; Nagel, E.; Zhang, C.; Rajappagowda, R. B.; Smirnova, A. L., Thermal liquefaction of lignin to aromatics: efficiency, selectivity, and product analysis. *ACS Sustainable Chem. Eng.* **2016,** *4* (10), 5106-5122.

22. Jiang, W.; Kumar, A.; Adamopoulos, S., Liquefaction of lignocellulosic materials and its applications in wood adhesives—A review. *Ind. Crops Prod.* **2018,** *124*, 325-342.

23. Riaz, A.; Kim, C. S.; Kim, Y.; Kim, J., High-yield and high-calorific bio-oil production from concentrated sulfuric acid hydrolysis lignin in supercritical ethanol. *Fuel* **2016,** *172*, 238-247.

24. Xu, J.; Xie, X.; Wang, J.; Jiang, J., Directional liquefaction coupling fractionation of lignocellulosic biomass for platform chemicals. *Green Chem.* **2016,** *18* (10), 3124-3138.

25. Li, Y.; Ragauskas, A. J., Kraft lignin-based rigid polyurethane foam. *J. Wood Chem. Technol.* **2012,** *32* (3), 210-224.

26. Wang, S.; Liu, W.; Yang, D.; Qiu, X., Highly resilient lignin-containing polyurethane foam. *Ind. Eng. Chem. Res.* **2018,** *58* (1), 496-504.

27. Pan, X.; Saddler, J. N., Effect of replacing polyol by organosolv and kraft lignin on the property and structure of rigid polyurethane foam. *Biotechnol. Biofuels* **2013,** *6* (1), 1-10.

28. Bernardini, J.; Cinelli, P.; Anguillesi, I.; Coltelli, M.-B.; Lazzeri, A., Flexible polyurethane foams green production employing lignin or oxypropylated lignin. *Eur. Polym. J.* **2015,** *64*, 147-156.

29. Cao, H.; Liu, R.; Li, B.; Wu, Y.; Wang, K.; Yang, Y.; Li, A.; Zhuang, Y.; Cai, D.; Qin, P., Biobased rigid polyurethane foam using gradient acid precipitated lignin from the black liquor: Revealing the relationship between lignin structural features and polyurethane performances. *Ind. Crops Prod.* **2022,** *177*, 114480.

30. https://www.pfa.org/foam-performance/.

31. Gondaliya, A.; Nejad, M., Lignin as a Partial Polyol Replacement in Polyurethane Flexible Foam. *Molecules* **2021,** *26* (8), 2302.

32. D'Souza, J.; George, B.; Camargo, R.; Yan, N., Synthesis and characterization of bio-polyols through the oxypropylation of bark and alkaline extracts of bark. *Ind. Crops Prod.* **2015,** *76*, 1-11.

33. Ramirez, B. J.; Gupta, V., High tear strength polyurea foams with low compression set and shrinkage properties at elevated temperatures. *Int. J. Mech. Sci.* **2019,** *150*, 29-34.

34. Kang, S.; Lee, S.; Kim, B., Shape memory polyurethane foams. *Express Polym. Lett.* **2012,** *6* (1), 63-69.

35. Ismail, A.; Khulbe, K.; Matsuura, T., Chapter 3-RO membrane characterization. *Reverse osmosis.* Elsevier Publications, London, **2019**; pp 57-90.

36.https://global.ihs.com/doc_detail.cfm?document_name=FORD%20WSB%2DM2D456%2DA&item_s_key=00354718.

3 Lignin with Tunable and Predictable Yield and Molecular Properties

3.1 Abstract

To control and predict lignin properties remains very challenging due to the complexity of chemical structures and recovery methods of lignin. Recently, an acid-catalyzed one-pot liquefaction technique was developed to produce Kraft lignin with improved molecular uniformity directly from black liquor. Herein, we investigated the effects of the liquefaction parameters (pH, reaction temperature, and reaction time) on the yield, molecular weights, polydispersity, and quantities of different types of hydroxyl groups of the Kraft lignin using the Box-Behnken response surface methodology (RSM). Computational models were generated and refined to establish the relationships between the liquefaction parameters and the Kraft lignin properties. The results showed that pH was the most influential factor followed by the reaction temperature affecting the properties of the Kraft lignin. The yield, molecular weight, and polydispersity were found to be more predictable ($R^2_{(pred)}$ values of 87.5-91.5%) than the type and quantity of hydroxyl groups ($R^2_{(pred)}$ values of 0) of the Kraft lignin. Additionally, the weight average molecular weight (Mw) could be used as a reliable predictor for both the number average molecular weight (Mn) and the polydispersity of the Kraft lignin, which was confirmed by both the experimental and the computational approaches. Such tunable and predictable molecular properties of the lignin may be associated with the clever use of acetic acid, subcritical methanol, and one-pot method. This study provided insights into understanding and predicting the properties of the lignin products from complex chemical reaction systems.

3.2 Introduction

Lignin has been highlighted as an attractive substitute for petroleum-derived products and to mitigate global climate change.[1-3] Lignin is a complex natural macromolecule that composes around 10-30% of plants and it contains chemically functional groups such as benzene rings and hydroxyl groups.[4,5] Owing to these molecular features, lignin can be directly employed in functional polymeric materials or as precursors to produce chemicals, fuels, and carbon materials.[6-9] A recent study that utilized lignin as a photocatalyst for the functionalization of C-H bonds has shown the potential multipurpose uses for lignin.[10]

Kraft lignin is considered the most available and most heterogenous technical lignin.[11] Its complex and recalcitrant molecular structures mainly result from three aspects. First, the lignin molecules in different types of lignocellulosic biomasses have inherent structural variety and heterogeneity.[12] Second, the severe isolation process further alters the lignin chemical structure. During the Kraft pulping process, a strong alkali solution (H_2O, Na_2S, and NaOH) is employed at elevated temperatures (~170 °C) to isolate and dissolve lignin from the cell walls of biomass, generating black liquor containing Kraft lignin.[13] As such, most Kraft lignin is in an irregular ionized form in the strong alkali black liquor.[14] Third, the complicated recovery process of Kraft lignin can further affect the structure. So far, the major recovery techniques for Kraft lignin are based on acid precipitation, in which the ionized lignin molecules are protonated and precipitated by carbon dioxide and diluted sulfuric acid.[15-17] During the precipitation process, polymerization reactions between the lignin molecules appear to be triggered by acid, aggravating the structural disorder of Kraft lignin molecules.[18] As a result, it is almost impossible to control and even predict the molecular properties of Kraft lignin.

However, it is crucial to control the molecular properties of the technical lignin to meet the requirements of applications. Generally, the molecular weight, polydispersity, and hydroxyl groups are important molecular properties of lignin. These properties were believed to affect the processability and performance of materials when lignin was used as the precursor. For example, the irregular variances in molecular weight and polydispersity of lignin lead to the difficulty of determining a standard processing route for lignin-based carbon fibers and their relatively weaker mechanical properties compared to petroleum-based carbon fibers.[19] Moreover, while lignin was used as a raw material to synthesize chemicals, the categories and quantity of hydroxyl groups may influence the chemical reactivity of lignin and thus determine the modification strategies that can be used such as oxidation, reduction, or grafting. For instance, Alireza and co-workers studied improving the yield of aromatics by modifying the aliphatic hydroxyl groups in lignin molecules by formic acid under the reductive catalysis.[20] Additionally, if there is an effective method of regulating those molecular properties, the relationship between the molecular properties and other physiochemical properties of lignin, such as thermal behaviors and solubility in solvents, can be better understood.[21,22]

So far, fractionation is the major strategy to obtain lignin with improved molecular uniformity, using methods such as sequential pH adjustment, solvents extraction, and ultrafiltration methods.[23,24] These fractionation methods enable the lignin fractions with unique molecular weight, polydispersity, and hydroxyl groups to be separated from one feedstock (black liquor or lignin). The sequential pH adjustment method usually involves the addition of acid to sequentially decrease the pH of black liquor and precipitate different lignin fractions. For example, Marina and co-workers used sulfuric acid to lower the pH of

softwood black liquor to 10.5, 5, and 2.5 successively, and the corresponding precipitated lignin products showed variable molecular weight and dispersity values.[25] The solvent extraction methods are based on the variable solubility of different lignin fractions in solvents. A system comprised of multiple solvents and/or a mixture of solvents but with different mixing ratios was frequently proposed to dissolve the lignin fractions from one isolated lignin feedstock. For instance, Shin's group employed five types of solvents, including ethyl acetate, 2-butanone, methanol, acetone, and a mixture of dioxane and water, to separate five fractions from milled wood lignin and organosolv lignin, respectively.[26] The molecular weight, dispersity, and hydroxyl numbers were found to vary among the five lignin fractions. In contrast, ultrafiltration is a state-of-the-art technology that relies on a series of membranes with a sequential decrease in molecular weight cutoff to fractionate the lignin. The membranes are commonly made of ceramic (e.g., TiO_2 and ZrO_2) or polymeric (e.g., cellulose and polyethersulfone) materials.[14] However, five technical issues prevent these fractionation methods from large-scale applications: (1) a low yield of target lignin fractions due to their limited amount in one feedstock; (2) operation complexity in the pH controlling and solvent extraction processes; (3) high solvent consumption in the solvent extraction methods; (4) a short lifespan of ultrafiltration membrane techniques; (5) poor tunability and predictability of the resulting lignin molecular properties.

More recently, our group reported an acid-catalyzed one-pot liquefaction technique that can produce Kraft lignin with improved molecular homogeneity directly from the Kraft black liquor, with subcritical methanol and acetic acid as the recovery solvent.[27] This liquefaction technique shows potential in overcoming the 1st-4th technical issues of the fractionation methods. Here we aimed to further explore if it is possible to control and

predict the yield and molecular characteristics of the resulting Kraft lignin by altering the liquefaction parameters including pH, reaction temperature, and reaction time. To achieve this goal, an experimental design was conducted based on the Box-Behnken response surface methodology (RSM). Then, the effect of the liquefaction parameters on the yield, molecular weight, polydispersity (PDI), and hydroxyl group categories and content of the resulting Kraft lignin was systematically studied. According to the relations between the liquefaction parameters and lignin properties, several computational models were subsequently developed and optimized to show the predictability of the investigated lignin properties. This study is expected to provide a new insight into the effective manipulation of the lignin properties.

3.3 Experimental Section

3.3.1 Materials

The Kraft black liquor (mixed hardwoods) used in this study was provided by Verso Corporation (Quinnesec, MI, USA), and the compositional information of black liquor has been reported by a previous study.[18] To avoid the effect of water on the liquefaction process, a two-stage drying process was conducted to remove water from the liquid black liquor before the liquefaction process. First, the black liquor was dried in an oven (Programmable Oven 838F, Fisher Scientific, USA) at 80 ℃ for 8 h, followed by vacuum drying (Models 89508-426, VWR, USA) at 50 ℃ for 24 h. The ash content of the solid derived from black liquor (SDBL) was determined as 47% using the thermogravimetric method which will be described later. Other chemical information involved in this study was provided in Table A1 (Appendix).

3.3.2 Acid-catalyzed One-pot Liquefaction Process

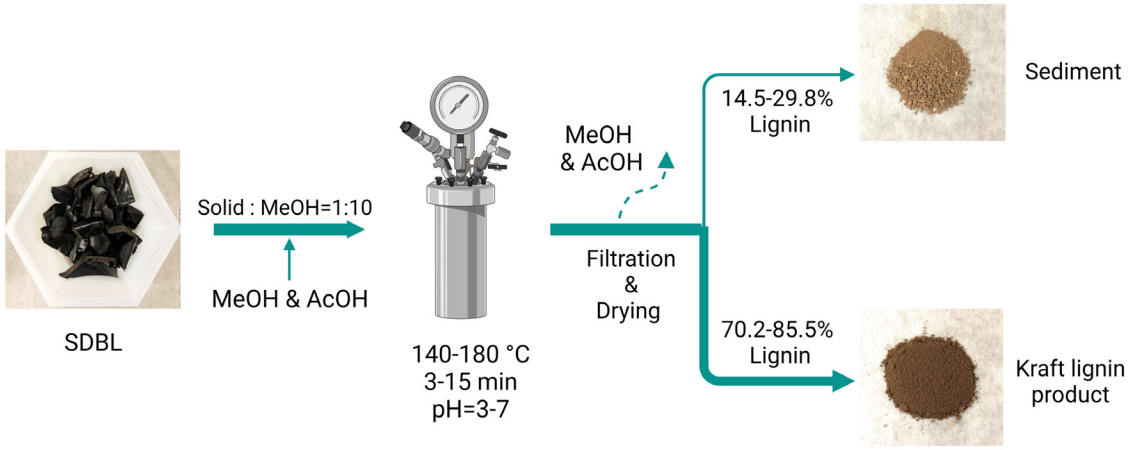

Scheme 3.1 The technical pathway from the solid derived from black liquor (SDBL) to Kraft lignin products. Reprinted (Adapted or Reprinted in part) with permission from [Created with BioRender.com]. Copyright [2022] [BioRender].

The details of the liquefaction process have been reported in our previous study.[27] In a typical experiment (Scheme 3.1), the solid derived from black liquor (SDBL) was mixed with methanol (MeOH) in a (1:10) mass ratio of SDBL: MeOH. The pH of the mixture was then adjusted by adding acetic acid. After that, the liquefaction processes on the mixtures were performed in a 300 ml Parr pressure reactor (Model No: 4560, Parr Instrument Company, USA). During the liquefaction process, the mixture was heated from room temperature to a target temperature (140-180 ℃) and then maintained at the temperature for a certain duration (3-15 min). At the end of the constant temperature stage, the reactor was cooled by removing the heater and passing cooling water through an internal coil. The mechanical stirring was kept on during the entire liquefaction process and cooling process. Subsequently, each sample was filtrated to separate the sediment and

the supernatant. The solvent in the supernatant was then removed by the two-stage drying process, generating the Kraft lignin products. In the view of sustainability, we recommend that the solvent should be recycled in the large-scale production of Kraft lignin, and it will consume less energy than recycling water due to the lower boiling point of methanol than that of water.

3.3.3 Determination of Lignin Yield

The yield of lignin after the liquefaction process was defined as below:

$$Yield(\%) = \left[1 - \frac{M_s \times (1 - AC_s)}{M_{SDBL} \times (1 - AC_{SDBL})}\right] \times 100 \qquad (1)$$

Where M_s refers to the mass of dry sediment, and the AC_s is the ash content of dry sediment; The M_{SDBL} represents the mass of dry solid derived from black liquor (SDBL); AC_{BL} is the ash content of dry solid derived from black liquor (SDBL). According to the previous study, the amount of carbohydrate in both black liquor and the sediments was ignored in the calculation as insignificant.[18]

The ash content of the dry samples was measured using a thermogravimetric analyzer (TGA, Model Q500, TA Instruments, USA). Briefly, the samples (~5 mg per sample) were heated from room temperature to 800 ℃ with a heating rate of 10 ℃·min^{-1} under airflow of 75 mL·min^{-1}. The samples were then cooled to room temperature under the same airflow. The ash content (AC) was calculated based on the following equation:

$$AC\ (\%) = \frac{M_r}{M_o} \times 100 \qquad (2)$$

Where M_r refers to the mass of residue solid after the heating process, and M_o is the original mass of the lignin sample. There were three replications of TGA tests to determine the average ash content of the samples.

3.3.4 Characterization of Lignin Molecular Weight

The number average (M_n) and weight average (M_w) molecular weights of the lignin samples were determined by a gel permeation chromatography (GPC) system (Waters e2695 Separation Module, Waters Corporation, USA) equipped with a refractive index detector and three 300 mm×7.8 mm columns including 1-Styragel HR 4, 2-Styragel HR 3, and 3-Ultrastyragel. Tetrahydrofuran (THF) was used as the mobile phase in the GPC system, and its flow rate was 1 mL·min^{-1}. Monodisperse polystyrene (162, 370, 580, 945, 1440, 1920, 3090, 4730, 6320, 9590, 10,400, and 16,200 Da) was used as calibration standards. The preparation and characterization processes were conducted according to a previous report.[28] The polydispersity (PDI) was used to reflect the molecular weight distribution of lignin molecules, which was defined using the following equation:[29]

$$PDI = \frac{M_w}{M_n} \quad (3)$$

3.3.5 Characterization for the Hydroxyl Groups of Lignin

The types and concentrations of hydroxyl groups in the lignin samples were determined by one-dimensional ^{31}P NMR (UNITY-INOVA 400 MHz, Varian, USA). The preparation procedures of lignin NMR samples followed a previous report.[30] Notably, endo-N-hydroxy-5-norbornene-2,3-dicarboximide (NHND) was used as the internal standard. Chromium acetylacetonate and 2-chloro-4,4,5,5-tetramethyl-1,3,2-dioxaphos-pholane (TMDP) were used as the relaxation and phosphating reagents respectively for the lignin

samples. The ^{31}P NMR spectra of phosphitylated lignin were obtained using an acquisition time of 1 s, a recycle delay time of 10 s, and 512 times scans. All the data were further treated using the MestReNova software. In the ^{31}P NMR spectra, the chemical shifts of the aliphatic and phenolic hydroxyl groups (-OHs) in the Kraft lignin respectively are: ~145.4-150.0 p.p.m (aliphatic -OH), ~140.0-144.5 p.p.m (C_5 substituted -OH), ~139.0-140.2 p.p.m (Guaiacyl -OH), and ~137.8 p.p.m (p-Hydroxyphenyl -OH).

3.3.6 Experimental Design and Computational Prediction

As shown in Scheme 3.2, the processing parameters for the acid-catalyzed one-pot liquefaction process included pH (3-7), reaction temperature (140-180 ℃), and reaction time (3-15 min). The Box-Behnken response surface method (RSM) was used for the experimental design in Minitab software. The details of the 15 experiments with different levels of variables were listed in Table A2.

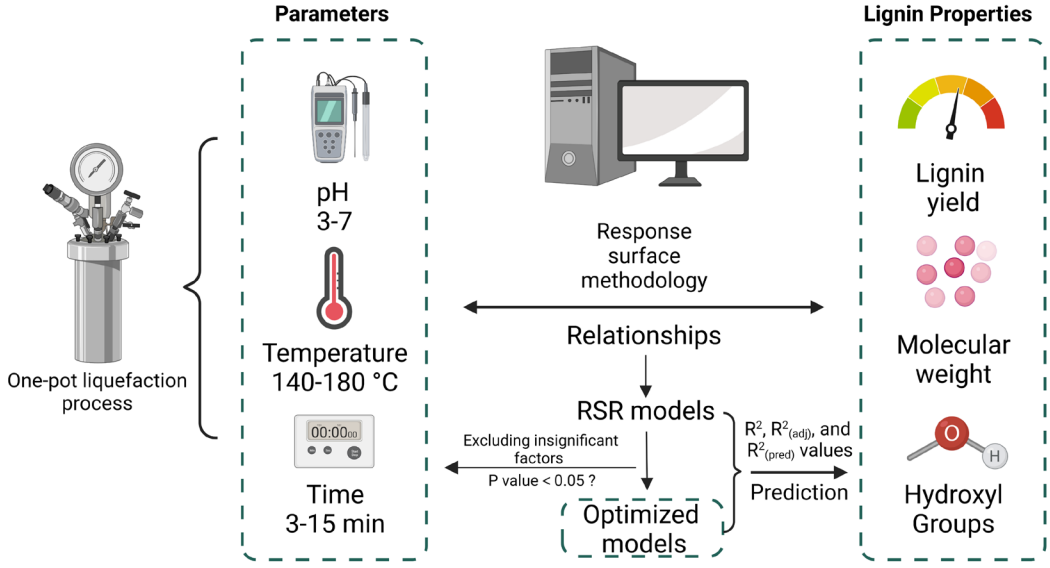

Scheme 3.2 The experimental design and computational prediction strategies. Reprinted (Adapted or Reprinted in part) with permission from [Created with BioRender.com]. Copyright [2022] [BioRender].

The experimental results, including the yield, number average molecular weight (Mn), weight average molecular weight (Mw), polydispersity (PDI), and hydroxyl group numbers of Kraft lignin, were statistically analyzed based on the Box-Behnken RSM. More specifically, full quadratic response surface regression (RSR) models were used first to identify the significant factors of the Kraft lignin properties using a significant level of 0.05 ($\alpha = 0.05$). The full quadratic RSR models were composed of linear terms (pH, temperature, and time), interaction terms (pH×temperature, pH×time, and temperature×time), and quadratic terms (pH×pH, temperature×temperature, and time×time). Then, the R^2, $R^2_{(adj)}$, and $R^2_{(pred)}$ values were utilized to evaluate the goodness of fit and predictability of the computational models in terms of the Kraft lignin's properties, with values closer to 100% indicating better goodness of fit and predictability of the models.[31,32] To increase the predictability, some of the RSR models were further optimized by excluding insignificant factors, generating optimized linear, linear + quadratic, or linear + squares models.

In addition, three polynomial models were used to fit the experimental data points of Mn versus Mw, PDI versus Mw, and PDI versus Mn to show the relationship among those molecular weight properties of the Kraft lignin. To further verify those relationships, the simulated Mn and Mw values were generated respectively by the optimized models that could predict those molecular parameters of Kraft lignin based on the liquefaction parameters. Then, the simulated PDI values were calculated based on Equation (3). A total

of 105 data points were generated by each model in which the pH values ranged from 3 to 7 with an increment interval of 0.2 and the temperatures in the range of 140-180 ℃ with an increment interval of 20 ℃. Subsequently, three polynomial models were also developed by fitting the simulated data points and made comparisons with those polynomial models based on the experimental results. The goodness of fit and predictability of the polynomial models were evaluated by the R^2, $R^2_{(adj)}$, and $R^2_{(pred)}$ values as well.

3.4 Results and Discussions

3.4.1 Lignin Yield

As shown in Figure 3.1, the yield of lignin varied in the range of 70.2-85.5%. The highest lignin yield value (85.5%) existed in the T-1 sample (pH=3, 160 ℃, and 3 min), while the lowest lignin yield (70.2%) occurred in the T-7 sample (pH=7, 140 ℃, and 9 min). Besides that, the lignin yield over 80% was also achieved by T-3, T-5, and T-13 samples, all of which had pH = 3. The results suggested that adjusting the liquefaction parameters could alter the yield of Kraft lignin.

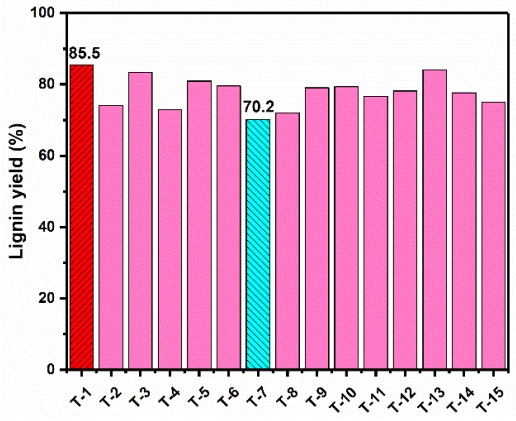

Figure 3.1 Lignin yield of the liquefaction processes based on the Box-Behnken RSM. (The highest and the lowest lignin yields were marked.)

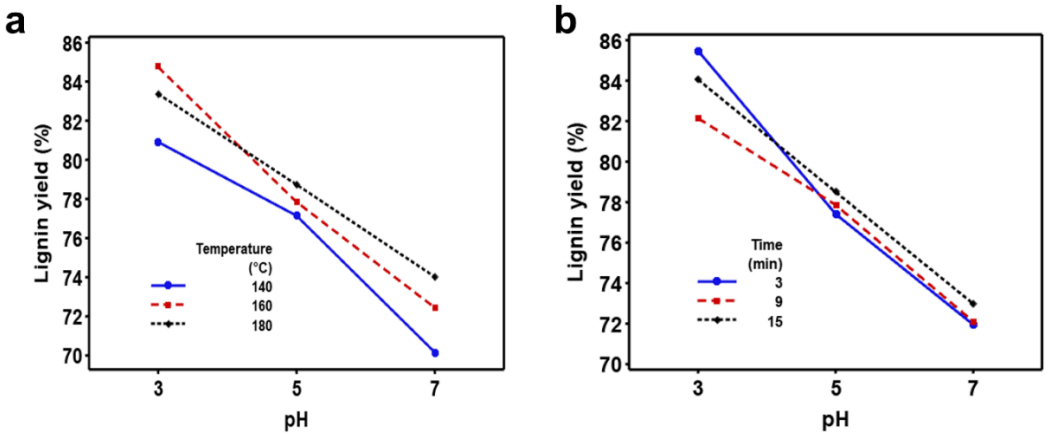

Figure 3.2 (a) The interaction plot of mean lignin yields (%) with the factors of pH and temperature; (b) The interaction plot of mean lignin yields (%) with the factors of pH and time.

To further disclose the effect of liquefaction parameters on the lignin yield, the experimental results were fitted with an RSR model, which is shown in Model A.1 (Supporting Information). For this RSR model, only the pH was the significant factor in lignin yield because of its statistically significant P-value < 0.001, and the interactive effects of the liquefaction parameters on the lignin yield were not statistically significant (P-value > 0.5) (Table A5). Moreover, the Pareto chart (Figure A.1, Appendix) further demonstrated that the pH was the major contributor to the lignin yield, and pH had a negative effect on the lignin yield due to the negative coefficient (Table A3). To more intuitively determine how the liquefaction parameters affect the lignin yield, interaction plots are shown in Figure 3.2. It was observed that the lignin yield decreased by

approximately 10% with the increase in pH values from 3 to 7 regardless of the reaction temperature and time, which further indicated the negative effect of pH on the lignin yield. At the same pH value, the variation of lignin yield was roughly in 5% when changing the reaction temperature and time, indicating that their influence on the lignin yield was less than that of the pH. Moreover, the intersections occurred among the lines, which implies the interactive effect of the liquefaction parameters on the lignin yield. However, such interactions were not statistically significant (P-value > 0.5) according to the analysis of variance (Table A5).

Such results seem to be contradictory to the common knowledge that lower pH precipitates rather than dissolves Kraft lignin in black liquor.[18] These differences may be explained by the organic acid used in this study. The conventional acid precipitation methods usually employ inorganic acid, such as sulfuric acid and CO_2 aqueous solution, to provide hydrogen ions for the protonation of lignin ionizes in alkaline black liquor. Then, the protonated lignin molecules may be drawn together due to the hydrogen bonding or may react with each other by acid-catalyzed polymerization reactions, leading to the precipitation of lignin molecules from the alkaline black liquor. In traditional lignin precipitation processes, decreasing the pH is able to provide more hydrogen ions for the protonation of lignin and the catalytic reactions, accelerating the precipitation of lignin macromolecules.[18] In contrast, acetic acid used in this study worked as a solvent for the lignin molecules in addition to as a donor of hydrogen ions.[33] Specifically, decreasing the pH of black liquor using acetic acid enabled more ionized lignin molecules to be neutralized and dissolved.

One of the objectives of this study was to predict the lignin yield using computational models. For the full quadratic RSR model of lignin yield, it showed great goodness-of-fit of experimental lignin yield results, which was indicated by the high R^2 (94.01%) and $R^2_{(adj)}$ (83.22%) values, but its predictive ability to the lignin yield was relatively weaker because of the lower $R^2_{(pred)}$ value (64.34%) (Table A4). The variance analysis results of the RSR model implied that a linear model may be more suitable to predict the lignin yield more precisely since the P-value of linear term was less than 0.05 (Table A.5). Two linear models were further developed by excluding the insignificant terms (Model A.2 and A.3). It was found that as compared to the RSR model, the R^2 values of the linear models declined, but their $R^2_{(adj)}$ and $R^2_{(pred)}$ values were increased, indicating that the RSR model was over-fitted (Table A.4, A.7, and A.10). Moreover, the linear model A.3 composed of pH and temperature exhibited the highest value (87.83%) of $R^2_{(pred)}$ among those models, indicating its superior prediction ability to the lignin yield compared to other models (Table A4, A7, and A10). For the linear models, the pH was still the major contributor to the lignin yield (Figure A.2 and A.3), and the temperature started to show a statistically significant positive effect on the lignin yield because of its P-value < 0.05 and coefficient = 1.195 (Table A6, A8, A9, and A11), which was not shown in the RSR model. Additionally, the pH showed a statistically significant negative effect (P-value < 0.001, coefficient = -5.595) on the lignin yield (Table A6, A8, A9, and A11). The reaction time was not a statistically significant variable (P-value = 0.66) for lignin yield.

To further exhibit the predictive behaviors of the models for lignin yield, scatter plots of actual and predicted lignin yield (%) are described in Figure 3.3. In each scatter plot, most of the data points were distributed around or fell in the diagonal (y = x), and the slight

differences of the data points distribution mainly occurred in the lignin yield of 70-74% and 83-85%. More specifically, after excluding the insignificant factors, the linear model A.2 and A.3 appeared to perform slightly better in the lignin yield of 70-74% but slightly worse in that of 83-85% compared to the RSR model. Beyond that, the linear models were obviously simpler than the RSR model, making them more feasible in practical prediction.

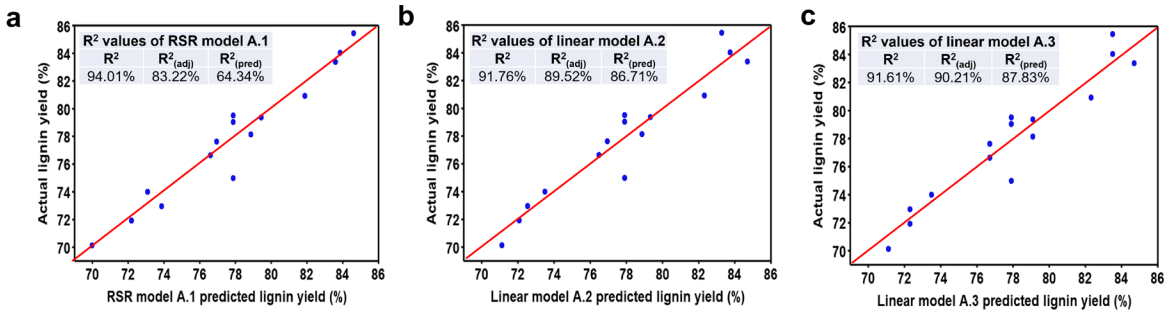

Figure 3.3 The scatter plots of actual lignin yield (%) versus different models predicted lignin yield (%).

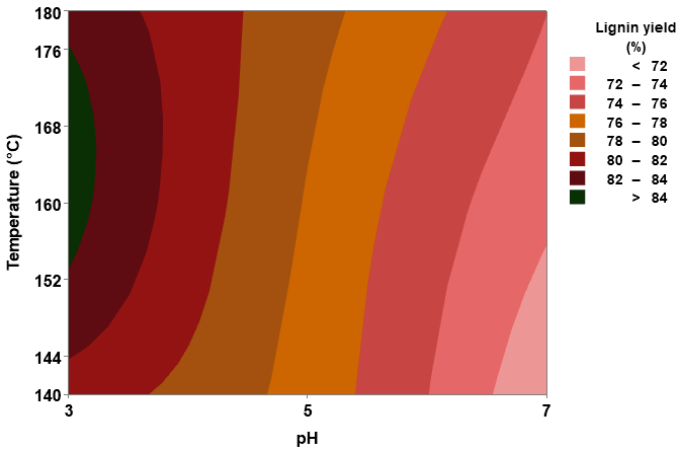

Figure 3.4 The contour plot of lignin yield versus liquefaction temperature and pH.

A contour map based on the model A.3 with the highest $R^2_{(pred)}$ value was plotted in Figure 3.4 to describe the optimized range of liquefaction temperature and pH toward the lignin yield more intuitively. The results indicated that high lignin yield (> 84%) can be achieved with the pH being approximately 3 and the temperature in the range of 155-175 ℃. As for the liquefaction time, its effect on the lignin yield appeared to be insignificant in both RSR and linear models, indicating that the shorter liquefaction time can be used for faster processing in the investigated range (3-15 min).

3.4.2 Molecular Weight and PDI of Kraft Lignin

The number average (Mn) and weight average (Mw) molecular weight values of the Kraft lignin are shown in Figure 3.5. The Mn value of the lignin from different tests was variable from 914 Da to 1351 Da (Figure 3.5a), and the Mw value of the lignin from different tests varied in the range of 1627~3189 Da (Figure 3.5b), indicating that adjusting the parameters of liquefaction processes could control the molecular weight of Kraft lignin. The lowest Mn (914 Da) and Mw (1627 Da) values were found in the T-2 sample (pH =7, 180 ℃, and 9 min), while the highest Mn (1351 Da) and Mw (3189 Da) occurred in T-11 sample (pH=5, 140 ℃, and 3 min) and T-13 sample (pH=3, 160 ℃, and 15 min), respectively (Figure 3.5a and b). Such Mw values were lower than that of the acid precipitated lignin (15000~77000 Da) reported by a previous study that employed the same black liquor source.[18] The difference can be explained by that the repolymerization reactions in traditional acid precipitation processes can be significantly reduced in the liquefaction process due to the existence of subcritical methanol.[18, 27] The relatively lower molecular weight range of the lignin is considered beneficial to its applications, such as in flexible polymer materials.[34] The PDI values of the Kraft lignin, shown in Figure 3.5c, varied in the range of 1.78-2.56,

suggesting that the molecular weight distribution of the Kraft lignin could be controlled by adjusting the parameters of the liquefaction process. The lowest PDI value (1.78) was obtained in the T-2 sample whose Mn and Mw values were the lowest as well, while the T-3 sample (pH=3, 180 °C, and 9 min) had the highest PDI value of 2.56 (Figure 3.5c). Most of those PDI values were lower than that of the Kraft lignin from acid precipitation processes (PDI = 2.2~5.4),[18] indicating that the uniformity of Kraft lignin molecules in this study was greater than that of the acid-precipitated Kraft lignin. The improved molecular homogeneity is preferred when using Kraft lignin in synthesis and preparation of high-value lignin-based products.[9, 14]

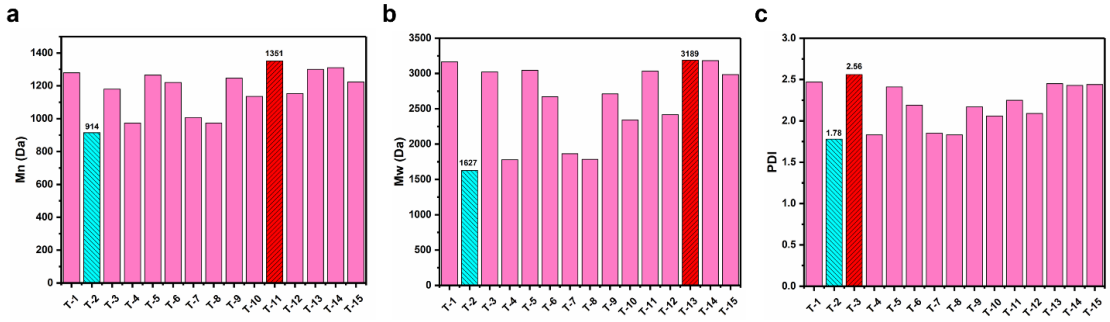

Figure 3.5 (a) Number average molecular weight (Mn), (b) weight average molecular weight (Mw), and (c) polydispersity (PDI) values of Kraft lignin obtained from the liquefaction processes based on the Box-Behnken RSM. (The highest and the lowest values were marked.)

To further understand the effect of the liquefaction parameters on the molecular weight properties of the Kraft lignin, three full quadratic RSR models were established to fit the experimental Mn, Mw, and PDI results (Model A.4, A.6, and A.8 respectively). In the RSR model A.4 of Mn, two linear terms (pH and temperature) and one square term (pH×pH)

were statistically significant factors (P-value < 0.05) (Table A.14). In the Pareto chart (Figure A.4), the contribution sequence of those significant factors to the Mn value of Kraft lignin was pH > pH×pH > temperature. The negative coefficient values (Table A.12) implies that those significant factors negatively affected the Mn values of the Kraft lignin. For the RSR model A.6 of Mw, the linear terms of pH and temperature, as well as the square term of pH×pH also had significantly influence on the Mw value of Kraft lignin (P < 0.05) (Table A.20). Meanwhile, the sequence of the contribution of those terms to the lignin's Mw values was the same as that to the Mn values (pH > pH×pH > temperature) (Figure A.6), and their coefficient values were negative as well (Table A.18), suggesting the negative effects of pH, temperature, and pH×pH on the Kraft lignin's Mw values. As for the RSR model A.8 of PDI, only the pH was found to be a statistically significant factor (P-value = 0.001) (Table A.26), and its coefficient value was negative (Table A.24), suggesting that the PDI value of the Kraft lignin was negatively affected by the pH.

Figure 3.6 shows the interaction plots of the effect of liquefaction parameters on the molecular properties of Kraft lignin. The Mn, Mw, and PDI values of the Kraft lignin tended to decline with increasing pH values. At the same pH value, the reaction temperature has more influence than the reaction time on the molecular features of the Kraft lignin. Higher reaction temperatures resulted in lower Mn, Mw, and PDI values of the Kraft lignin at pH = 5 and 7, but no obvious trend in the changes of the same molecular parameters was observed at pH = 3 as shown in Figure 3.6 a-c. However, such interactive effects of pH and reaction temperature on the molecular properties were statistically insignificant according to the analysis of variance (Table A.14, A.20, and A.26).

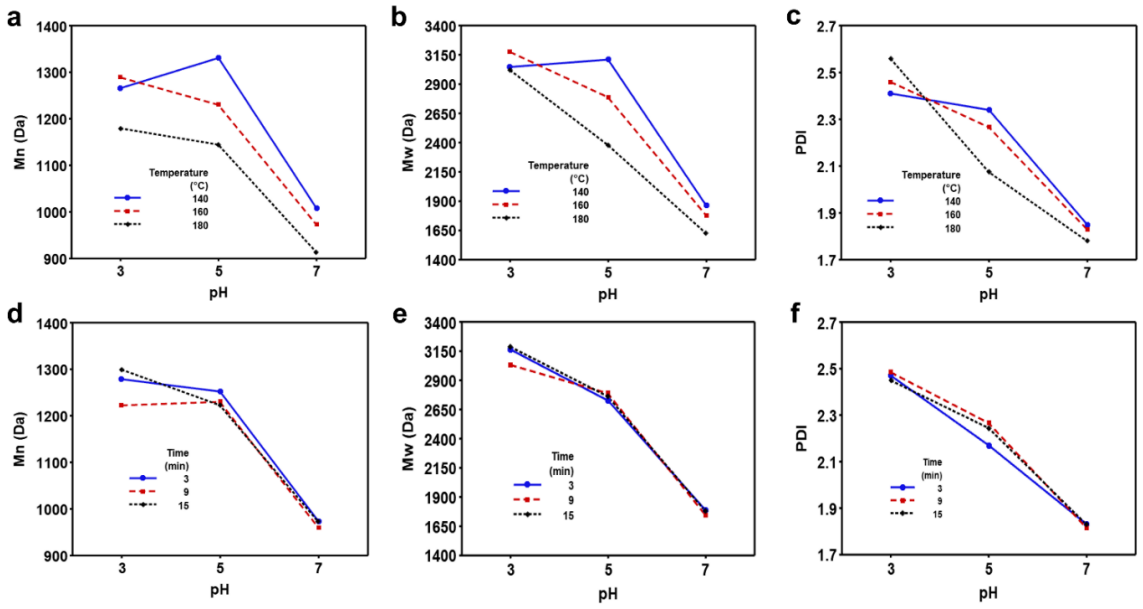

Figure 3.6 The interaction plot of (a) mean number average molecular weight (Mn), (b) mean weight average molecular weight (Mw), and (c) mean polydispersity (PDI) of the Kraft lignin with the pH and temperature; The interaction plot of (d) mean number average molecular weight (Mn), (e) mean weight average molecular weight (Mw), and (f) mean polydispersity (PDI) of the Kraft lignin with the pH and time.

The negative effects of pH on the Mn, Mw, and PDI values of the Kraft lignin can be attributed to fewer hydrogen ions available for the polymerization of the lignin molecules with increasing pH values. Consequently, the repolymerization reactions among the lignin molecules catalyzed by the acid could be reduced, leading to lower molecular weight values and greater molecular uniformity of the Kraft lignin. As for the negative effect of reaction temperature on the Mn and Mw values of the Kraft lignin, it could be explained by that higher temperatures could be beneficial for the alcoholysis reaction of lignin molecules in the presence of acid and result in a lower lignin molecular weight.[35] More

specifically, as the liquefaction temperature was higher, more heat was provided for activating the lignin and methanol molecules, accelerating inter-molecule collisions. Such collisions may cleave a greater amount of ether linkages, such as β-O-4 and 4-O-5 linkages, in lignin macromolecules and then form more small lignin molecules. Those demonstrations also implied that the polymerization and depolymerization reactions of the Kraft lignin molecules could be simultaneously controlled by adjusting the pH and reaction temperature of the liquefaction processes.

To show the goodness-of-fit and predictive ability of the computational models for the molecular weight features of the Kraft lignin, the R^2, $R^2_{(adj)}$, and $R^2_{(pred)}$ values were generated. For the full quadratic RSR models of Mn, Mw, and PDI values of the lignin, they displayed great goodness-of-fit with all the R^2 values greater than 90% but low predictability with low $R^2_{(pred)}$ values of 59.60%, 33.75%, and 10.58%, respectively (Table A.13, A.19, and A.25). To obtain higher predictability of the molecular properties of Kraft lignin, the RSR models of the Mn and Mw were fine tuned to model A.5 and model A.7, respectively, in which the pH, reaction temperature, and pH×pH were included as they were statistically significant in the RSR models. Consequently, the $R^2_{(pred)}$ values of model A.5 and model A.7 were increased to 91.54% and 87.51%, respectively (Table A.16 and A.22), implying that these models were able to predict the Mn and Mw values of Kraft lignin better than the original RSR models. Nevertheless, as shown in the Pareto charts (Figure A.5 and A.7), the contribution sequence of those variables in model A.5 and model A.7 was the same as the RSR models (pH > pH×pH > temperature). Moreover, model A.9 was developed based on the pH since it was the only significant factor in the RSR model of the PDI values of the Kraft lignin (Table A.26). Compared to the RSR model, a higher

$R^2_{(pred)}$ value of 78.81% was obtained by model A.9 (Table A.25 and A.28), indicating a better prediction for the molecular polydispersity of the Kraft lignin.

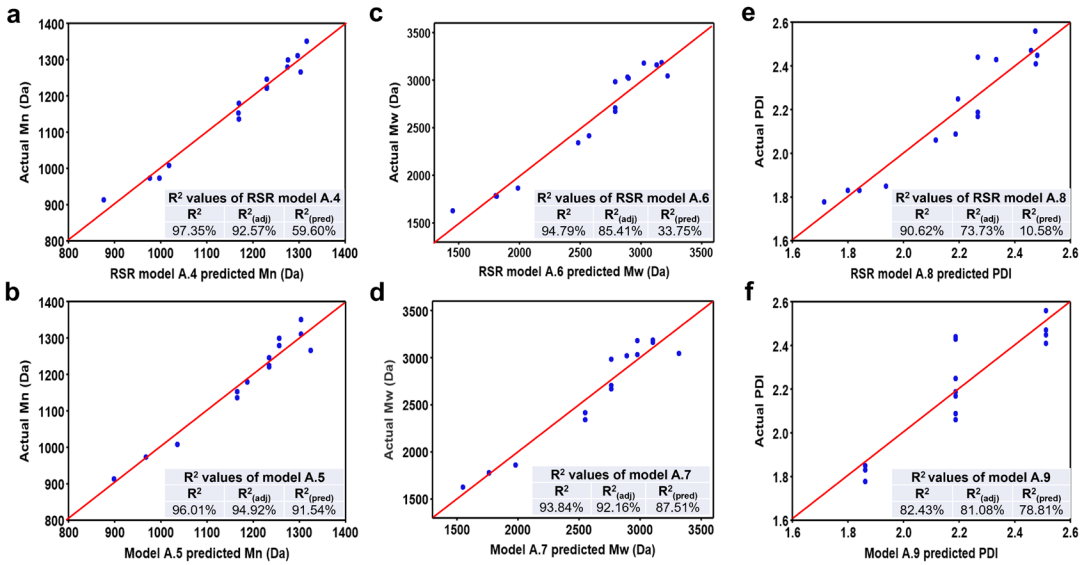

Figure 3.7 The scatter plots of (a) actual Mn versus RSR model A.4 predicted Mn, (b) actual Mn versus model A.5 predicted Mn, (c) actual Mw versus RSR model A.6 predicted Mw, (d) actual Mw versus model A.7 predicted Mw, (e) actual PDI versus RSR model A.8 predicted PDI, and (f) actual PDI versus model A.9 predicted PDI.

To compare the predictive behaviors of the models for the Mn, Mw, and PDI of the Kraft lignin, the scatter plots were shown in Figure 3.7. As for the Mn, most data points were distributed close to or fell in the diagonal (y = x), but their positions were slightly changed when comparing Figure 3.7 a and b, implying the different predictive behaviors of RSR model A.4 and model A.5. More specifically, after removing the insignificant terms, model A.5 performed better in predicting the lower Mn values (900-1000 Da) but worse in predicting the higher Mn values (1200-1300 Da) compared to RSR model A.4.

Furthermore, the distribution of Mw data points was looser than that of Mn data points (Figure 3.7a-d), suggesting that the predictability of Mw was relatively lower than that of Mn as in agreement with their $R^2_{(pred)}$ values (Table A.13 vs. Table A.19 and Table A.16 vs. Table A.22). Similarly, the model A.7 without insignificant factors was more advantageous for the prediction of Mw at lower values (1500-2000 Da) but less advantageous for that at higher values (~3000 Da) in comparison to RSR model A.6 (Figure 3.7c and d). For the PDI, the data points were distributed around or fell in the diagonal (y = x) (Figure 3.7e), while the data points in Figure 3.7f were arranged in three columns. This predictive behavior distinction was caused by the different number of terms in RSR model A.8 and model A.9. Although the model A.9 had a higher $R^2_{(pred)}$ value relative to RSR model A.8 (Table A.25 and A.28), it only generated three PDI values to represent all the actual PDI values, which is not appropriate in practice. A more feasible method of generating the PDI values will be directly using the simulated Mw and Mn values in the calculations of Equation 3.

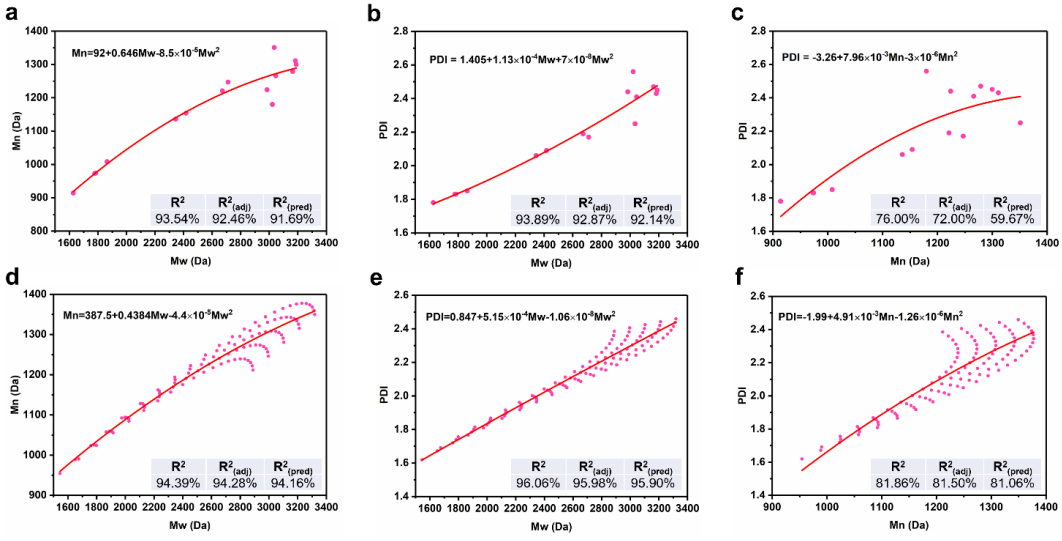

Figure 3.8 The correlation plots of experimental (a) Mn versus Mw, (b) PDI versus Mw, and (c) PDI versus Mn; The correlation plots of simulated (d) Mn versus Mw, (e) PDI versus Mw, and (f) PDI versus Mn.

Additionally, three polynomial models were developed to fit the three experimental data sets of Mn versus Mw, PDI versus Mw, and PDI versus Mn (Figure 3.8a-c). In the polynomial models of Mn versus Mw and PDI versus Mw, both goodness-of-fit and predictability were performed very well since their R^2, $R^2_{(adj)}$, and $R^2_{(pred)}$ values were greater than 90% (Figure 3.8a and b). In contrast, relatively lower R^2, $R^2_{(adj)}$, and $R^2_{(pred)}$ values of the polynomial model of PDI versus Mn indicated its weaker goodness-of-fit and predictability (Figure 3.8c). These results implied that the Mw value of the Kraft lignin could be employed to predict its Mn and PDI values and vice versa. Moreover, the positive relationship between the Mn values and the Mw values of the Kraft lignin was significant (Table A.30 and A.32). Additionally, there was a statistically significant positive correlation between the PDI values and the Mw values of the lignin with a constant coefficient of 1.405 (Table A.33 and A.35). These results indicated that adjusting the liquefaction parameters was able to effectively control the molecular weight while maintaining the molecular homogeneity of Kraft lignin, which has not been reported previously and is very beneficial to its down-stream applications.[23]

To confirm the relationships demonstrated above, we simulated the Mn and Mw values of the Kraft lignin using the model A.5 and A.7 respectively, and the PDI values of the Kraft lignin were calculated based on Equation 3 using the simulated Mn and Mw values. The simulation processes have been detailed in the experimental section, and the simulated data

were shown in Table A.39-41. Three polynomial models were also developed to fit three simulated data sets of Mn versus Mw, PDI versus Mw, and PDI versus Mn, respectively (Figure 3.8 d-f). Among these models, both goodness-of-fit and predictability were performed very well by the polynomial models of Mn versus Mw and PDI versus Mw (Figure 3.8d and e), while they were relatively poor in the model of PDI versus Mn (Figure 3.8f). Particularly, high $R^2_{(pred)}$ values of 94.16% and 95.90% were found in the polynomial models of Mn versus Mw and PDI versus Mw, respectively, suggesting that the simulated Mw value could be used as a predictor of both simulated Mn and PDI values of the Kraft lignin (Figure 3.8d and e). Such results were highly in agreement with the experimental results discussed earlier, which further implied the strong possibility of predicting the molecular weight parameters of the Kraft lignin by tuning the liquefaction parameters.

3.4.3 The Hydroxyl Groups of Kraft Lignin

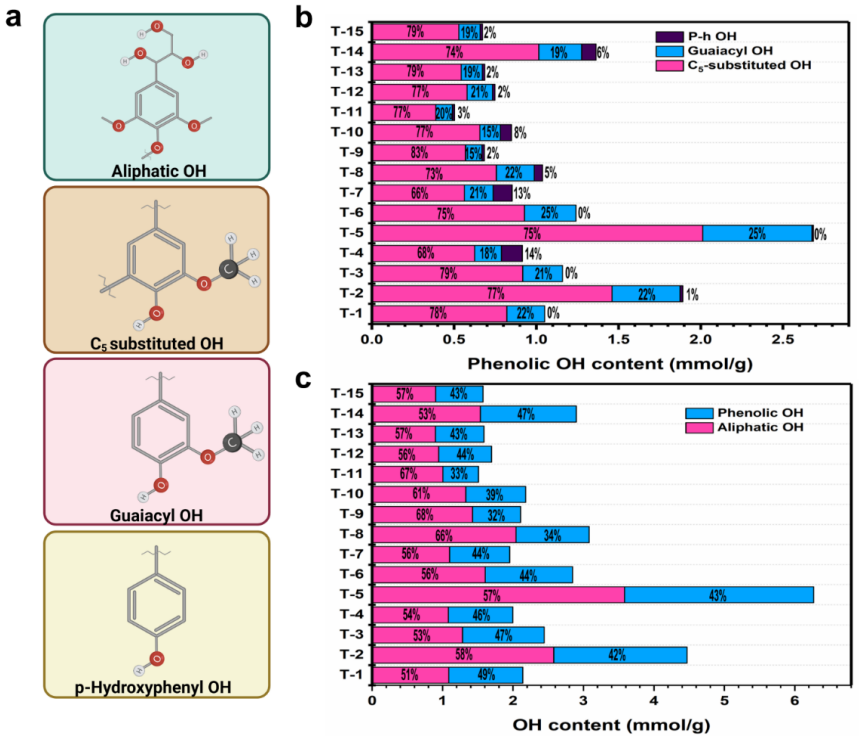

Figure 3.9 (a) The structural models of different types of hydroxyl groups in the lignin; reprinted (adapted or reprinted in part) with permission from [Created with BioRender.com]. Copyright [2022] [BioRender]; (b) The contents of different types of phenolic -OHs in the Kraft lignin; (c) the ratio of total phenolic to aliphatic -OHs content in the Kraft lignin.

In addition to the molecular weight characteristics, the hydroxyl groups (-OHs) are also an important feature of lignin since they determine the chemical reactivity and solubility of lignin in solvents.[36] The aliphatic and phenolic -OHs, which are the major types of hydroxyl groups in the lignin molecules,[37] were investigated using ^{31}P NMR in this study. The typical structural models of aliphatic and phenolic OHs are shown in Figure 3.9a. In the 15 tests, the total amount of phenolic -OHs in the Kraft lignin samples varied from 0.50

mmol/g to 2.68 mmol/g (Figure 3.9b). The minimum value existed in the T-11 sample with the processing parameters of pH=5, 140 ℃, and 3 min, while the maximum value existed in the T-5 sample with the processing parameters of pH=3, 140 ℃, and 9 min (Figure 3.9b). It was found that the C_5-substituted -OHs occupied 66-83% of the phenolic -OH content, while 15-25% and 0-14% of the phenolic -OHs were in the Guaiacyl and p-Hydroxyphenyl (p-H) units respectively (Figure 3.9b). These results indicated that the C_5-substituted -OHs dominated the phenolic -OHs in the Kraft lignin. Moreover, the influence of the liquefaction parameters on the quantity of the phenolic -OHs was studied based on the Box-Behnken response surface methodology (RSM) as well. Only the pH×Temperature, as an interaction term, significantly affected the total amount of phenolic -OHs in the lignin ($P < 0.05$) (Table A.53). Additionally, two full quadratic RSR models were developed for the total amount of phenolic -OHs and the content ratio of the C_5 substituted -OHs to the Guaiacyl -OHs to show the predictive possibility (Model A.16 and A.17). Although the R^2 values of these RSR models achieved 84.16% and 52.9%, respectively, their $R^2_{(pred)}$ values were 0 (Table A.52 and A.55). These results indicated that the RSR models fitted the experimental phenolic -OH contents of the Kraft lignin to some extent, but they were unable to forecast the phenolic -OH contents in the Kraft lignin.

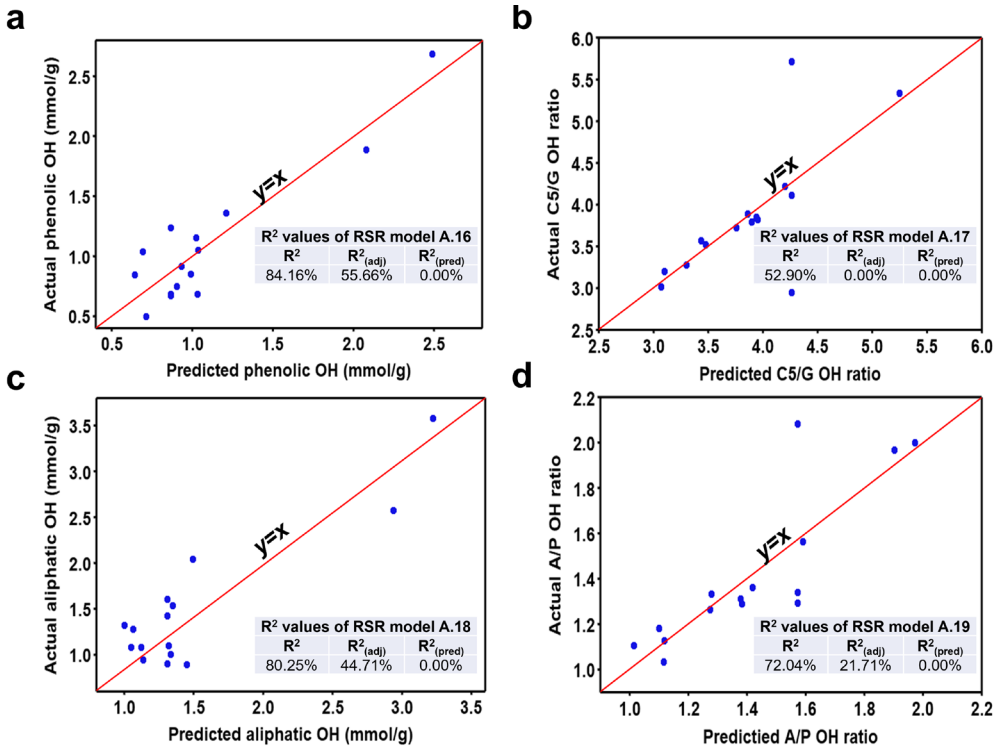

Figure 3.10 (a) Scatter plots of actual versus predicted phenolic -OHs content of the Kraft lignin; (b) scatter plots of actual versus predicted content ratio of C5 substituted -OHs to Guaiacyl -OHs of the Kraft lignin; (c) scatter plots of actual versus predicted aliphatic -OHs content; (d) scatter plots of actual versus predicted content ratio of aliphatic to phenolic -OHs of the Kraft lignin.

In Figure 3.10a, most of the data points were loosely distributed around the diagonal (y = x), further demonstrating the poor capacity of RSR model A.16 for predicting the phenolic -OHs content in the Kraft lignin. In Figure 3.10b, most of the data points were fell in the diagonal (y = x), while two data points were far away from the diagonal, which likely contributed to the poor ability of RSR model A.17 to forecast the content ratio of the C5 substituted -OHs to the Guaiacyl -OHs. The RSR models were not further modified

because no clear modification directions were discovered from the analysis of variances (Table A.53 and A.56).

The aliphatic -OHs contents of the Kraft lignin varied in the range of 0.90-3.58 mmol/g. The minimum and the maximum values were found in T-13 (pH=3, 160 ℃, and 15 min) and T-5 samples (pH=3, 140 ℃, and 9 min), respectively (Figure 3.9c). The pH×Temperature term was the only significant factor ($P < 0.05$) that affected the aliphatic -OHs content in the Kraft lignin molecules (Table A.59). Similarly, the experimental aliphatic -OHs content in the Kraft lignin molecules could be fitted well by the RSR model A.18 as indicated by the R^2 value of 80.25%; nevertheless, this model was overfitted and could not be used to predict the aliphatic -OHs content as the $R^2_{(adj)}$ and $R^2_{(pred)}$ values were 44.71% and 0, respectively (Table A.58). Moreover, for all lignin samples, the aliphatic -OHs content was higher than the phenolic -OHs content (Figure 3.9c). This result suggested a great potential of the Kraft lignin to be used as a polyol system in the synthesis of polyurethanes. Additionally, none of the liquefaction parameters showed significant influences on the ratio of aliphatic -OHs to phenolic -OHs contents ($P > 0.05$) (Table A.62). Similarly, although the established RSR model A.19 could fit those ratio results in some degree ($R^2 = 72.04\%$), it was overfitted and could not be used to forecast the content ratio of the aliphatic -OHs and the phenolic -OHs because the $R^2_{(adj)}$ and $R^2_{(pred)}$ values were 21.71% and 0, respectively (Table A.61). Such low $R^2_{(pred)}$ values of the RSR model A.18 and A.19 were consistent with the loose distributions of the data points around the diagonals ($y = x$) in Figure 3.10c and d. The RSR models were not further improved since no clear improvement directions were obtained from the results of analysis of variances

(Table A.59 and A.62). Those results showed the challenges of estimating the amount of OHs relative to the molecular weight parameters of the Kraft lignin.

3.4.4 Proposed Mechanisms and Outlooks

Why are the Kraft lignin properties controllable and predictable? Overall, we believe that they are associated with the clever use of acetic acid and subcritical methanol. In this study, acetic acid may function as a hydrogen ions donor, solvent, and catalyst for the Kraft lignin, and subcritical methanol plays triple roles of solvent, hydroxylation, and methylation reactants for the Kraft lignin. Four major chemical reactions among the acetic acid, methanol, and Kraft lignin molecules are proposed. First, hydrogen ions are dissociated by a part of acetic acid molecules in methanol, and some of them neutralize the ionized Kraft lignin molecules (Figure 3.11a). Second, hydrogen bonds are formed among the neutralized lignin molecules, methanol, and the non-dissociated acetic acid molecules, generating a stable mixture (Figure 3.11b). Third, some of the hydrogen ions dissociated by the acetic acid molecules may catalyze the polymerization reactions among the lignin molecules (Figure 3.11c). Fourth, under the acidic catalysis, the subcritical methanol molecules could attack and cleave the C-O bonds (eg., β-O-4) in the lignin molecules. Afterward, the methanol molecules will be decomposed into the methyl radicals and -OHs and react with the decomposed lignin molecules, generating hydroxylated and methylated products (Figure 3.11d). To increase the lignin yield, lower pH values and higher temperatures are required because they can accelerate the first, second reactions, and fourth reactions and allow more lignin molecules to be dissolved in the solvents. Regarding the molecular weight properties of the lignin, when the reaction temperature is fixed, increasing pH offers more hydrogen ions (H^+) as the catalyst for the third and fourth

reactions, while the third reaction may occur easier than the fourth reaction, leading to higher molecular weights and PDI values of the lignin; when the pH is fixed, higher temperature could trigger more the fourth reaction than the third reaction, resulting in lower molecular weights of the lignin. Also, the unexpected strong correlations among the molecular weight properties of the Kraft lignin may be associated with the synergistic effect of third and fourth reactions. Thus, making full use of the functions of acetic acid and subcritical methanol is the core of this study. It should be noted that although only Kraft lignin was involved in this study, we believe that the acid-catalyzed one-pot liquefaction method would also work for other lignin sources based on the proposed mechanisms.

This study also inspired that to better understand and even predict the properties of products from complex chemical reaction systems, the effective use of research methodologies and the simple design of the reaction systems are crucial. Response surface methodology (RSM) is a traditional approach that is usually employed to optimize the processing parameters and the relevant product properties. In this study, we did not stop at the optimization processes and continued to refine and simplify the computational models by excluding the insignificant factors, obtaining remarkably improved prediction and feasibility in practice. Recently, machine learning is an emerging method that has been used in predicting the product properties, but it often requires a large amount of data sets, which is time-consuming in data collection.[38, 39] In contrast, our research strategy may have superiority in that aspect. On the other hand, integrating all chemical reactions in one device is beneficial to reducing system uncertainty, enabling the prediction of product properties to be possible.

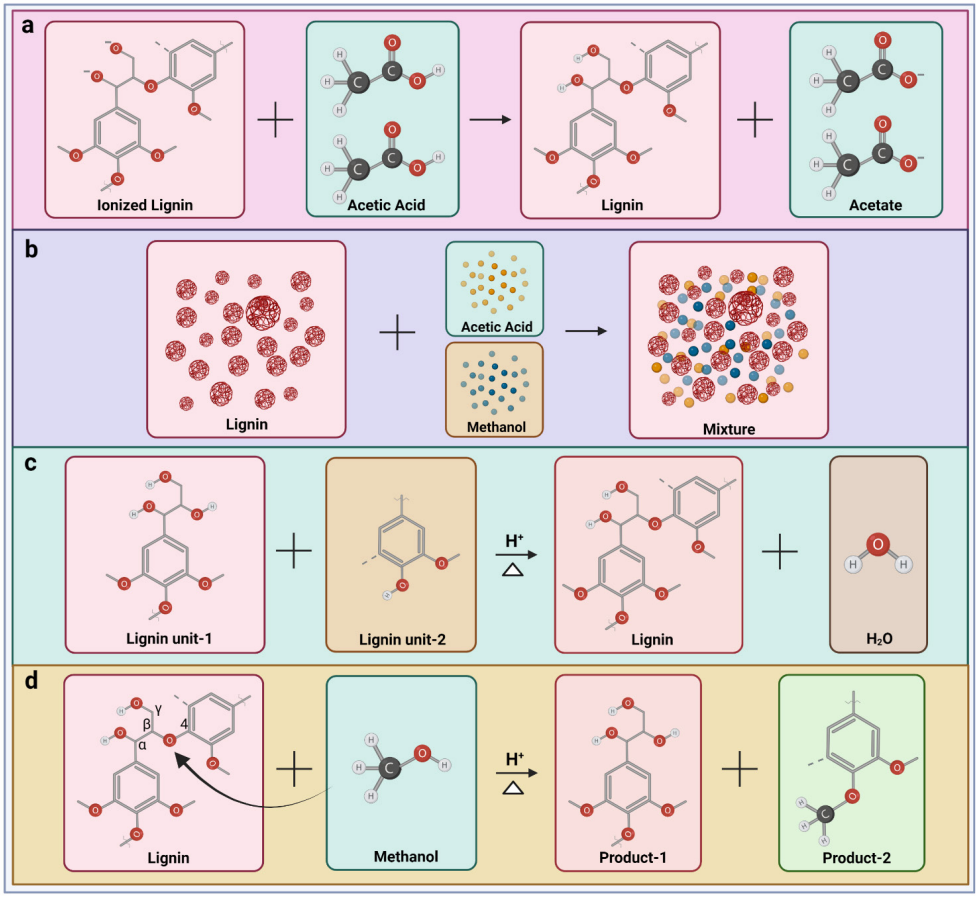

Figure 3.11 (a) The neutralization reactions between ionized lignin and acetic acid; (b) The formation of the stable mixture of lignin, acetic acid, and methanol; (c) The polymerization reactions among the lignin units with acidic catalysis and heating; (d) The reactions between the lignin molecules and subcritical methanol molecules with acidic catalysis and heating. Reprinted (Adapted or Reprinted in part) with permission from [Created with BioRender.com]. Copyright [2022] [BioRender].

3.5 Conclusions

In this study, we investigated the correlation between the processing parameters of the acid-catalyzed one-pot liquefaction process and the molecular properties as well as the yield of

the Kraft lignin using response surface methodology (RSM). The pH was found to be the most influential parameter followed by the reaction temperature of the liquefaction process. The pH had negative effects on the yield (70.2-85.5%), molecular weight, and polydispersity of Kraft lignin, and the reaction temperature positively affected the lignin yield but negatively influenced the molecular weight values of the Kraft lignin. Specifically, the Kraft lignin with a higher yield tended to exhibit higher molecular weight and polydispersity values. The relatively higher R^2, $R^2_{(adj)}$, and $R^2_{(pred)}$ values of the computational models of yield and molecular weight features indicated their better goodness-of-fit and predictability than the models of hydroxyl groups natures of the Kraft lignin. Both experimental and simulated approaches verified that the weight average molecular weight (Mw) of the Kraft lignin could be used as a predictor of the number average molecular weight (Mn) and the polydispersity of the Kraft lignin. The controllable and predictable properties of the lignin may benefit from the clever use of acetic acid, subcritical methanol, and one-pot method. We expect that the research strategies adopted in this study offer new insights into understanding and predicting the product properties from complicated chemical reaction systems.

3.6 References

1. Hu, J.; Zhang, Q.; Lee, D.-J., Kraft lignin biorefinery: A perspective. *Bioresource Technology* **2018,** *247*, 1181-1183.

2. Ragauskas, A. J.; Beckham, G. T.; Biddy, M. J.; Chandra, R.; Chen, F.; Davis, M. F.; Davison, B. H.; Dixon, R. A.; Gilna, P.; Keller, M., Lignin valorization: improving lignin processing in the biorefinery. *Science* **2014,** *344* (6185).

3. Cao, Y.; Chen, S. S.; Zhang, S.; Ok, Y. S.; Matsagar, B. M.; Wu, K. C.-W.; Tsang, D. C., Advances in lignin valorization towards bio-based chemicals and fuels: Lignin biorefinery. *Bioresource Technology* **2019,** *291*, 121878.

4. Garlapati, V. K.; Chandel, A. K.; Kumar, S. J.; Sharma, S.; Sevda, S.; Ingle, A. P.; Pant, D., Circular economy aspects of lignin: Towards a lignocellulose biorefinery. *Renewable and Sustainable Energy Reviews* **2020,** *130*, 109977.

5. Ponnusamy, V. K.; Nguyen, D. D.; Dharmaraja, J.; Shobana, S.; Banu, J. R.; Saratale, R. G.; Chang, S. W.; Kumar, G., A review on lignin structure, pretreatments, fermentation reactions and biorefinery potential. *Bioresource Technology* **2019,** *271*, 462-472.

6. Moreno, A.; Sipponen, M. H., Lignin-based smart materials: a roadmap to processing and synthesis for current and future applications. *Materials Horizons* **2020,** *7* (9), 2237-2257.

7. Xu, C.; Arancon, R. A. D.; Labidi, J.; Luque, R., Lignin depolymerisation strategies: towards valuable chemicals and fuels. *Chemical Society Reviews* **2014,** *43* (22), 7485-7500.

8. Torres, L. A. Z.; Woiciechowski, A. L.; de Andrade Tanobe, V. O.; Karp, S. G.; Lorenci, L. C. G.; Faulds, C.; Soccol, C. R., Lignin as a potential source of high-added value compounds: A review. *Journal of Cleaner Production* **2020,** *263*, 121499.

9. Li, Q.; Serem, W. K.; Dai, W.; Yue, Y.; Naik, M. T.; Xie, S.; Karki, P.; Liu, L.; Sue, H.-J.; Liang, H., Molecular weight and uniformity define the mechanical performance of lignin-based carbon fiber. *Journal of Materials Chemistry A* **2017,** *5* (25), 12740-12746.

10. Kim, J.; Nguyen, T. V. T.; Kim, Y. H.; Hollmann, F.; Park, C. B., Lignin as a multifunctional photocatalyst for solar-powered biocatalytic oxyfunctionalization of C–H bonds. *Nature Synthesis* **2022,** *1* (3), 217-226.

11. Gioia, C.; Colonna, M.; Tagami, A.; Medina, L.; Sevastyanova, O.; Berglund, L. A.; Lawoko, M., Lignin-based epoxy resins: Unravelling the relationship between structure and material properties. *Biomacromolecules* **2020,** *21* (5), 1920-1928.

12. Crestini, C.; Lange, H.; Sette, M.; Argyropoulos, D. S., On the structure of softwood kraft lignin. *Green Chemistry* **2017,** *19* (17), 4104-4121.

13. Gierer, J., Chemical aspects of kraft pulping. *Wood Science and Technology* **1980,** *14* (4), 241-266.

14. Sadeghifar, H.; Ragauskas, A., Perspective on technical lignin fractionation. *ACS Sustainable Chemistry & Engineering* **2020**, 8 (22), 8086-8101.

15. Tomani, P., The lignoboost process. *Cellulose Chemistry & Technology* **2010,** *44* (1), 53.

16. Kouisni, L.; Holt-Hindle, P.; Maki, K.; Paleologou, M., The lignoforce system: a new process for the production of high-quality lignin from black liquor. *J. Sci. Technol. For. Prod. Processes* **2012,** *2* (4), 6-10.

17. Zhu, W.; Westman, G.; Theliander, H., Investigation and characterization of lignin precipitation in the lignoboost process. *Journal of Wood Chemistry and Technology* **2014,** *34* (2), 77-97.

18. Andeme Ela, R. C.; Spahn, L.; Safaie, N.; Ferrier Jr, R. C.; Ong, R. G., Understanding the effect of precipitation process variables on hardwood lignin characteristics and recovery from black liquor. *ACS Sustainable Chemistry & Engineering* **2020,** *8* (37), 13997-14005.

19. Qu, W.; Yang, J.; Sun, X.; Bai, X.; Jin, H.; Zhang, M., Towards producing high-quality lignin-based carbon fibers: a review of crucial factors affecting lignin properties and conversion techniques. *International Journal of Biological Macromolecules* **2021,** *189*, 768-784.

20. Rahimi, A.; Ulbrich, A.; Coon, J. J.; Stahl, S. S., Formic-acid-induced depolymerization of oxidized lignin to aromatics. *Nature* **2014,** *515* (7526), 249-252.

21. Araújo, L. C. P.; Yamaji, F. M.; Lima, V. H.; Botaro, V. R., Kraft lignin fractionation by organic solvents: Correlation between molar mass and higher heating value. *Bioresource Technology* **2020,** *314*, 123757.

22. Vermaas, J. V.; Crowley, M. F.; Beckham, G. T., Molecular lignin solubility and structure in organic solvents. *ACS Sustainable Chemistry & Engineering* **2020,** *8* (48), 17839-17850.

23. Pang, T.; Wang, G.; Sun, H.; Sui, W.; Si, C., Lignin fractionation: Effective strategy to reduce molecule weight dependent heterogeneity for upgraded lignin valorization. *Industrial Crops and Products* **2021,** *165*, 113442.

24. Xu, J.; Li, C.; Dai, L.; Xu, C.; Zhong, Y.; Yu, F.; Si, C., Biomass fractionation and lignin fractionation towards lignin valorization. *ChemSusChem* **2020,** *13* (17), 4284-4295.

25. Alekhina, M.; Ershova, O.; Ebert, A.; Heikkinen, S.; Sixta, H., Softwood kraft lignin for value-added applications: Fractionation and structural characterization. *Industrial Crops and Products* **2015,** *66*, 220-228.

26. Park, S. Y.; Kim, J.-Y.; Youn, H. J.; Choi, J. W., Fractionation of lignin macromolecules by sequential organic solvents systems and their characterization for further valuable applications. *International Journal of Biological Macromolecules* **2018,** *106*, 793-802.

27. Quan, P.; Kiziltas, A.; Gondaliya, A.; Siahkamari, M.; Nejad, M.; Xie, X., Kraft Lignin with Improved Homogeneity Recovered Directly from Black Liquor and Its Application in Flexible Polyurethane Foams. *ACS Omega* **2022**.

28. Siahkamari, M.; Emmanuel, S.; Hodge, D. B.; Nejad, M., Lignin-Glyoxal: A Fully Biobased Formaldehyde-Free Wood Adhesive for Interior Engineered Wood Products. *ACS Sustainable Chemistry & Engineering* **2022,** *10* (11), 3430-3441.

29. Tolbert, A.; Akinosho, H.; Khunsupat, R.; Naskar, A. K.; Ragauskas, A. J., Characterization and analysis of the molecular weight of lignin for biorefining studies. *Biofuels, Bioproducts and Biorefining* **2014,** *8* (6), 836-856.

30. Meng, X.; Crestini, C.; Ben, H.; Hao, N.; Pu, Y.; Ragauskas, A. J.; Argyropoulos, D. S., Determination of hydroxyl groups in biorefinery resources via quantitative ^{31}P NMR spectroscopy. *Nature Protocols* **2019,** *14* (9), 2627-2647.

31. Veerasamy, R.; Rajak, H.; Jain, A.; Sivadasan, S.; Varghese, C. P.; Agrawal, R. K., Validation of QSAR models-strategies and importance. *Int. J. Drug Des. Discov* **2011,** *3*, 511-519.

32. Umar, B. A.; Uzairu, A.; Shallangwa, G. A., Quantum Modeling and Molecular Dynamic Simulation of Some Amino Acids and Related Compounds on Their Corrosion Inhibition of Steel in Acidic Media. *Port. Electrochim. Acta* **2020,** *38*, 313-329.

33. Melro, E.; Alves, L.; Antunes, F. E.; Medronho, B., A brief overview on lignin dissolution. *Journal of Molecular Liquids* **2018,** *265*, 578-584.

34. Yoshida, H.; Mörck, R.; Kringstad, K. P.; Hatakeyama, H., Kraft lignin in polyurethanes. II. Effects of the molecular weight of kraft lignin on the properties of polyurethanes from a kraft lignin–polyether triol–polymeric MDI system. *Journal of Applied Polymer Science* **1990,** *40* (11-12), 1819-1832.

35. Zhu, S.; Guo, J.; Wang, X.; Wang, J.; Fan, W., Alcoholysis: a promising technology for conversion of lignocellulose and platform chemicals. *ChemSusChem* **2017,** *10* (12), 2547-2559.

36. Hatakeyama, H.; Hatakeyama, T., Lignin structure, properties, and applications. In *Biopolymers*, Springer: 2009; pp 1-63.

37. Cateto, C. A.; Barreiro, M. F.; Rodrigues, A. E.; Brochier-Salon, M. C.; Thielemans, W.; Belgacem, M. N., Lignins as macromonomers for polyurethane synthesis: A comparative study on hydroxyl group determination. *Journal of Applied Polymer Science* **2008,** *109* (5), 3008-3017.

38. Elmaz, F.; Yücel, Ö.; Mutlu, A. Y., Predictive modeling of biomass gasification with machine learning-based regression methods. *Energy* **2020,** *191*, 116541.

39. Tang, Q.; Chen, Y.; Yang, H.; Liu, M.; Xiao, H.; Wang, S.; Chen, H.; Naqvi, S. R., Machine learning prediction of pyrolytic gas yield and compositions with feature reduction methods: effects of pyrolysis conditions and biomass characteristics. *Bioresource Technology* **2021,** *339*, 125581.

4 The Iron-based Desulfurization Process of Lignin

4.1 Abstract

Residual covalently bonded sulfur is one of the intractable issues that prevent Kraft lignin from value-added applications in large scale. In this study, an iron-based desulfurization process was developed to reduce the amount of covalently bonded sulfur in the lignin. The effects of reaction temperature, reaction time, and amount of iron on the sulfur content and desulfurization rate of the lignin were investigated. The results showed that the covalently bonded sulfur group in the lignin molecules was thiol (-C-S-H), and the thiol group may react with iron atoms after the desulfurization processes, generating iron sulfate compounds. Moreover, the reaction temperature was the most influential factor of the sulfur content and desulfurization rate of the lignin, and the highest desulfurization rate of 39.3% occurred at 90 ℃, 16h, and 0.3 g iron.

4.2 Introduction

Sulfur is one of the major issues that prevent the Kraft lignin from the value-added applications. Kraft lignin, a main technical lignin on the earth, originates from the Kraft pulping process in which uses sodium hydroxide (NaOH), sodium sulfide (Na_2S), and hot water (~170 ℃) to deconstruct and dissolve the lignin molecules from the cell walls of biomass, generating black liquor with lignin.[1,2] Owing to the use of sodium sulfide (Na_2S), the resultant Kraft lignin usually contains 1.5-8% sulfur compounds in the inorganic and organic forms.[3,4] As a result, the applications of Kraft lignin are still limited. For example, if the fuels are made by Kraft lignin, they will generate sulfur dioxide (SO_2) during the combustion and cause acid rain when they are emitted into the atmosphere. The acid rain is known to be harmful to ecosystems such as aquatic and soil environments.[5,6] Thus, to

expand the applications of Kraft lignin, it is necessary to develop effective methods to remove the sulfur compounds.

So far, a few of methods have been proposed to remove the sulfur from the lignin. The sulfur in the lignin includes sulfur-based salts, elemental sulfur, and covalently bonded sulfur.[7,8] For the sulfur-based salts, acid-water wash is an effective removal method since they can be easily dissolved in water. For the elemental sulfur, it can be removed by organic solvent extraction methods to some extent. The most challenging task is removing the covalently bonded sulfur from the lignin molecules because of the covalent bonds between carbon atoms and sulfur atoms.[7,8] To remove the covalently bonded sulfur, the hydrogenation method using Raney nickel (Ni-Al alloy) as the catalyst have been proved to be more effective than the oxidative methods using oxygen as the oxidant.[8] Afterward, silver (Ag) or copper (Cu) were used to reduce the covalently bonded sulfur from Kraft lignin or black liquor soap.[7,9] However, these studies were based on the total sulfur content without the experimental evidence of removed covalently bonded sulfur groups. Also, the metals or alloy involved in such methods are quite expensive, making the desulfurization process not cost-effective.

Iron (Fe) is one of the most common elements on the earth, and it is cheap and has been used as a reductive catalyst in other fields.[10,11] In this study, we hypothesized that iron may work as a catalyst and a desulfurizer for the organic sulfur in the Kraft lignin molecules. To verify the hypothesis, a thermochemical method was developed involving methanol (solvent), lignin, and iron. The effects of the reaction temperature, time, and the amount of iron on the sulfur content and desulfurization rate of the lignin were investigated in this

study. The elemental analyzer, FTIR, XPS, and XRD were used to reveal the desulfurization mechanisms.

4.3 Experimental Section

4.3.1 Materials

The Kraft lignin was produced from the acid-catalyzed one-pot liquefaction process, which has been reported in the chapter 3. The methanol (ACS reagent) and iron powder (≥99%) were purchased from Sigma-Aldrich company, and they were directly used without any modifications. Hydrochloric acid (37%) was purchased from VWR Chemicals company. The distilled water was produced in our lab.

4.3.2 Removal of Inorganic Salts from the Lignin

To remove the inorganic salts, a purification process was conducted on the Kraft lignin. The Kraft lignin was first mixed with a certain amount of distilled water, then the pH of the lignin-water mixture was adjusted to 1 by adding hydrochloric acid. Afterward, the mixture was filtered by a vacuum filtration followed by a wash of diluted hydrochloric acid aqueous solution (pH = 1). The residue was collected and vacuum dried at 50 ℃ overnight, generating the pretreated lignin, while the filtrate was discarded. Such a purification process aims to minimize the effects of inorganic salts on the desulfurization process of the lignin.

4.3.3 Desulfurization

In a typical experiment, 1.5 g pretreated lignin was mixed with 15 g methanol followed by the addition of a certain amount of iron powder. Then, the mixture was refluxed at a certain temperature for a certain duration. At the end, the flask with the mixture was sunk in cold

water for 10 min. Then, the mixture was filtered by vacuum filtration to separate the supernatant and residue. Afterward, the methanol in the supernatant was evaporated at room temperature in the hood overnight followed by an overnight vacuum drying process at 50 ℃, forming desulfurized lignin. The desulfurization rate (DR) of lignin was defined as below:

$$DR = \frac{SC_p - SC_d}{SC_p} \times 100\%$$

Where the SC_p refers to the sulfur content of the pretreated lignin, SC_d is the sulfur content of the desulfurized lignin.

4.3.4 Experimental Design of the Desulfurization Processes

The processing parameters of the desulfurization processes included reaction temperature (70, 80, and 90 ℃), reaction time (8, 16, and 24 h), and the amount of iron powder (0.15, 0.30, and 0.45 g). To explore the effect of each parameter on the sulfur content and desulfurization rate (%) of lignin, an experimental design was detailed in Table 4.1. Each of the tests was conducted once.

Table 4.1 The details of the experimental design

Tests	Temperature (℃)	Time (h)	Amount of iron (g)
1	70	16	0.30
2	80	16	0.30
3	90	16	0.30
4	80	8	0.30
5	80	24	0.30

6	80	16	0.15
7	80	16	0.45

4.3.5 Determination of Sulfur Content of Lignin

The sulfur content (wt%) of lignin samples was characterized by an elemental combustion system (Costech EAS 4010, USA). Approximately 2 mg of each sample was weighed into tin capsules for analysis. Vanadium pentoxide was added to each sample as a combustion aid. The instrument was calibrated with sulfanilamide with standards run every 12 samples to check for instrument stability. For the lignin sample from one desulfurization test, it had three replications to obtain an average sulfur content value.

4.3.6 Statistical Analysis

The sulfur content of lignin was shown in average values with standard deviations. The average values were calculated based on the results of three replications of sulfur content tests. Also, one-way ANOVA ($\alpha = 0.05$) for these data was conducted in SPSS software to show the significant factors.

4.3.7 Fourier-transform Infrared (FTIR) Spectroscopy

To understand the basic desulfurization mechanisms of the lignin, a Fourier-transform Infrared (FTIR) Spectrometer (IRTracer-100, SHIMADZU, USA) was used to observe the variations of sulfur groups and other chemical groups in the pretreated and desulfurized lignin. Before the tests for lignin samples, an air background scan was carried out. The wavenumbers range of FTIR spectra ranged from 400 cm^{-1} to 4000 cm^{-1}, and the resolution and number of scans were 4 cm^{-1} and 10 respectively.

4.3.8 X-ray Photoelectron Spectroscopy (XPS)

The XPS measurements were conducted on the lignin and the iron powder before and after the desulfurization processes. An X-ray photoelectron spectrometer (PHI 5800, Physical Electronics, USA) with a dual X-ray source (Mg and Al) was utilized to perform XPS measurements using the Mg X-ray source at 100 W. High-resolution energy spectra were collected for C 1s, O 1s, S 2p, and Fe 2p using a pass energy of 23.50 eV, a step size of 0.1 eV, and a dwell time of 100 ms/step. All the XPS spectra were fitted using CasaXPS software.

4.4 Results and Discussions

4.4.1 The sulfur content (wt%) and desulfurization rate (%) of lignin

As shown in Figure 4.1 a, the sulfur content in the pretreated lignin was approximately 4.24 wt%, and it decreased to be lower than 3.66 wt% after the desulfurization processes. With the increasing reaction temperature, the sulfur content of the lignin was reduced from 3.66 wt% to 2.57 wt% (Figure 4.1 a), and the desulfurization rate increased from 13.5% to 39.3% (Figure 4.1 b). The desulfurization rates were similar to that of the method using silver (9.6-46.4%) but lower than that of methods using copper (85.7-93.7%) for black liquor soap and Raney nickel (60-63.9%) for Kraft lignin.[7-9] However, although the reference methods had very high desulfurization rates, those are based on total sulfur contents without the experimental evidence of covalently bonded sulfur forms. Thus, it is difficult to judge what the covalently bonded sulfur groups were and if they were removed or not.

The statistical analysis results showed that the reduction of sulfur content of the desulfurized lignin compared with the pretreated lignin was statistically significant (P value < 0.001), while the difference between the sulfur content of lignin desulfurized at 70 and 80 ℃ was not statistically significant (P value = 0.721) (Table 4.2). Such results could be explained by the activation energy of collisional reactions.[12] At 90 ℃, the lignin molecules with sulfur groups may obtain the specific activation energy that can accelerate the collisional reactions between the sulfur groups and iron atoms, resulting in the significant reduction of sulfur content compared to the lignin desulfurized at 70 and 80 ℃. Such results also implied that continuing to increase the temperature higher than 90 ℃ may remove more sulfur groups from the lignin molecules.

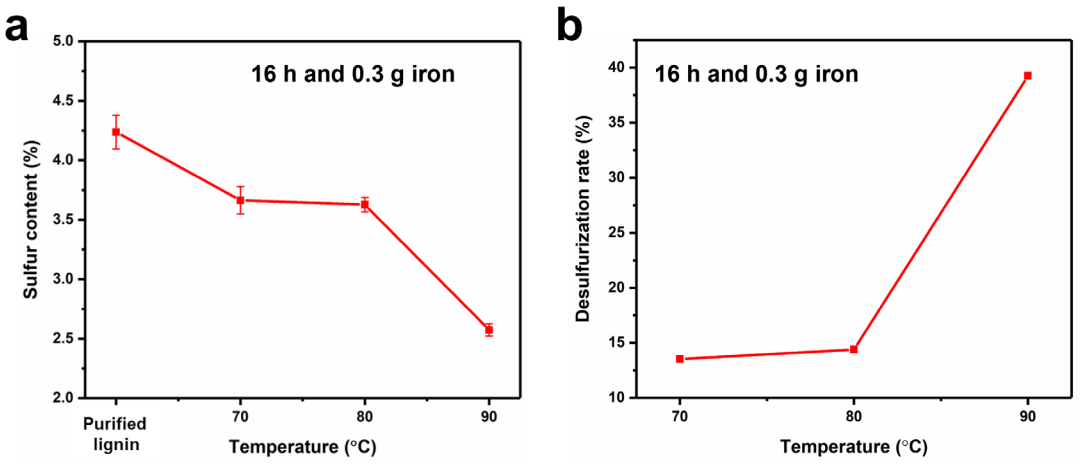

Figure 4.1 The sulfur content (wt%) (a) and desulfurization rate (%) (b) of lignin with different reaction temperatures, 16 h, and 0.3 g iron.

Table 4.2 Statistically multiple comparisons of the sulfur content of lignin with different reaction temperatures (70-90 ℃).

(I) Temperature (℃)	(J) Temperature (℃)	Mean Difference (I-J)	Sig.
Pretreated lignin	70	0.57333*	<0.001
	80	0.61000*	<0.001
	90	1.66333*	<0.001
70	80	0.03667	0.721
	90	1.09000*	<0.001
80	90	1.05333*	<0.001

* The mean difference is significant at the 0.05 level.

Figure 4.2a shows the effect of reaction time on the sulfur content (wt%) and desulfurization rate (%) of lignin. Compared with the sulfur content of pretreated lignin (4.24 wt%), the lignin desulfurized at different reaction times had lower sulfur content (3.12-3.63 wt%), but it flunctuated with longer reaction time. Such variations were statistically significant (P value < 0.02) as shown in Table 4.3. Accordingly, the desulfurzation rates at different reaction times were in the range of 14.4-26.4% with a fluctuation (Figure 4.2b). The fluctuation was related to the complex structures of lignin molecules. Actually, the extracted lignin is a mixture of molecules with complicated three-dimensional structures rather than a single compound.[13,14] The distribution of the sulfur groups in the lignin molecules was very likely not as regular as the model compounds with sulfur groups which were frequently used in previous studies.[15-17] Also, the size and shape

of carbon skeletons of lignin molecules were variable due to the polydispersity, and they may cause different steric effects when the sulfur groups reacted with the iron atoms.[18] Thus, the desulfurization rate of lignin fluctuated.

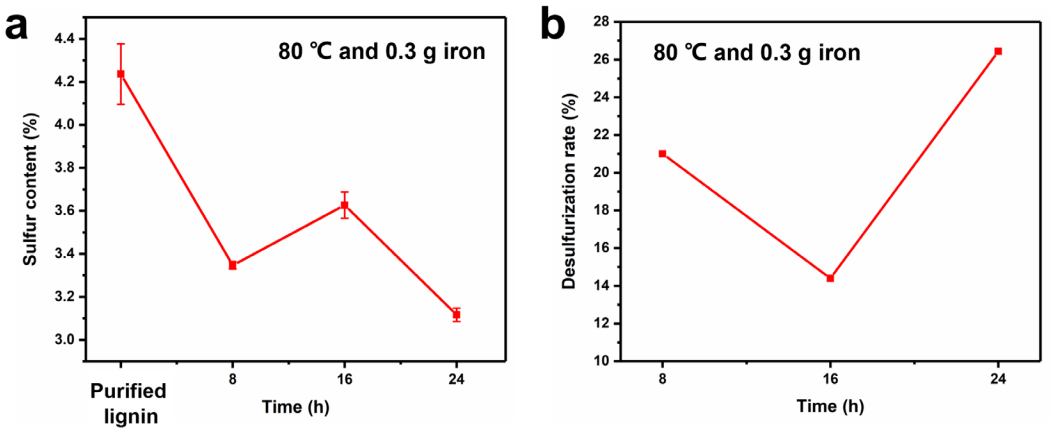

Figure 4.2 The sulfur content (wt%) (a) and desulfurization rate (%) (b) of lignin with different reaction times, 80 ℃, and 0.3 g iron.

Table 4.3 Statistically multiple comparisons of the sulfur content (wt%) of lignin with different reaction times (8-24 h).

(I) Time (h)	(J) Time (h)	Mean Difference (I-J)	Sig.
Pretreated lignin	8	0.89000*	<0.001
	16	0.61000*	<0.001
	24	1.12000*	<0.001
8	16	-0.28000*	0.007
	24	0.23000*	0.019
16	24	0.51000*	<0.001

* The mean difference is significant at the 0.05 level.

The effect of amount of iron on the sulfur content (wt%) and desulfurization rate (%) of lignin is shown in the Figure 4.3. When the reaction temperature and time were fixed at 80 ℃ and 16 h respectively, the lignin desulfurized with the different amounts of iron (0.15-0.45 g) possessed the sulfur contents ranging from 3.27-3.63 wt% which was lower than that of pretreated lignin (4.24 wt%). Such reductions of sulfur content were statistically significant (P value < 0.005) (Table 4.4). Similarly, there were fluctuations in the sulfur contents and desulfurization rates of lignin within the range of iron amounts. However, the sulfur content of desulfurized lignin with the iron amount of 0.15 g in comparison to that of desulfurized lignin with the iron amounts of 0.30 g and 0.45 g was not statistically significant (P value > 0.2) (Table 4.4). Such fluctuations may be associated with the ununiform distribution of sulfur groups and the different steric effects of the lignin molecules as well.

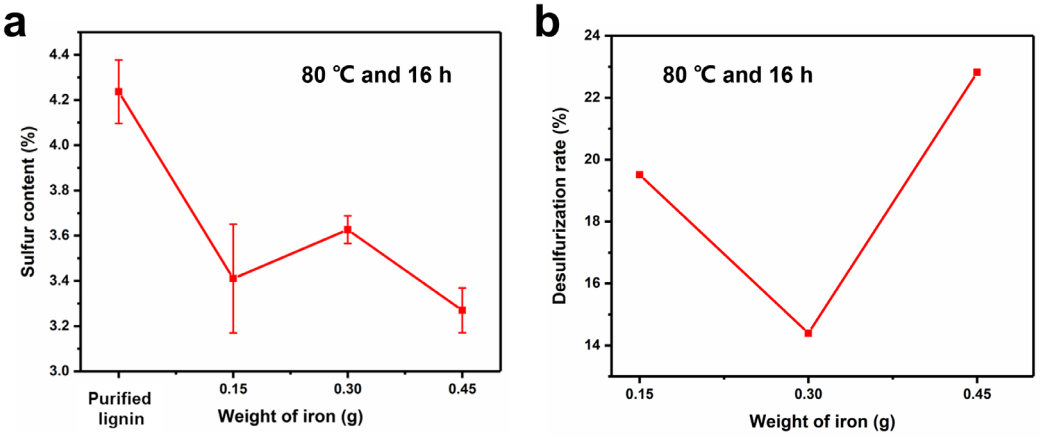

Figure 4.3 The sulfur content (wt%) (a) and desulfurization rate (%) (b) of lignin with different amounts of iron (g), 80 ℃, and 16 h.

Table 4.4 Statistically multiple comparisons of the sulfur content (wt%) of lignin with different amounts of iron (0.15-0.45 g).

(I) Amount of iron (g)	(J) Amount of iron (g)	Mean Difference (I-J)	Sig.
Pretreated lignin	0.15	0.82667*	<0.001
	0.30	0.61000*	0.004
	0.45	0.96667*	<0.001
0.15	0.30	-0.21667	0.189
	0.45	0.14000	0.381
0.30	0.45	0.35667*	0.046

The mean difference is significant at the 0.05 level.

4.4.2 FTIR Spectra

The FTIR spectra of the pretreated lignin and the selected desulfurized lignin are shown in Figure 4.4. The peaks in the FTIR spectra mainly existed in the range of 750-2000 cm^{-1} and 2500-3500 cm^{-1}, and the profile of each spectrum was very similar. For the carbon-based groups, there were C=C of alkene (829 cm^{-1}), C-O of aliphatic ether (1105 cm^{-1}), C-O of ester (1207 cm^{-1}), O-H and C=O of carboxylic acid (1437 and 1709 cm^{-1}), C-H of alkane (1504 and 2941 cm^{-1}), C=C of cyclic alkene (1608 cm^{-1}), and O-H of alcohol (3400 cm^{-1}).[19] For the sulfur-based groups, the peaks at 1031 and 1329 cm^{-1} may be S=O of sulfoxide and S=O of sulfone respectively, while they could be also C-O of ether and O-H of phenol respectively since there is overlapping of peaks among these chemical groups.[19] The S-H of thiol that was estimated to exist in the lignin molecules could not be observed clearly since its peak range (2600-2550 cm^{-1}) was overlapped with the air background in

the FTIR spectra.[19] These results indicated that the main molecular characteristics of the lignin was maintained well after the desulfurization processes.

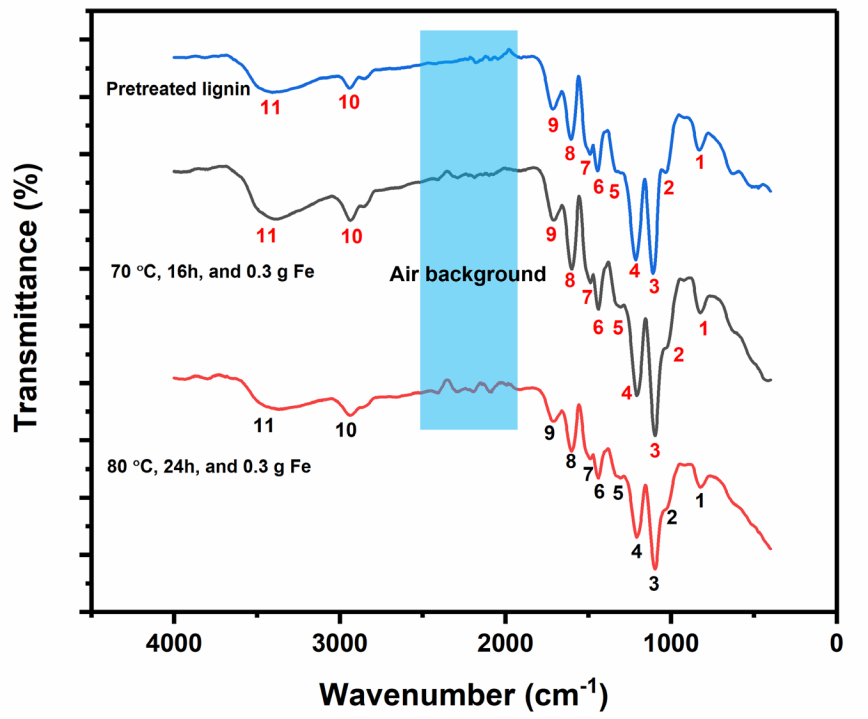

Figure 4.4 FTIR spectra of the pretreated lignin and the selected desulfurized lignin.

Table 4.5 Major functional groups of the pretreated lignin and the selected desulfurized lignin shown in the FTIR spectra.

Peaks	Wavenumber (cm^{-1})	Assignment	Functional groups
1	829	C=C	Alkene
2	1031	S=O or C-O	Sulfoxide or ether
3	1105	C-O	Aliphatic ether
4	1207	C-O	Ester
5	1329	O-H or S=O	Phenol or sulfone

6	1437	O-H	Carboxylic acid
7	1504	C-H	Alkane
8	1608	C=C	Cyclic alkene
9	1709	C=O	Carboxylic acid dimer
10	2941	C-H	Alkane
11	3400	O-H	Alcohol

4.4.3 XPS Spectra

Figure 4.5a shows the high resolution XPS spectrum with the S 2p peak of the pretreated lignin. It was found that there was a peak existing at approximately 164 eV, indicating the existence of thiol (-C-S-H) in the lignin molecules.[20] Such a chemical group was not observed in the FTIR spectra due to its low concentration and different sensitivity of FTIR and XPS instruments. After the desulfurization processes, the signal of thiol still existed in the XPS spectrum of the lignin, while the intensity of the signal was significantly lower than that of the pretreated lignin (Figure 4.5b). This result was in accordance with the reduction of sulfur content of the desulfurized lignin compared to the pretreated lignin. Moreover, there were no signals of sulfoxide and sulfone groups which should occur at 167.0 and 167.7 eV respectively.[21,22] These results refuted that the peaks at 1031 and 1329 cm^{-1} in the FTIR spectra belonged to the sulfoxide and sulfone groups. Moreover, typical Fe 2p peaks (~710 eV and ~725 eV) and no sulfur peaks were observed in the high XPS spectra of pure iron powder (Figure 4.6a and b).[20,23] After the desulfurization processes, the signal of Fe 2p peaks became weaker, and an iron-sulfate peak (~168 eV) and a thiol peak (~164 eV) occurred. The iron-sulfate peak may be due to the reaction between the covalently bonded thiol groups in the lignin molecules and iron atoms under the aid of

oxygen, and it still needs to be verified by further studies. The thiol peak may be related to the residual lignin on the surface of the reacted iron sample.

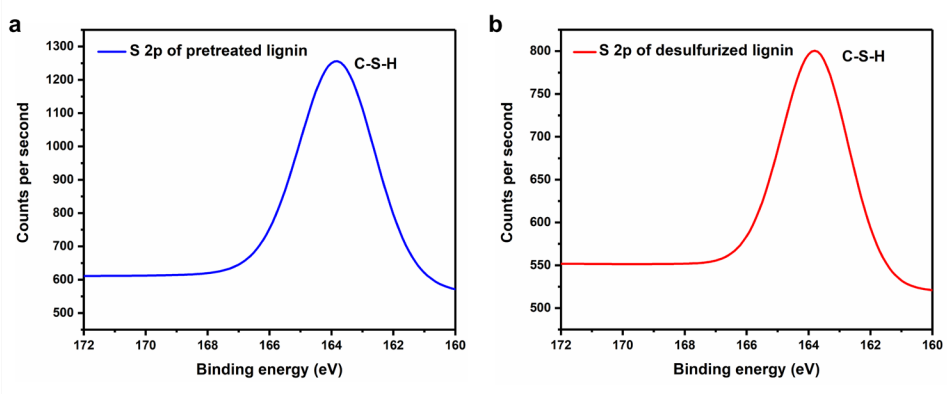

Figure 4.5 The high resolution XPS spectrum with the S 2p peak of (a) pretreated lignin and (b) desulfurized lignin.

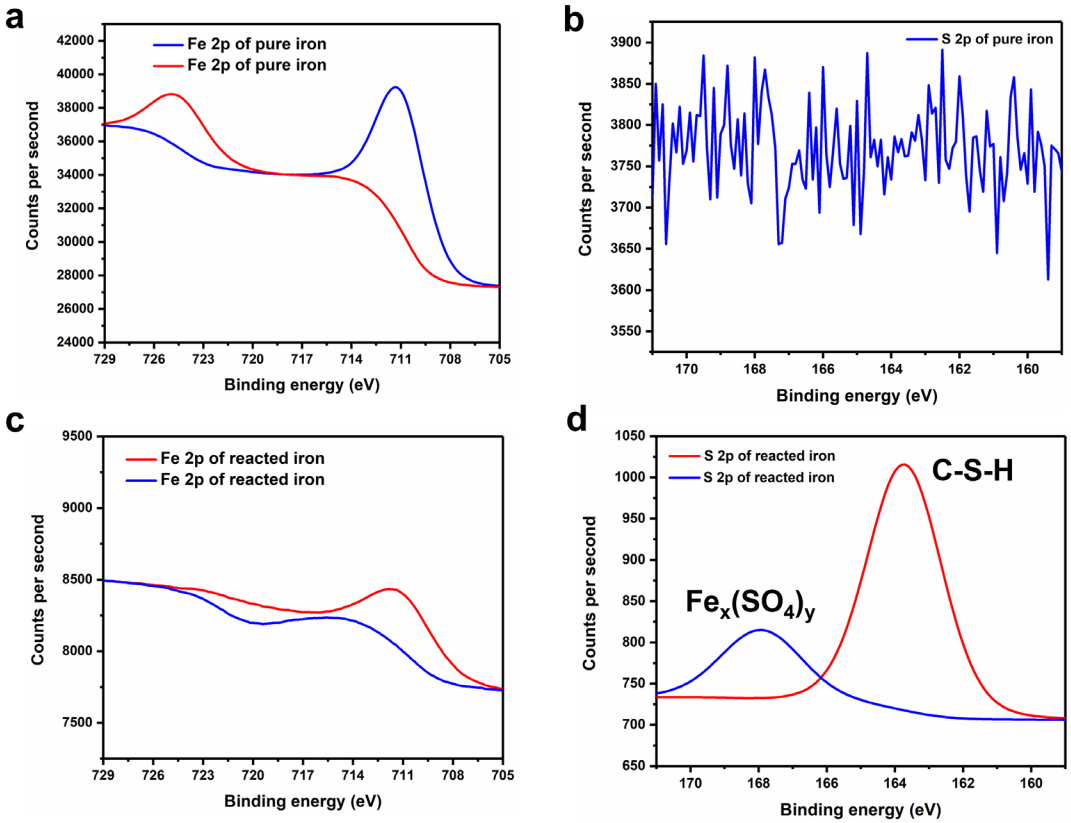

Figure 4.6 The high resolution XPS spectra with (a) Fe 2p peaks and (b) S 2p peaks of pure iron; the high resolution XPS spectra with (c) Fe 2p peaks and (b) S 2p peaks of reacted iron.

4.5 Conclusions

In summary, an iron-based desulfurization process was developed to reduce the amount of covalently bonded sulfur in the Kraft lignin molecules. The results verified that the thiol group (-C-S-H) existed in the lignin molecules. The reaction temperature was the most influential factor of the sulfur content and desulfurization rate of lignin. The highest desulfurization rate of 39.3% existed at 90 ℃, 16h, and 0.3 g iron. After the desulfurization processes, the thiol groups may react with iron atoms under the aid of oxygen and generate iron sulfate compounds, while other major chemical groups in the lignin molecules were maintained well. The reaction mechanism still needs to be verified by further studies. Although the developed method could reduce the covalently bonded sulfur to some extent, the lignin still had sulfur contents higher than 2 wt%. Thus, it is necessary to seek for more efficient desulfurization ways of Kraft lignin.

4.6 References

1. Gierer, J., Chemical aspects of kraft pulping. *Wood Science and Technology* **1980,** *14* (4), 241-266.

2. Norgren, M.; Lindstrom, B., Dissociation of Phenolic Groups in Kraft Lignin at Elevated Temperatures. *Holzforschung* **2000,** (5), 54.

3. Tomani, P.; Axegård, P.; Berglin, N.; Lovell, A.; Nordgren, D., Integration of lignin removal into a kraft pulp mill and use of lignin as a biofuel. *Cellulose Chemistry and*

Technology **2011,** *45* (7), 533.

4. Vishtal; Kraslawski, CHALLENGES IN INDUSTRIAL APPLICATIONS OF TECHNICAL LIGNINS. *Bioresources* **2011,** *6* (3), 3547-3568.

5. https://www.epa.gov/acidrain/what-acid-rain#.

6. https://www.epa.gov/acidrain/effects-acid-rain.

7. Evdokimov, A. N.; Kurzin, A. V.; Fedorova, O. V.; Lukanin, P. V.; Kazakov, V. G.; Trifonova, A. D., Desulfurization of kraft lignin. *Wood Science and Technology* **2018,** *52* (4), 1165-1174.

8. Svensson, S., 2008. Minimizing the sulphur content in Kraft lignin.

9. Evdokimov, A. N.; Kurzin, A. V.; Trifonova, A. D.; Popova, L. M.; Buisman, G. J. H., Desulfurization of black liquor soap for production of crude tall oil with lower sulfur content. *Wood Science and Technology* **2017,** *51* (6), 1353-1363.

10. Casey, C. P.; Guan, H., An efficient and chemoselective iron catalyst for the hydrogenation of ketones. *Journal of the American Chemical Society* **2007,** *129* (18), 5816-5817.

11. Boddien, A.; Mellmann, D.; Gärtner, F.; Jackstell, R.; Junge, H.; Dyson, P. J.; Laurenczy, G.; Ludwig, R.; Beller, M., Efficient dehydrogenation of formic acid using an iron catalyst. *Science* **2011,** *333* (6050), 1733-1736.

12. Menzinger, M.; Wolfgang, R., The Meaning and Use of the Arrhenius Activation Energy. *Angewandte Chemie International Edition* **1969,** *8* (6), 438-444.

13. Ralph, J.; Lapierre, C.; Boerjan, W., Lignin structure and its engineering. *Current Opinion in Biotechnology* **2019,** *56*, 240-249.

14. Vanholme, R.; Demedts, B. B.; Morreel, K.; Ralph, J.; Boerjan, W., Lignin

Biosynthesis and Structure. *Plant Physiology* **2010,** *153* (3), 895-905.

15. Zhang, M.; Wei, Y.; Li, R.; Zhu, W.; Li, H.; Zhang, Q.; Wang, M.; Chen, X.; Li, H., Magnetic POM-based mesoporous silica for fast oxidation of aromatic sulfur compounds. *Fuel* **2017,** *209* (dec.1), 545-551.

16. Abazari, R.; Esrafili, L.; Morsali, A.; Wu, Y.; Gao, J., PMo12@ UiO-67 nanocomposite as a novel non-leaching catalyst with enhanced performance durability for sulfur removal from liquid fuels with exceptionally diluted oxidant. *Applied Catalysis B: Environmental* **2021,** *283*, 119582.

17. Al-Hammadi, S. A.; Al-Amer, A. M.; Saleh, T. A., Alumina-carbon nanofiber composite as a support for MoCo catalysts in hydrodesulfurization reactions. *Chemical Engineering Journal* **2018,** *345*, 242-251.

18. Hill, T. L., On Steric Effects. *The Journal of Chemical Physics* **1946,** *14* (7), 465-465.

19. https://chem.libretexts.org/Ancillary_Materials/Reference/Reference

20.https://www.thermofisher.com/us/en/home/materials-science/learning-center/periodic-table.html

21. Louette, P.; Bodino, F.; Pireaux, J. J., Poly(sulfone resin) XPS Reference Core Level and Energy Loss Spectra. *Surface Science Spectra* **2005,** *12* (1).

22. Avval, T. G.; Cushman, C. V.; Bahr, S.; Dietrich, P.; Linford, M. R., Dimethyl sulfoxide by near-ambient pressure XPS. *Surface Science Spectra* **2019,** *26* (1), 014020.

23. https://xpsdatabase.com/iron-fe-z26-chemicals/

A Supporting Information for Chapter 3

Table A.1 The information of chemicals used in this study.

Purpose	Name	Company	Purity
Liquefaction processes	Methanol	Sigma-Aldrich	≥99.8%
	Acetic acid	Sigma-Aldrich	≥99.7%
	Tetrahydrofuran	Sigma-Aldrich	≥99.9%
Molecular weight (GPC) tests	Pyridine	Fisher Chemical™	≥99%
	Acetic anhydride	Sigma-Aldrich	≥99%
	Hydrochloric acid	Sigma-Aldrich	37%
	Polystyrene standards	Agilent Technologies	
^{31}P NMR tests	Deuterated chloroform	Sigma-Aldrich	99.8atom %D
	Pyridine (Certified ACS)	Fisher Chemical™	≥99%
	Endo-N-Hydroxy-5-norbornene-2,3-dicarboximide	Alfa Aesar	97%
	Chromium(III) acetylacetonate	Acros Organics	97%
	2-Chloro-4,4,5,5-tetramethyl-1,3,2-dioxaphospholane	Sigma-Aldrich	95%

Table A.2 Experimental parameters and variables based on the Box-Behnken response surface methodology (RSM).

Test	pH	Temperature (°C)	Time (min)
1	3	160	3
2	7	180	9
3	3	180	9
4	7	160	15
5	3	140	9
6	5	160	9
7	7	140	9
8	7	160	3
9	5	160	9
10	5	180	15
11	5	140	3
12	5	180	3
13	3	160	15
14	5	140	15
15	5	160	9

A.1 Response Surface Regression (Full Quadratic): Lignin Yield versus pH, Temperature, and Time

Table A.3 Coded coefficients of each term in the RSR model of lignin yield.

Term	Coef	SE Coef	T-Value	P-Value	VIF
Constant	77.86	1.07	72.87	0.000	
pH	-5.595	0.654	-8.55	0.000	1.00
Temperature	1.195	0.654	1.83	0.127	1.00
Time	0.234	0.654	0.36	0.736	1.00
pH×pH	-0.040	0.963	-0.04	0.968	1.01
Temperature×Temperature	-0.699	0.963	-0.73	0.500	1.01
Time×Time	0.785	0.963	0.81	0.452	1.01
pH×Temperature	0.348	0.925	0.38	0.722	1.00
pH×Time	0.611	0.925	0.66	0.538	1.00
Temperature×Time	0.055	0.925	0.06	0.955	1.00

Table A.4 R^2, $R^2_{(adj)}$, and $R^2_{(pred)}$ values of the RSR model of lignin yield.

R^2	$R^2_{(adj)}$	$R^2_{(pred)}$
94.01%	83.22%	64.34%

Table A.5 Analysis of variance of terms in the RSR model of lignin yield.

Source	DF	Adj SS	Adj MS	F-Value	P-Value
Model	9	268.716	29.857	8.72	0.014
Linear	3	262.298	87.433	25.52	0.002
pH	1	250.437	250.437	73.11	0.000
Temperature	1	11.424	11.424	3.33	0.127
Time	1	0.437	0.437	0.13	0.736
Square	3	4.427	1.476	0.43	0.740
pH×pH	1	0.006	0.006	0.00	0.968
Temperature×Temperature	1	1.806	1.806	0.53	0.500
Time×Time	1	2.275	2.275	0.66	0.452
2-Way Interaction	3	1.991	0.664	0.19	0.896
pH×Temperature	1	0.486	0.486	0.14	0.722
pH×Time	1	1.493	1.493	0.44	0.538
Temperature×Time	1	0.012	0.012	0.00	0.955
Error	5	17.128	3.426		
Lack-of-Fit	3	4.610	1.537	0.25	0.860
Pure Error	2	12.519	6.259		
Total	14	285.844			

Model A.1 The RSR model for the prediction of lignin yield.

$$\begin{aligned}\text{Lignin Yield} = {} & 48.6 - 4.55\ \text{pH} + 0.572\ \text{Temperature} - 0.68\ \text{Time} \\ & - 0.010\ \text{pH}\times\text{pH} \\ & - 0.00175\ \text{Temperature}\times\text{Temperature} + 0.0218\ \text{Time}\times\text{Time} \\ & + 0.0087\ \text{pH}\times\text{Temperature} \\ & + 0.0509\ \text{pH}\times\text{Time} + 0.00046\ \text{Temperature}\times\text{Time}\end{aligned}$$

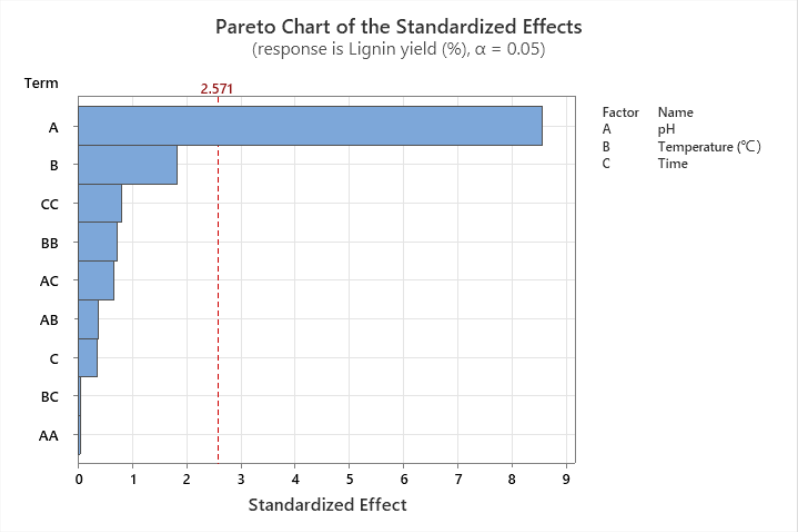

Figure A.1 Pareto chart of the standardized effects of each term in the RSR model on the lignin yield**.**

A.2 Response Surface Regression (Linear Terms): Lignin Yield versus pH, Temperature, and Time

Table A.6 Coded coefficients of each term in the linear model-1 of lignin yield.

Term	Coef	SE Coef	T-Value	P-Value	VIF
Constant	77.888	0.378	206.18	0.000	
pH	-5.595	0.517	-10.82	0.000	1.00
Temperature	1.195	0.517	2.31	0.041	1.00
Time	0.234	0.517	0.45	0.660	1.00

Table A.7 R^2, $R^2_{(adj)}$, and $R^2_{(pred)}$ values of the linear model-1 of lignin yield.

R^2	$R^2_{(adj)}$	$R^2_{(pred)}$
91.76%	89.52%	86.71%

Table A.8 Analysis of variance of terms in the linear model-1 of lignin yield.

Source	DF	Adj SS	Adj MS	F-Value	P-Value
Model	3	262.298	87.433	40.85	0.000
Linear	3	262.298	87.433	40.85	0.000
pH	1	250.437	250.437	117.00	0.000
Temperature	1	11.424	11.424	5.34	0.041
Time	1	0.437	0.437	0.20	0.660
Error	11	23.546	2.141		
Lack-of-Fit	9	11.028	1.225	0.20	0.967
Pure Error	2	12.519	6.259		
Total	14	285.844			

Model A.2 The linear model-1 for the prediction of lignin yield.

Lignin Yield = 81.97 - 2.798 pH + 0.0597 Temperature + 0.0390 Time

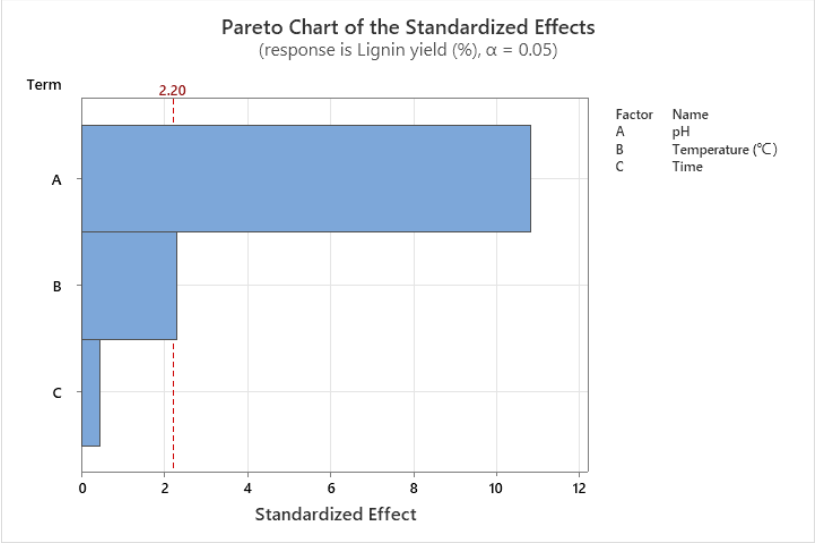

Figure A.2 Pareto chart of the standardized effects of each term in the linear model-1 on the lignin yield.

A.3 Response Surface Regression (Linear Terms): Lignin yield versus pH, Temperature

Table A.9 Coded coefficients of each term in the linear model-2 of lignin yield.

Term	Coef	SE Coef	T-Value	P-Value	VIF
Constant	77.888	0.365	213.38	0.000	
pH	-5.595	0.500	-11.19	0.000	1.00
Temperature	1.195	0.500	2.39	0.034	1.00

Table A.10 R^2, $R^2_{(adj)}$, and $R^2_{(pred)}$ values of the linear model-2 of lignin yield.

R^2	$R^2_{(adj)}$	$R^2_{(pred)}$
91.61%	90.21%	87.83%

Table A.11 Analysis of variance of terms in the linear model-2 of lignin yield.

Source	DF	Adj SS	Adj MS	F-Value	P-Value
Model	2	261.86	130.930	65.51	0.000
Linear	2	261.86	130.930	65.51	0.000
pH	1	250.44	250.437	125.31	0.000
Temperature	1	11.42	11.424	5.72	0.034
Error	12	23.98	1.999		
Lack-of-Fit	10	11.46	1.146	0.18	0.975
Pure Error	2	12.52	6.259		
Total	14	285.84			

Model A.3 The linear model-2 for the prediction of lignin yield.

Lignin Yield = 82.32 - 2.798 pH + 0.0597 Temperature

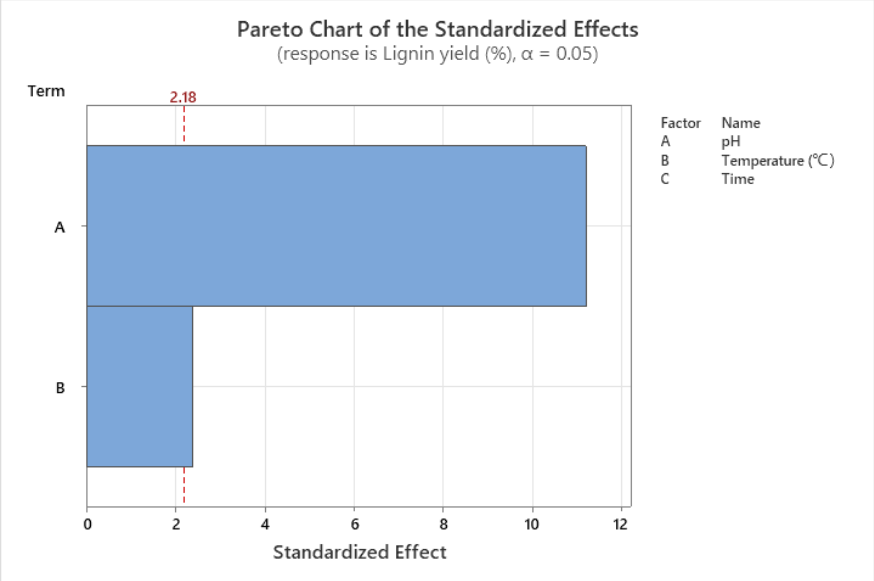

Figure A.3 Pareto chart of the standardized effects of each term in the linear model-2 on the lignin yield.

A.4 Response Surface Regression (Full Quadratic): Mn versus pH, Temperature, Time

Table A.12 Coded coefficients of each term in the RSR model of Mn of lignin.

Term	Coef	SE Coef	T-Value	P-Value	VIF
Constant	1230.7	22.0	56.05	0.000	
pH	-144.5	13.4	-10.75	0.000	1.00
Temperature	-69.0	13.4	-5.13	0.004	1.00
Time	-4.8	13.4	-0.35	0.738	1.00
pH×pH	-122.6	19.8	-6.19	0.002	1.01
Temperature×Temperature	-16.1	19.8	-0.81	0.453	1.01
Time×Time	23.4	19.8	1.18	0.290	1.01
pH×Temperature	-2.0	19.0	-0.11	0.920	1.00
pH×Time	-5.5	19.0	-0.29	0.784	1.00
Temperature×Time	5.5	19.0	0.29	0.784	1.00

Table A.13 R^2, $R^2_{(adj)}$, and $R^2_{(pred)}$ values of the RSR model of Mn of lignin.

R^2	$R^2_{(adj)}$	$R^2_{(pred)}$
97.35%	92.57%	59.60%

Table A.14 Analysis of variance of terms in the RSR model of Mn of lignin.

Source	DF	Adj SS	Adj MS	F-Value	P-Value
Model	9	265361	29485	20.39	0.002
Linear	3	205311	68437	47.32	0.000
pH	1	167042	167042	115.50	0.000

Temperature	1	38088	38088	26.34	0.004
Time	1	181	181	0.12	0.738
Square	3	59793	19931	13.78	0.007
pH×pH	1	55483	55483	38.36	0.002
Temperature × Temperature	1	955	955	0.66	0.453
Time×Time	1	2025	2025	1.40	0.290
2-Way Interaction	3	258	86	0.06	0.979
pH× Temperature	1	16	16	0.01	0.920
pH×Time	1	121	121	0.08	0.784
Temperature ×Time	1	121	121	0.08	0.784
Error	5	7231	1446		
Lack-of-Fit	3	6826	2275	11.25	0.083
Pure Error	2	405	202		
Total	14	272592			

Model A.4 The RSR model for the prediction of Mn of lignin.

Mn = 414 + 246.3 pH + 9.3 Temperature - 17.5 Time - 30.65 pH×pH
- 0.0402 Temperature × Temperature + 0.650 Time×Time
- 0.050 pH× Temperature - 0.46 pH×Time + 0.046 Temperature ×Time

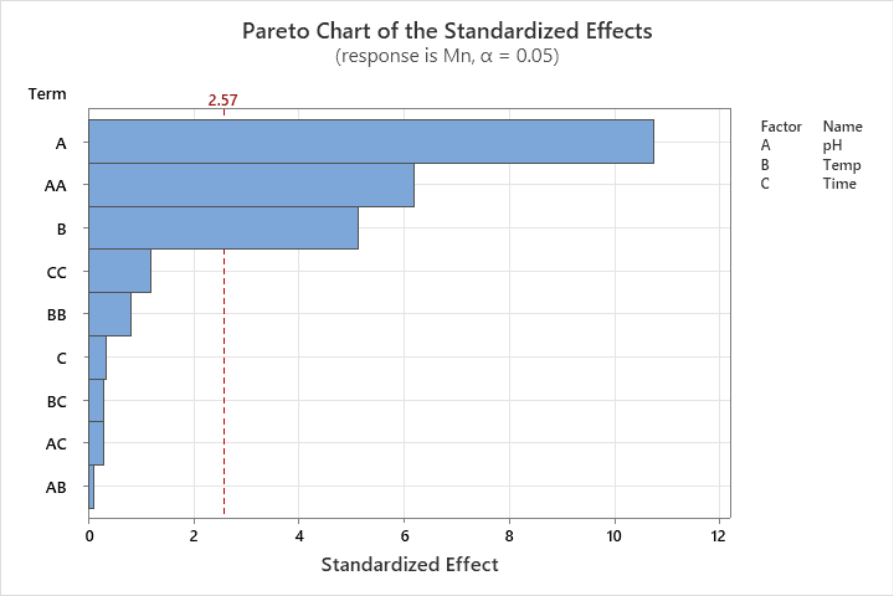

Figure A.4 Pareto chart of the standardized effects of each term in the RSR model on the lignin's Mn.

A.5 Response Surface Regression: Mn versus pH, Temperature

Table A.15 Coded coefficients of each term in the optimized model of Mn of lignin.

Term	Coef	SE Coef	T-Value	P-Value	VIF
Constant	1234.9	11.9	103.87	0.000	
pH	-144.5	11.1	-12.99	0.000	1.00
Temperature	-69.0	11.1	-6.20	0.000	1.00
pH×pH	-123.1	16.3	-7.56	0.000	1.00

Table A.16 R^2, $R^2_{(adj)}$, and $R^2_{(pred)}$ values of the optimized model of Mn of lignin.

R^2	$R^2_{(adj)}$	$R^2_{(pred)}$
96.01%	94.92%	91.54%

Table A.17 Analysis of variance of terms in the optimized model of Mn of lignin.

Source	DF	Adj SS	Adj MS	F-Value	P-Value
Model	3	261710	87237	88.18	0.000
Linear	2	205130	102565	103.67	0.000
pH	1	167042	167042	168.85	0.000
Temperature	1	38088	38088	38.50	0.000
Square	1	56580	56580	57.19	0.000
pH×pH	1	56580	56580	57.19	0.000
Error	11	10882	989		
Lack-of-Fit	9	10478	1164	5.75	0.157
Pure Error	2	405	202		

Total	14	272592	

Model A.5 The optimized model for the prediction of Mn of lignin.

Mn = 1379 + 235.5 pH - 3.450 Temperature - 30.78 pH×pH

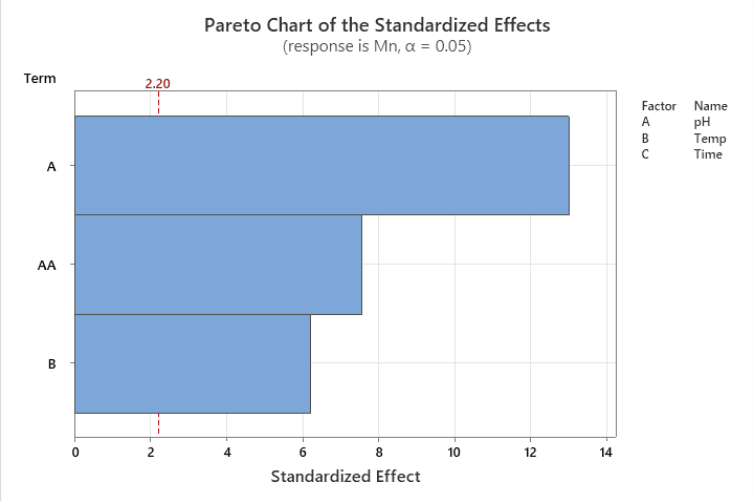

Figure A.5 Pareto chart of the standardized effects of each term in the optimized model on the lignin' s Mn.

A.6 Response Surface Regression (Full Quadratic): Mw versus pH, Temperature, Time

Table A.18 Coded coefficients of each term in the RSR model of Mw of lignin.

Term	Coef	SE Coef	T-Value	P-Value	VIF
Constant	2790	127	21.92	0.000	
pH	-670.8	77.9	-8.61	0.000	1.00
Temperature	-214.8	77.9	-2.76	0.040	1.00
Time	11.7	77.9	0.15	0.886	1.00
pH×pH	-333	115	-2.90	0.034	1.01
Temperature × Temperature	-67	115	-0.59	0.583	1.01
Time×Time	22	115	0.19	0.854	1.01
pH× Temperature	-53	110	-0.48	0.649	1.00
pH×Time	-8	110	-0.07	0.947	1.00
Temperature ×Time	-55	110	-0.50	0.637	1.00

Table A.19 R^2, $R^2_{(adj)}$, and $R^2_{(pred)}$ values of the RSR model of Mw of lignin.

R^2	$R^2_{(adj)}$	$R^2_{(pred)}$
94.79%	85.41%	33.75%

Table A.20 Analysis of variance of terms in the RSR model of Mw of lignin.

Source	DF	Adj SS	Adj MS	F-Value	P-Value
Model	9	4417890	490877	10.11	0.010
Linear	3	3969290	1323097	27.24	0.002
pH	1	3599245	3599245	74.11	0.000

Temperature	1	368940	368940	7.60	0.040
Time	1	1105	1105	0.02	0.886
Square	3	424808	141603	2.92	0.140
pH×pH	1	408719	408719	8.42	0.034
Temperature × Temperature	1	16678	16678	0.34	0.583
Time×Time	1	1835	1835	0.04	0.854
2-Way Interaction	3	23793	7931	0.16	0.917
pH× Temperature	1	11342	11342	0.23	0.649
pH×Time	1	240	240	0.00	0.947
Temperature ×Time	1	12210	12210	0.25	0.637
Error	5	242845	48569		
Lack-of-Fit	3	184812	61604	2.12	0.336
Pure Error	2	58033	29016		
Total	14	4660735			

Model A.6 The RSR model for the prediction of Mw of lignin.

Mw = -1921 + 715 pH + 53.8 Temperature + 68 Time - 83.2 pH×pH
- 0.168 Temperature × Temperature + 0.62 Time×Time- 1.33 pH× Temperature
- 0.65 pH×Time - 0.460 Temperature ×Time

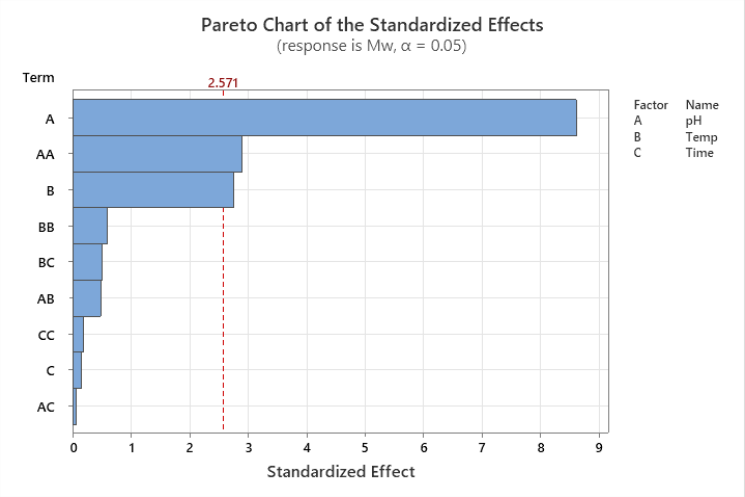

Figure A.6 Pareto chart of the standardized effects of each term in the RSR model on the lignin' s Mw.

A.7 Response Surface Regression: Mw versus pH, Temperature

Table A.21 Coded coefficients of each term in the optimized model of Mw of lignin.

Term	Coef	SE Coef	T-Value	P-Value	VIF
Constant	2764.0	61.1	45.26	0.000	
pH	-670.8	57.1	-11.74	0.000	1.00
Temperature	-214.8	57.1	-3.76	0.003	1.00
pH×pH	-329.5	83.6	-3.94	0.002	1.00

Table A.22 R^2, $R^2_{(adj)}$, and $R^2_{(pred)}$ values of the optimized model of Mw of lignin.

S	R^2	$R^2_{(adj)}$	$R^2_{(pred)}$
161.589	93.84%	92.16%	87.51%

Table A.23 Analysis of variance of terms in the optimized model of Mw of lignin.

Source	DF	Adj SS	Adj MS	F-Value	P-Value
Model	3	4373514	1457838	55.83	0.000
Linear	2	3968185	1984092	75.99	0.000
pH	1	3599244	3599244	137.84	0.000
Temperature	1	368940	368940	14.13	0.003
Square	1	405329	405329	15.52	0.002
pH×pH	1	405329	405329	15.52	0.002
Error	11	287221	26111		
Lack-of-Fit	9	229188	25465	0.88	0.638
Pure Error	2	58033	29016		

Total	14	4660735

Model A.7 The optimized model for the prediction of Mw of lignin.

$$Mw = 4100 + 488\ pH - 10.74\ Temperature - 82.4\ pH \times pH$$

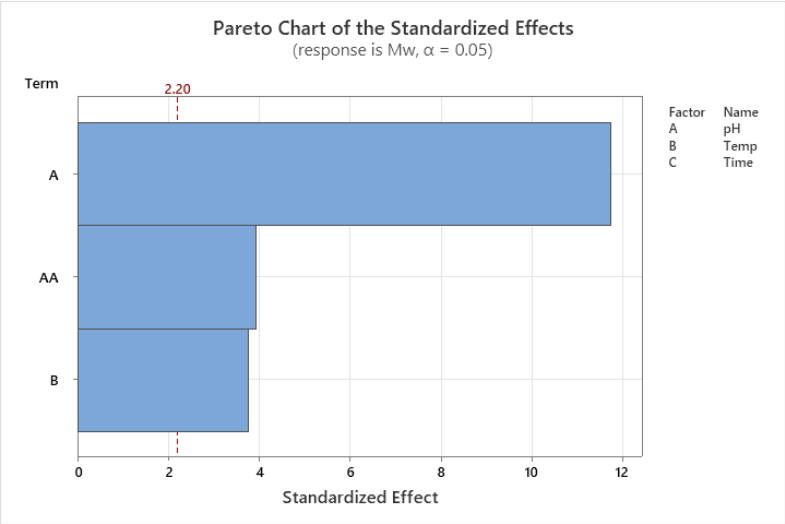

Figure A.7 Pareto chart of the standardized effects of each term in the optimized model on the lignin' s Mw.

A.8 Response Surface Regression (Full Quadratic): PDI versus pH, Temperature, Time

Table A.24 Coded coefficients of each term in the RSR model of PDI of lignin.

Term	Coef	SE Coef	T-Value	P-Value	VIF
Constant	2.2667	0.0801	28.31	0.000	
pH	-0.3250	0.0490	-6.63	0.001	1.00
Temperature	-0.0563	0.0490	-1.15	0.303	1.00
Time	0.0163	0.0490	0.33	0.754	1.00
pH×pH	-0.0896	0.0722	-1.24	0.270	1.01
Temperature×Temperature	-0.0271	0.0722	-0.38	0.723	1.01
Time×Time	-0.0321	0.0722	-0.44	0.675	1.01
pH×Temperature	-0.0550	0.0694	-0.79	0.464	1.00
pH×Time	0.0050	0.0694	0.07	0.945	1.00
Temperature×Time	-0.0525	0.0694	-0.76	0.483	1.00

Table A.25 R^2, $R^2_{(adj)}$, and $R^2_{(pred)}$ values of the RSR model of PDI of lignin.

R^2	$R^2_{(adj)}$	$R^2_{(pred)}$
90.62%	73.73%	10.58%

Table A.26 Analysis of variance of terms in the RSR model of PDI of lignin.

Source	DF	Adj SS	Adj MS	F-Value	P-Value
Model	9	0.92890	0.103211	5.36	0.039
Linear	3	0.87243	0.290808	15.12	0.006
pH	1	0.84500	0.845000	43.92	0.001

Temperature	1	0.02531	0.025313	1.32	0.303
Time	1	0.00211	0.002112	0.11	0.754
Square	3	0.03325	0.011084	0.58	0.655
pH×pH	1	0.02963	0.029631	1.54	0.270
Temperature×Temperature	1	0.00271	0.002708	0.14	0.723
Time×Time	1	0.00380	0.003801	0.20	0.675
2-Way Interaction	3	0.02322	0.007742	0.40	0.758
pH×Temperature	1	0.01210	0.012100	0.63	0.464
pH×Time	1	0.00010	0.000100	0.01	0.945
Temperature×Time	1	0.01102	0.011025	0.57	0.483
Error	5	0.09619	0.019238		
Lack-of-Fit	3	0.05092	0.016975	0.75	0.615
Pure Error	2	0.04527	0.022633		
Total	14	1.02509			

Model A.8 The RSR model for the prediction of PDI of lignin.

PDI = -0.57 + 0.278 pH + 0.0297 Temperature + 0.087 Time - 0.0224 pH×pH
- 0.000068 Temperature×Temperature
- 0.00089 Time×Time - 0.00137 pH×Temperature + 0.00042 pH×Time
- 0.000437 Temperature×Time

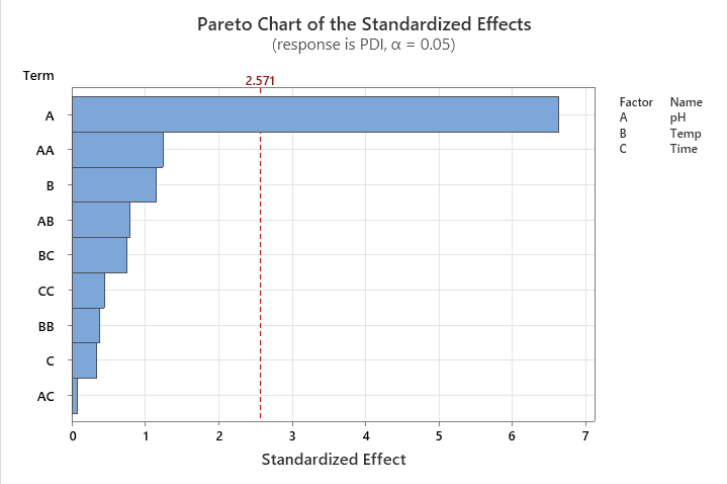

Figure S8. Pareto chart of the standardized effects of each term in the RSR model on the lignin' s PDI.

A.9 Response Surface Regression: PDI versus pH

Table A.27 Coded coefficients of each term in the optimized model of PDI of lignin.

Term	Coef	SE Coef	T-Value	P-Value	VIF
Constant	2.1873	0.0304	71.98	0.000	
pH	-0.3250	0.0416	-7.81	0.000	1.00

Table A.28 R^2, $R^2_{(adj)}$, and $R^2_{(pred)}$ values of the optimized model of PDI of lignin.

R^2	$R^2_{(adj)}$	$R^2_{(pred)}$
82.43%	81.08%	78.81%

Table A.29 Analysis of variance of terms in the optimized model of PDI of lignin.

Source	DF	Adj SS	Adj MS	F-Value	P-Value
Model	1	0.84500	0.84500	61.00	0.000
Linear	1	0.84500	0.84500	61.00	0.000
pH	1	0.84500	0.84500	61.00	0.000
Error	13	0.18009	0.01385		
Lack-of-Fit	11	0.13483	0.01226	0.54	0.797
Pure Error	2	0.04527	0.02263		
Total	14	1.02509			

Model A.9 The optimized model for the prediction of PDI of lignin.

$$PDI = 3.000 - 0.1625\ pH$$

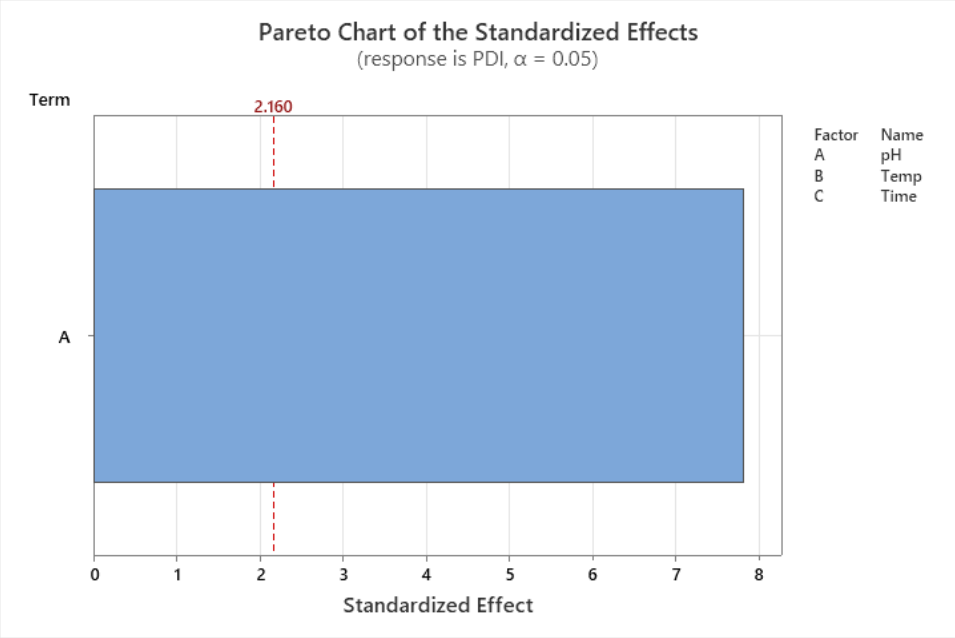

Figure S9. Pareto chart of the standardized effects of each term in the optimized model on the lignin' s PDI.

A.10 Regression Analysis: Experimental Mn versus Experimental Mw

Model A.10 The model for the prediction of experimental Mn of lignin using experimental Mw of lignin.

$$Mn = 92 + 0.646\ Mw - 0.000085\ Mw \times Mw$$

Table A.30 Coefficients of the terms in the Model A.10.

Term	Coef	SE Coef	T-Value	P-Value	VIF
Constant	92	276	0.33	0.745	
Mw	0.646	0.237	2.73	0.018	177.83
Mw×Mw	-0.000085	0.000048	-1.76	0.104	177.83

Table A.31 R^2, $R^2_{(adj)}$, and $R^2_{(pred)}$ values of Model A.10.

R^2	$R^2_{(adj)}$	$R^2_{(pred)}$
93.54%	92.46%	91.69%

Table A.32 Analysis of variance of terms in the Model A.10.

Source	DF	Adj SS	Adj MS	F-Value	P-Value
Regression	2	254974	127487	86.83	0.000
Mw	1	10951	10951	7.46	0.018
Mw×Mw	1	4531	4531	3.09	0.104
Error	12	17618	1468		
Total	14	272592			

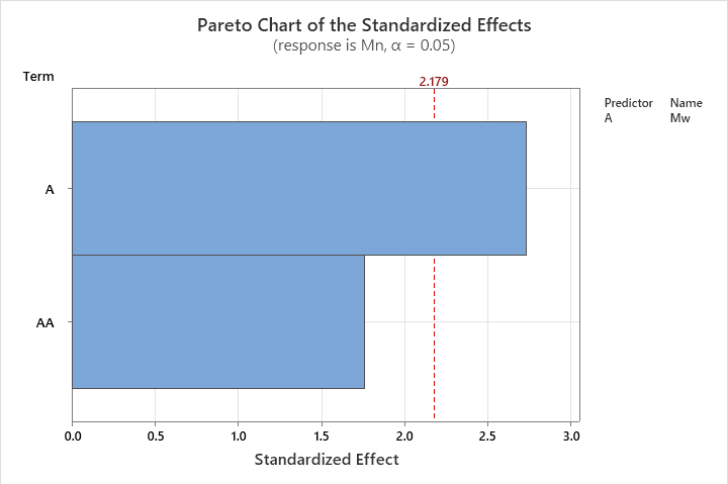

Figure S10. Pareto chart of the standardized effects of each term in the Model A. 10 on the experimental Mn.

A.11 Regression Analysis: Experimental PDI versus Experimental Mw

Model A.11 The model for the prediction of experimental PDI of lignin using experimental Mw of lignin.

PDI = 1.405 + 0.000113 Mw + 0.000000 Mw×Mw

Table A.33 Coefficients of terms in the Model A.11.

Term	Coef	SE Coef	T-Value	P-Value	VIF
Constant	1.405	0.520	2.70	0.019	
Mw	0.000113	0.000446	0.25	0.804	177.83
Mw×Mw	0.000000	0.000000	0.77	0.459	177.83

Table A.34 R^2, $R^2_{(adj)}$, and $R^2_{(pred)}$ values of the Model A.11.

R^2	$R^2_{(adj)}$	$R^2_{(pred)}$
93.89%	92.87%	92.14%

Table A.35 Analysis of variance of terms in the Model A.11.

Source	DF	Adj SS	Adj MS	F-Value	P-Value
Regression	2	0.96245	0.481226	92.19	0.000
Mw	1	0.00034	0.000336	0.06	0.804
Mw×Mw	1	0.00305	0.003055	0.59	0.459
Error	12	0.06264	0.005220		
Total	14	1.02509			

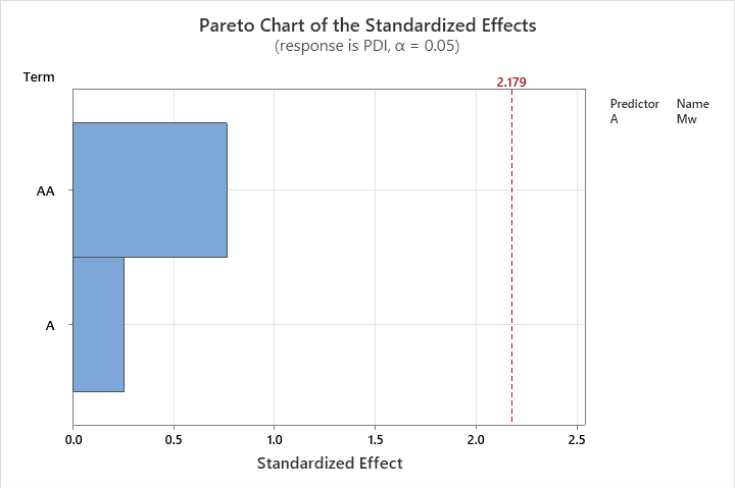

Figure A.11 Pareto chart of the standardized effects of each term in the Model A.11 on the experimental PDI.

A.12 Regression Analysis: Experimental PDI versus Experimental Mn

Model A.12 The model for the prediction of experimental PDI of lignin using experimental Mn of lignin.

PDI = -3.26 + 0.00796 Mn - 0.000003 Mn×Mn

Table A.36 Coefficients of terms in the Model A.12.

Term	Coef	SE Coef	T-Value	P-Value	VIF
Constant	-3.26	3.18	-1.03	0.325	
Mn	0.00796	0.00569	1.40	0.187	430.18
Mn×Mn	-0.000003	0.000003	-1.11	0.289	430.18

Table A.37 R^2, $R^2_{(adj)}$, and $R^2_{(pred)}$ values of the Model A.12.

R^2	$R^2_{(adj)}$	$R^2_{(pred)}$
76.00%	72.00%	59.67%

Table A.38 Analysis of variance of terms in the Model A.12.

Source	DF	Adj SS	Adj MS	F-Value	P-Value
Regression	2	0.77905	0.38952	19.00	0.000
Mn	1	0.04019	0.04019	1.96	0.187
Mn×Mn	1	0.02522	0.02522	1.23	0.289
Error	12	0.24605	0.02050		
Total	14	1.02509			

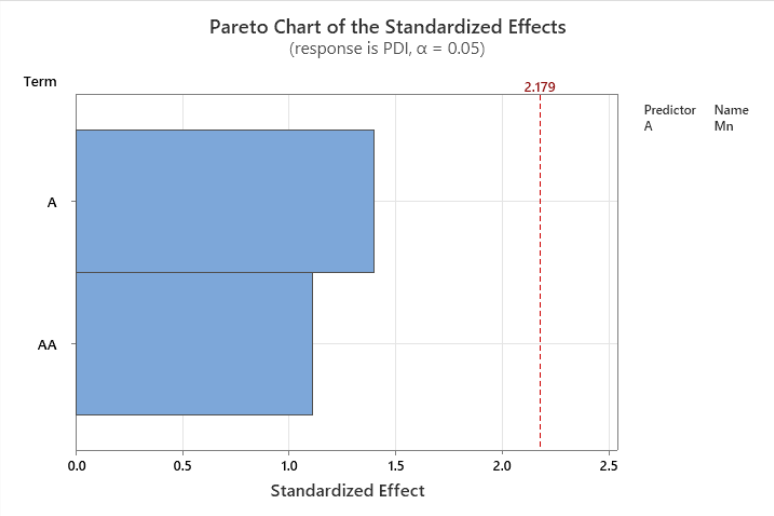

Figure A.12 Pareto chart of the standardized effects of each term in Model A.12 on the experimental PDI.

A.13 Computational Simulation of Mn, Mw, and PDI Values of Kraft Lignin

Table A.39 Simulated Mn values of Kraft lignin generated by Model A.5.

pH \ °C	140	150	160	170	180
3.0	1349	1315	1280	1246	1211
3.2	1360	1326	1291	1257	1222
3.4	1368	1334	1299	1265	1230
3.6	1374	1339	1305	1270	1236
3.8	1377	1342	1308	1273	1239
4.0	1378	1343	1309	1274	1240
4.2	1376	1341	1307	1272	1238
4.4	1371	1337	1302	1268	1233
4.6	1365	1330	1296	1261	1227
4.8	1356	1321	1287	1252	1218
5.0	1344	1310	1275	1241	1206
5.2	1330	1295	1261	1226	1192
5.4	1313	1279	1244	1210	1175
5.6	1294	1260	1225	1191	1156
5.8	1273	1238	1204	1169	1135
6.0	1249	1214	1180	1145	1111
6.2	1223	1188	1154	1119	1085
6.4	1194	1159	1125	1090	1056

6.6	1162	1128	1093	1059	1024
6.8	1129	1094	1060	1025	991
7.0	1092	1058	1023	989	954

Table A.40 Simulated Mw values of Kraft lignin generated by Model A.7.

°C / pH	**140**	**150**	**160**	**170**	**180**
3.0	3319	3211	3104	2997	2889
3.2	3314	3207	3099	2992	2885
3.4	3303	3196	3088	2981	2873
3.6	3285	3178	3070	2963	2856
3.8	3261	3154	3046	2939	2831
4.0	3230	3123	3015	2908	2800
4.2	3192	3085	2978	2870	2763
4.4	3148	3041	2934	2826	2719
4.6	3098	2990	2883	2775	2668
4.8	3040	2933	2826	2718	2611
5.0	2976	2869	2762	2654	2547
5.2	2906	2799	2691	2584	2476
5.4	2829	2721	2614	2507	2399
5.6	2745	2638	2530	2423	2316
5.8	2655	2547	2440	2333	2225
6.0	2558	2451	2343	2236	2128
6.2	2455	2347	2240	2132	2025

6.4	2344	2237	2130	2022	1915
6.6	2228	2120	2013	1906	1798
6.8	2105	1997	1890	1782	1675
7.0	1975	1867	1760	1653	1545

Table A.41 Simulated PDI values of Kraft lignin based on the simulated Mn and Mw values using the equation (3) in the main text.

pH \ **℃**	**140**	**150**	**160**	**170**	**180**
3.0	2.5	2.4	2.4	2.4	2.4
3.2	2.4	2.4	2.4	2.4	2.4
3.4	2.4	2.4	2.4	2.4	2.3
3.6	2.4	2.4	2.4	2.3	2.3
3.8	2.4	2.3	2.3	2.3	2.3
4.0	2.3	2.3	2.3	2.3	2.3
4.2	2.3	2.3	2.3	2.3	2.2
4.4	2.3	2.3	2.3	2.2	2.2
4.6	2.3	2.2	2.2	2.2	2.2
4.8	2.2	2.2	2.2	2.2	2.1
5.0	2.2	2.2	2.2	2.1	2.1
5.2	2.2	2.2	2.1	2.1	2.1
5.4	2.2	2.1	2.1	2.1	2.0
5.6	2.1	2.1	2.1	2.0	2.0
5.8	2.1	2.1	2.0	2.0	2.0

6.0	2.0	2.0	2.0	2.0	1.9
6.2	2.0	2.0	1.9	1.9	1.9
6.4	2.0	1.9	1.9	1.9	1.8
6.6	1.9	1.9	1.8	1.8	1.8
6.8	1.9	1.8	1.8	1.7	1.7
7.0	1.8	1.8	1.7	1.7	1.6

A.14 Regression Analysis: Simulated Mn versus Simulated Mw

Model A.13 The model for the prediction of simulated Mn of lignin using simulated Mw of lignin.

Mn = 387.5 + 0.4384 Mw - 0.000044 Mw*Mw

Table A.42 Coefficients of terms in the Model A.13.

Term	Coef	SE Coef	T-Value	P-Value	VIF
Constant	387.5	72.7	5.33	0.000	
Mw	0.4384	0.0588	7.45	0.000	125.13
Mw*Mw	-0.000044	0.000012	-3.78	0.000	125.13

Table A.43 R^2, $R^2_{(adj)}$, and $R^2_{(pred)}$ values of Model A.13.

R^2	R^2 (adj)	R^2(pred)
94.39%	94.28%	94.16%

Table A.44 Analysis of variance of terms in Model A.13.

Source	DF	Adj SS	Adj MS	F-Value	P-Value
Regression	2	997400	498700	857.98	0.000
Mw	1	32292	32292	55.56	0.000
Mw*Mw	1	8310	8310	14.30	0.000
Error	102	59287	581		
Total	104	1056687			

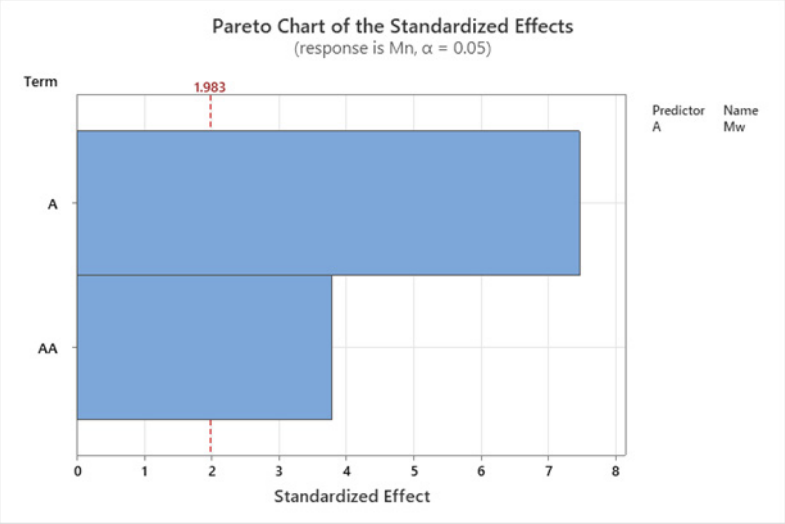

Figure A.13. Pareto chart of the standardized effects of each term in the Model A.13 on the simulated Mn.

A.15 Regression Analysis: Simulated PDI versus Simulated Mw

Model A.14 The model for the prediction of simulated PDI of lignin using simulated Mw of lignin.

PDI = 0.847 + 0.000515 Mw- 0.000000 Mw*Mw

Table A.45 Coefficients of terms in the Model A.14.

Term	Coef	SE Coef	T-Value	P-Value	VIF
Constant	0.847	0.128	6.62	0.000	
Mw	0.000515	0.000104	4.98	0.000	125.13
Mw*Mw	-0.000000	0.000000	-0.52	0.605	125.13

Table A.46 R^2, $R^2_{(adj)}$, and $R^2_{(pred)}$ values of Model A.14.

R^2	$R^2_{(adj)}$	$R^2_{(pred)}$
96.06%	95.98%	95.90%

Table A.47 Analysis of variance of terms in Model A.14.

Source	DF	Adj SS	Adj MS	F-Value	P-Value
Regression	2	4.48161	2.24081	1243.52	0.000
Mw	1	0.04461	0.04461	24.75	0.000
Mw*Mw	1	0.00049	0.00049	0.27	0.605
Error	102	0.18380	0.00180		
Total	104	4.66541			

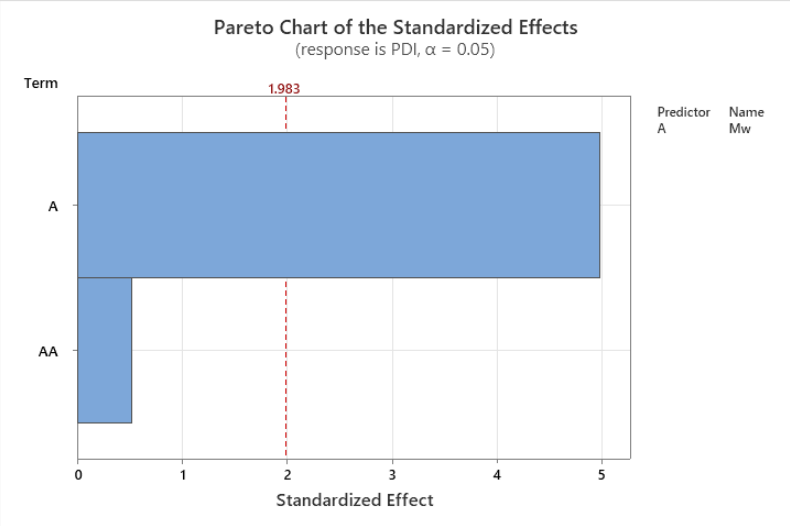

Figure A.14 Pareto chart of the standardized effects of each term in the Model A.14 on the simulated PDI.

A.16 Regression Analysis: Simulated PDI versus Simulated Mn

Model A.15 The model for the prediction of simulated PDI of lignin using simulated Mn of lignin.

PDI = -1.99 + 0.00491 Mn - 0.000001 Mn*Mn

Table A.48 Coefficients of terms in the Model A.15.

Term	Coef	SE Coef	T-Value	P-Value	VIF
Constant	-1.99	1.10	-1.81	0.073	
Mn	0.00491	0.00184	2.66	0.009	432.62
Mn*Mn	-0.000001	0.000001	-1.64	0.105	432.62

Table A.49 R^2, $R^2_{(adj)}$, and $R^2_{(pred)}$ values of Model A.15.

R^2	$R^2_{(adj)}$	$R^2_{(pred)}$
81.86%	81.50%	81.06%

Table A.50 Analysis of variance of terms in Model A.15.

Source	DF	Adj SS	Adj MS	F-Value	P-Value
Regression	2	3.81913	1.90956	230.15	0.000
Mn	1	0.05888	0.05888	7.10	0.009
Mn*Mn	1	0.02224	0.02224	2.68	0.105
Error	102	0.84628	0.00830		
Total	104	4.66541			

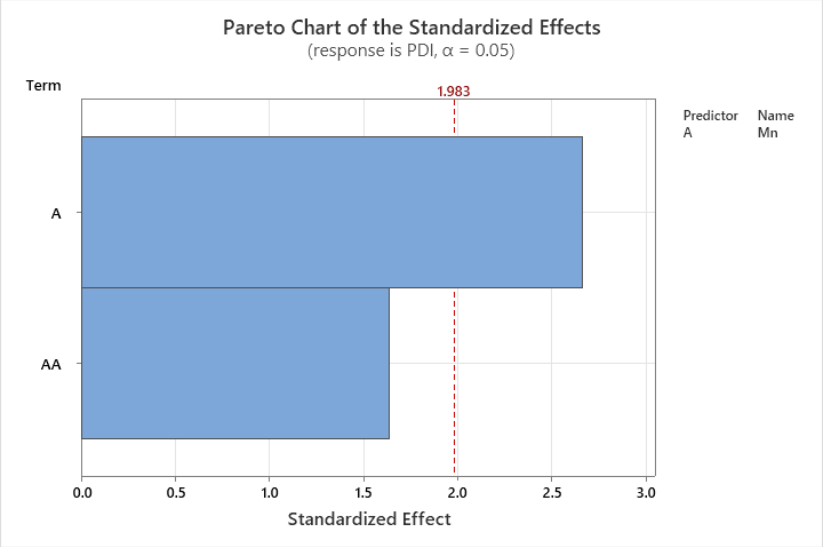

Figure S15. Pareto chart of the standardized effects of each term in the Model A.15 on the simulated PDI.

A.17 Response Surface Regression (Full Quadratic): Phenolic OH versus pH, Temperature, Time

Table A.51 Coded coefficients of terms in the RSR model of phenolic OH content of lignin.

Term	Coef	SE Coef	T-Value	P-Value	VIF
Constant	0.865	0.216	4.02	0.010	
pH	-0.111	0.132	-0.84	0.440	1.00
Temperature	-0.094	0.132	-0.72	0.506	1.00
Time	0.059	0.132	0.45	0.673	1.00
pH×pH	0.419	0.194	2.16	0.084	1.01
Temperature×Temperature	0.362	0.194	1.86	0.121	1.01
Time×Time	-0.362	0.194	-1.86	0.121	1.01
pH×Temperature	0.641	0.187	3.43	0.019	1.00
pH×Time	0.061	0.187	0.33	0.758	1.00
Temperature×Time	-0.190	0.187	-1.02	0.356	1.00

Table A.52 R^2, $R^2_{(adj)}$, and $R^2_{(pred)}$ values of the RSR model of phenolic OH content of lignin.

R^2	$R^2_{(adj)}$	$R^2_{(pred)}$
84.16%	55.66%	0.00%

Table A.53 Analysis of variance of terms in the RSR model of phenolic OH content of lignin.

Source	DF	Adj SS	Adj MS	F-Value	P-Value
Model	9	3.70264	0.41140	2.95	0.123

Linear	3	0.19714	0.06571	0.47	0.715
pH	1	0.09780	0.09780	0.70	0.440
Temperature	1	0.07132	0.07132	0.51	0.506
Time	1	0.02801	0.02801	0.20	0.673
Square	3	1.70444	0.56815	4.08	0.082
pH×pH	1	0.64776	0.64776	4.65	0.084
Temperature×Temperature	1	0.48447	0.48447	3.48	0.121
Time×Time	1	0.48429	0.48429	3.48	0.121
2-Way Interaction	3	1.80106	0.60035	4.31	0.075
pH×Temperature	1	1.64230	1.64230	11.79	0.019
pH×Time	1	0.01475	0.01475	0.11	0.758
Temperature×Time	1	0.14400	0.14400	1.03	0.356
Error	5	0.69667	0.13933		
Lack-of-Fit	3	0.48509	0.16170	1.53	0.419
Pure Error	2	0.21158	0.10579		
Total	14	4.39931			

Model A.16 The RSR model for the prediction of phenolic OH content of lignin.

Phenolic OH = 37.6 - 3.711 pH - 0.360 Temperature + 0.419 Time + 0.1047 pH×pH
+ 0.000906 Temperature×Temperature
- 0.01006 Time×Time + 0.01602 pH×Temperature + 0.0051 pH×Time
- 0.00158 Temperature×Time

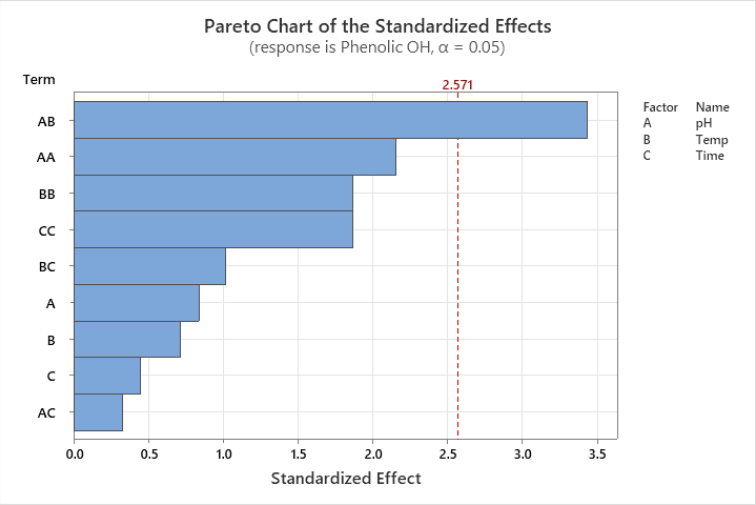

Figure A.16 Pareto chart of the standardized effects of each term in the RSR model on the phenolic OH content.

A.18 Response Surface Regression (Full Quadratic): C5/G OH versus pH, Temperature, Time

Table A.54 Coded coefficients of terms in the RSR model of C5/G OH content of lignin.

Term	Coef	SE Coef	T-Value	P-Value	VIF
Constant	4.260	0.511	8.33	0.000	
pH	-0.097	0.313	-0.31	0.769	1.00
Temperature	0.301	0.313	0.96	0.381	1.00
Time	0.355	0.313	1.13	0.308	1.00
pH×pH	-0.677	0.461	-1.47	0.202	1.01
Temperature×Temperature	-0.197	0.461	-0.43	0.687	1.01
Time×Time	0.139	0.461	0.30	0.775	1.01
pH×Temperature	-0.113	0.443	-0.25	0.809	1.00
pH×Time	-0.028	0.443	-0.06	0.953	1.00
Temperature×Time	0.394	0.443	0.89	0.415	1.00

Table A.55 R^2, $R^2_{(adj)}$, and $R^2_{(pred)}$ values of the RSR model of C5/G OH content of lignin.

R^2	$R^2_{(adj)}$	$R^2_{(pred)}$
52.90%	0.00%	0.00%

Table A.56 Analysis of variance of terms in the RSR model of C5/G OH content of lignin.

Source	DF	Adj SS	Adj MS	F-Value	P-Value
Model	9	4.39993	0.48888	0.62	0.746
Linear	3	1.80703	0.60234	0.77	0.559

pH	1	0.07553	0.07553	0.10	0.769
Temperature	1	0.72425	0.72425	0.92	0.381
Time	1	1.00725	1.00725	1.29	0.308
Square	3	1.91933	0.63978	0.82	0.538
pH×pH	1	1.69024	1.69024	2.16	0.202
Temperature×Temperature	1	0.14321	0.14321	0.18	0.687
Time×Time	1	0.07113	0.07113	0.09	0.775
2-Way Interaction	3	0.67357	0.22452	0.29	0.834
pH×Temperature	1	0.05091	0.05091	0.06	0.809
pH×Time	1	0.00304	0.00304	0.00	0.953
Temperature×Time	1	0.61962	0.61962	0.79	0.415
Error	5	3.91805	0.78361		
Lack-of-Fit	3	0.07536	0.02512	0.01	0.997
Pure Error	2	3.84269	1.92135		
Total	14	8.31798			

Model A.17 The RSR model for the prediction of C5/G OH content of lignin.

C5/G OH = -12.6 + 2.11 pH + 0.157 Temperature - 0.524 Time - 0.169 pH×pH
- 0.00049 Temperature×Temperature
+ 0.0039 Time×Time - 0.0028 pH×Temperature - 0.0023 pH×Time
+ 0.00328 Temperature×Time

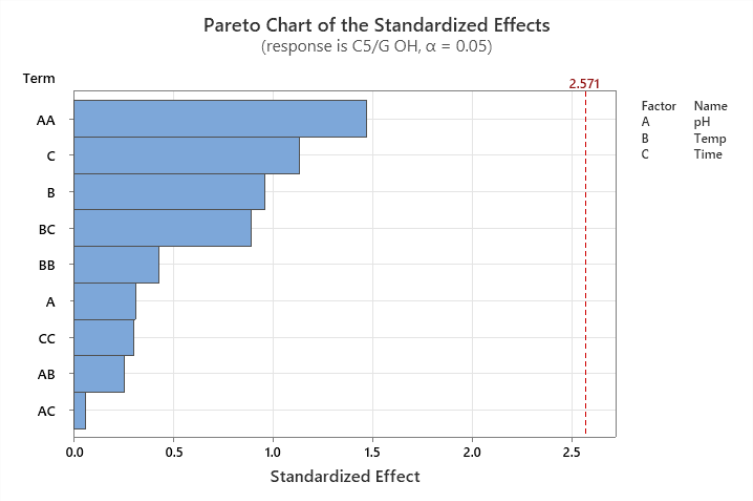

Figure A.17 Pareto chart of the standardized effects of each term in the RSR model on the C5/G OH content of lignin.

A.19 Response Surface Regression (Full Quadratic): Aliphatic OH versus pH, Temperature, Time

Table A.57 Coded coefficients of terms in the RSR model of aliphatic OH content of lignin.

Term	Coef	SE Coef	T-Value	P-Value	VIF
Constant	1.310	0.318	4.12	0.009	
pH	-0.006	0.195	-0.03	0.976	1.00
Temperature	-0.136	0.195	-0.70	0.516	1.00
Time	-0.029	0.195	-0.15	0.887	1.00
pH×pH	0.450	0.286	1.57	0.177	1.01
Temperature×Temperature	0.376	0.286	1.31	0.246	1.01
Time×Time	-0.482	0.286	-1.68	0.153	1.01
pH×Temperature	0.945	0.275	3.43	0.019	1.00
pH×Time	-0.193	0.275	-0.70	0.513	1.00
Temperature×Time	-0.037	0.275	-0.14	0.898	1.00

Table A.58 R^2, $R^2_{(adj)}$, and $R^2_{(pred)}$ values of the RSR model of aliphatic OH content of lignin.

R^2	$R^2_{(adj)}$	$R^2_{(pred)}$
80.25%	44.71%	0.00%

Table A.59 Analysis of variance of terms in the RSR model of aliphatic OH content of lignin.

Source	DF	Adj SS	Adj MS	F-Value	P-Value
Model	9	6.15308	0.68368	2.26	0.192

Linear	3	0.15511	0.05170	0.17	0.912
pH	1	0.00031	0.00031	0.00	0.976
Temperature	1	0.14799	0.14799	0.49	0.516
Time	1	0.00681	0.00681	0.02	0.887
Square	3	2.27436	0.75812	2.50	0.174
pH×pH	1	0.74765	0.74765	2.47	0.177
Temperature×Temperature	1	0.52231	0.52231	1.72	0.246
Time×Time	1	0.85855	0.85855	2.84	0.153
2-Way Interaction	3	3.72362	1.24121	4.10	0.081
pH×Temperature	1	3.56836	3.56836	11.78	0.019
pH×Time	1	0.14973	0.14973	0.49	0.513
Temperature×Time	1	0.00552	0.00552	0.02	0.898
Error	5	1.51409	0.30282		
Lack-of-Fit	3	1.24638	0.41546	3.10	0.253
Pure Error	2	0.26770	0.13385		
Total	14	7.66717			

Model A.18 The RSR model for the prediction of aliphatic OH content of lignin.

Aliphatic OH = 46.0 - 4.76 pH - 0.423 Temperature + 0.366 Time + 0.1125 pH×pH
+ 0.000940 Temperature×Temperature
- 0.01339 Time×Time + 0.02361 pH×Temperature - 0.0161 pH×Time
- 0.00031 Temperature×Time

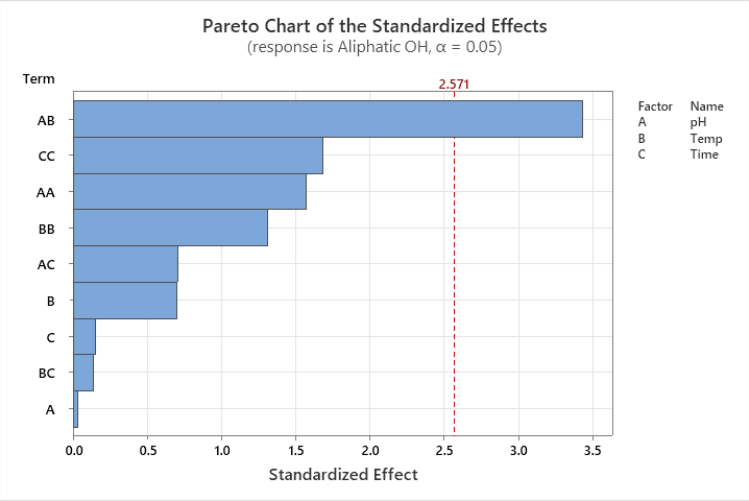

Figure A.18 Pareto chart of the standardized effects of each term in the RSR model on the aliphatic OH content of lignin.

A.20 Response Surface Regression (Full Quadratic): A/P OH versus pH, Temperature, Time

Table A.60 Coded coefficients of terms in the RSR model of A/P OH content of lignin.

Term	Coef	SE Coef	T-Value	P-Value	VIF
Constant	1.572	0.171	9.18	0.000	
pH	0.127	0.105	1.21	0.280	1.00
Temperature	-0.057	0.105	-0.54	0.613	1.00
Time	-0.135	0.105	-1.29	0.254	1.00
pH×pH	-0.206	0.154	-1.34	0.239	1.01
Temperature×Temperature	-0.092	0.154	-0.60	0.577	1.01
Time×Time	0.009	0.154	0.06	0.958	1.01
pH×Temperature	0.075	0.148	0.51	0.633	1.00
pH×Time	-0.266	0.148	-1.80	0.132	1.00
Temperature×Time	0.293	0.148	1.98	0.105	1.00

Table A.61 R^2, $R^2_{(adj)}$, and $R^2_{(pred)}$ values of the RSR model of A/P OH content of lignin.

S	R^2	$R^2_{(adj)}$	$R^2_{(pred)}$
0.296566	72.04%	21.71%	0.00%

Table A.62 Analysis of variance of of terms in the RSR model of A/P OH content of lignin.

Source	DF	Adj SS	Adj MS	F-Value	P-Value
Model	9	1.13309	0.125899	1.43	0.362

Linear	3	0.30070	0.100234	1.14	0.418
pH	1	0.12929	0.129287	1.47	0.280
Temperature	1	0.02557	0.025566	0.29	0.613
Time	1	0.14585	0.145848	1.66	0.254
Square	3	0.18227	0.060756	0.69	0.596
pH×pH	1	0.15742	0.157423	1.79	0.239
Temperature×Temperature	1	0.03123	0.031233	0.36	0.577
Time×Time	1	0.00027	0.000273	0.00	0.958
2-Way Interaction	3	0.65012	0.216707	2.46	0.177
pH×Temperature	1	0.02272	0.022716	0.26	0.633
pH×Time	1	0.28360	0.283596	3.22	0.132
Temperature×Time	1	0.34381	0.343810	3.91	0.105
Error	5	0.43976	0.087951		
Lack-of-Fit	3	0.04716	0.015722	0.08	0.965
Pure Error	2	0.39259	0.196296		
Total	14	1.57285			

Model A.19 The RSR model for the prediction of A/P OH content of lignin.

A/P OH = -1.2 + 0.478 pH + 0.039 Temperature - 0.307 Time - 0.0516 pH×pH
- 0.000230 Temperature×Temperature
+ 0.00024 Time×Time + 0.00188 pH×Temperature - 0.0222 pH×Time
+ 0.00244 Temperature×Time

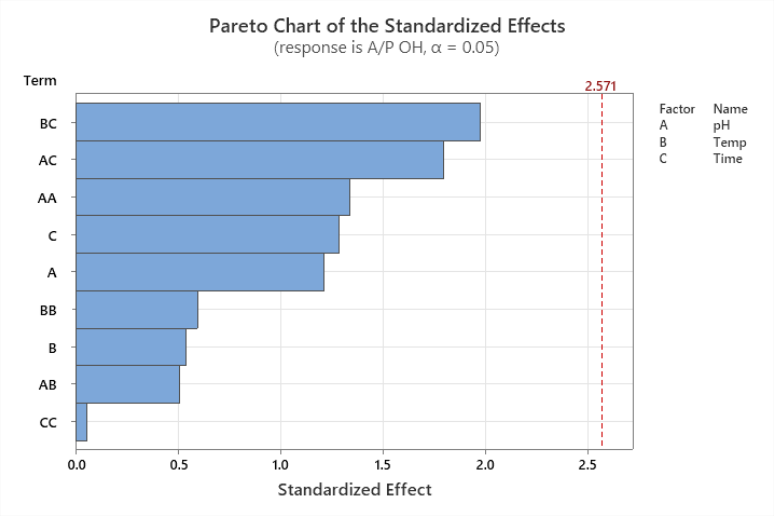

Figure S19. Pareto chart of the standardized effects of each term in the RSR Model on the A/P OH content of lignin.

B Life Cycle Assessment of the Lignin Recovery Processes

B.1 Abstract

In previous chapters, an acid-catalyzed liquefaction process was proposed to recover lignin directly from Kraft black liquor. Herein, Life Cycle Assessment (LCA) was performed on the processes based on the Cradle-to-Gate strategy to evaluate their environmental impacts, and they were compared with the fossil-based polyols. The results showed that process-2 (140 ℃, pH=7, and 9 min) with the lowest lignin recovery rate (70%) had lower greenhouse gas emissions and energy consumption than the process-1 (160 ℃, pH=3, and 3 min) with the highest lignin recovery rate (85%). The methanol, acetic acid, and heat used in the liquefaction processes were the major contributors to the environmental impacts. Also, if using lignin to replace fossil-based polyols to prepare flexible polyurethane foams, the process-2 lignin would be better a choice because it had less greenhouse gas emissions and similar energy consumption in comparison to the fossil-based polyols.

B.2 Introduction

As a typical petroleum-based product, polyurethane (PU) foams have extensively served in different fields of both industry and people's daily life thanks to their attractive features such as lightweight, unique mechanical performance (e.g., elasticity), and low thermal conductivity.[1-3] However, such a situation also raises growing concerns about the environmental impacts caused by PU foams since they consume a large amount of fossil-based chemicals and are difficult to recycle at the end-of-life of products.[4,5] To relieve this issue, partially replacing petroleum-based polyols with lignin was proposed to make lignin-

based PU foams as lignin contains plenty of hydroxyl groups which can react with isocyanate.[6-8]

So far, a few of Life Cycle Assessment (LCA) studies on the lignin-based PU foams have been reported. For example, Kulas et al. conducted a LCA on the Aqueous Lignin Purification with Hot Agents (ALPHA) process.[9] The ALPHA process was used to fractionate and purify the lignin from the ethanol production with corn stover as the raw material. The lignin fraction with low molecular weight was used to produce polyurethane foams. It was found that the use of ethanol in the ALPHA process resulted in lower greenhouse gas (GHG) emissions and energy consumption than acetic acid. Also, the GHG emissions and energy consumption of ethanol solvent lignin-based PU foams were similar to that of fossil-based PU foams due to the low replacement ratio (30 wt%) of lignin to fossil-based polyols. Another example is the LCA conducted by Manzardo et al. on the lignin-based rigid PU foams. (Ref.) It was found that the introduction of lignin in the formulations of PU foams leaded to up to 30% reduction in the GHG emissions and depletion of fossil resources.[10]

In previous chapters, a novel acid-catalyzed liquefaction process was developed to recover lignin directly from Kraft black liquor. In this process, the lignin was recovered using methanol and acetic acid with heating. Then, the lignin was directly used to replace 20 wt% fossil-based polyols in the formula of flexible PU foams. In this chapter, the life cycle assessment (LCA) of the lignin production processes was performed based on the Cradle-to-Gate strategy since the use and disposal stages were not considered in this study, and it

was compared with the fossil-based polyol for the flexible PU foams to show the differences of their environmental impacts on energy consumption and CO_2 emissions.

B.3 The Objectives of Life Cycle Assessment

The LCA aims at determining the environmental impacts of the production of lignin from the liquefaction processes with different parameters and making comparisons with that of fossil-based polyols. There are four objectives of the LCA. The first is to analyze the feasibility of the lignin production from the liquefaction process according to the LCA. The second goal is to optimize the parameters of the liquefaction process based on the LCA. The third is to quantify and compare the environmental impacts between the production process of lignin-based polyols and that of fossil-based polyols. The last goal is to outline the future development directions of lignin production and applications from environmental life cycle point-of-view.

B.4 The Scope of Life Cycle Assessment

This investigation was conducted based on the Cradle-to-Gate strategy including the stages from raw materials to products. In this study, fossil-based polyol was used as the reference to evaluate the environmental performance of the lignin. The raw material for the lignin recovery is black liquor which is a byproduct of the Kraft pulping process. The polyol was assumed as the polyol ether that is commonly used in the formula of the flexible PU foams. It was also assumed that the liquefaction process follows the Kraft pulping process in the same plant.

B.5 Functional Unit

As shown in Chapter 2, the recovered lignin could be used to directly replace 20 wt% fossil-based polyols in the formula of the flexible polyurethane foams without any modifications. Thus, the functional unit was defined as 1 kg polyols in this study.

B.6 Data Sources and Environmental Impact Categories

The data of Kraft pulping process originated from literature sources. Ecoinvent database provided the information of involved materials, chemicals, and energy. This assessment was simulated in the SimaPro 9.0 LCA software.

Environmental impact categories investigated in this study was global warming gas (CO_2) emission and energy consumption. The CO_2 emission (kg CO_2 eq) was simulated based on the IPCC GWP 100 assessment method; the cumulative energy demand of the processes was estimated using the Cumulative Energy Demand 1.1 methodology.

B.7 Assumptions

(1) The methanol and acetic acid used in the liquefaction processes can be recycled in industry, and their recovery rates were 95%. It is because previous chapters have verified that those chemicals reacted with the lignin and caused their mass loss.

(2) The water and chemicals (NaOH and Na_2S) used in the Kraft pulping processes can be recycled in industry, and their recovery rates were 90%.[11]

(3) The heat used in the liquefaction process can be recycled in industry. It should be noted that a paper published in 2000 mentioned the recovery rate of heat should be 25-45% when the temperature of hot stream is cooled.[12] In this study, the recovery rate of heat was assumed as 60% because heat recovery systems may have been improved over past

20 years.

(4) The residue after the liquefaction process can be burned to generate energy.

B.8 System Boundaries

The system boundary for the life cycle of assessment is shown in Figure B.1. In this study, the system boundary includes the Kraft pulping process, black liquor, and the liquefaction process. The mass allocation method was used to split up the environmental burden of Kraft pulping processes and liquefaction processes among different products. The details of the mass allocation are shown in the Table B.1. The pulp is the major product of the Kraft pulping process, and the pulp yield was assumed as 80%.[13] Thus, the mass allocation factor of pulp was 0.8, and that of lignin in black liquor was 0.2. Moreover, the black liquor used in the liquefaction process was assumed as 10% of the total black liquor produced by the pulping process, and rest of the black liquor was used for burning to recover the cooking chemicals and generate heat. Thus, the allocation factor of black liquor used in the liquefaction process was 0.1. Also, the allocation factors of lignin polyols were based on their recovery rates of liquefaction process-1 (85%) and process-2 (70%). The lignin mass balance flows from woodchips to lignin polyols are shown in the Figure B.2 and B.3.

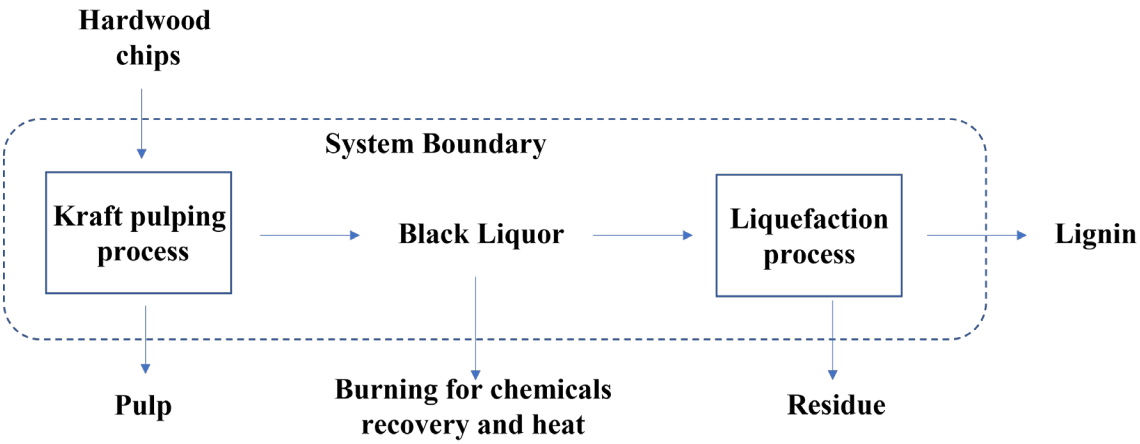

Figure B.1 Life cycle assessment system boundary of the lignin production.

Table B.1 Mass allocation factors of LCA.

Products	**Mass allocation of Kraft pulping process**
Pulp	0.8
Lignin in black liquor	0.2
Products	**Mass allocation of lignin in black liquor**
Lignin for burning	0.9
Lignin for liquefaction processes	0.1
Products	**Mass allocation of liquefaction processes**
Lignin polyols	0.85 (process-1) or 0.70 (process-2)
Lignin in residue	0.15 (process-1) or 0.30 (process-2)

The operation conditions of the Kraft pulping process are listed in Table B.2. For the Kraft pulping process, the raw materials are mixed hardwood chips of red maple and aspen (7:3); the sodium hydroxide (NaOH) and sodium sulfide (Na_2S) are used as processing chemicals, and they are dissolved in water. The pulping process for the wood chips is maintained at

approximately 170 ℃ for 2 h, and the delignification rate can be 90% according to previous reports.[9] After the pulping process, pulp and black liquor with most separated lignin are produced.

Table B.2 Operation conditions of the Kraft pulping process.

Parameters	Conditions
Red maple: aspen	7:3
Mass ratio of NaOH: Na_2S	3:1
Mass ratio of NaOH: wood	0.18:1
White liquor (water, NaOH, and Na_2S): wood	2:1
Temperature	170 ℃
Time	2 h
Delignification rate	90%

The compositions of the hardwood are shown in Table B.3, which were referred to a reference.[14]

Table B.3 Compositions of hardwood.

Compositions	Percentage
Cellulose	45%
Hemicellulose	30%
lignin	22%
Others	3%

The compositions of the black liquor are shown in Table B.4, which is referred to a previous study with the same black liquor sources.[15]

Table B.4 Compositions of the hardwood black liquor.

Compositions	Percentage
Moisture content	25.2%
Lignin	32.8%
Ash	39.4%
Hemicellulose	2.1%

The operation conditions of the liquefaction process are shown in Table B.5 and B.6. As discussed in chapter 3, the liquefaction process-1 with 160 ℃, pH = 3, and 3 min had the highest lignin recovery rate of 85%, while the liquefaction process-2 with 140 ℃, pH = 7, and 9 min had the lowest lignin recovery rate of 70%. The mass ratio of methanol to the solid of black liquor was maintained at 1:10 for both liquefaction processes. In this study, the environmental impacts of the liquefaction process-1 and the liquefaction process-2 were analyzed and compared, and they were compared with the fossil-based polyols as well.

Table B.5 Operation conditions of the liquefaction process-1.

Parameters	Conditions
Mass ratio of solid in black liquor: methanol	1:10
Temperature	160 ℃
pH	3

Time	3 min
Ash-free lignin recovery rate	85%

Table B.6 Operation conditions of the liquefaction process-2.

Parameters	Conditions
Mass ratio of solid in black liquor: methanol	1:10
Temperature	140 ℃
pH	7
Time	9 min
Ash-free lignin recovery rate	70%

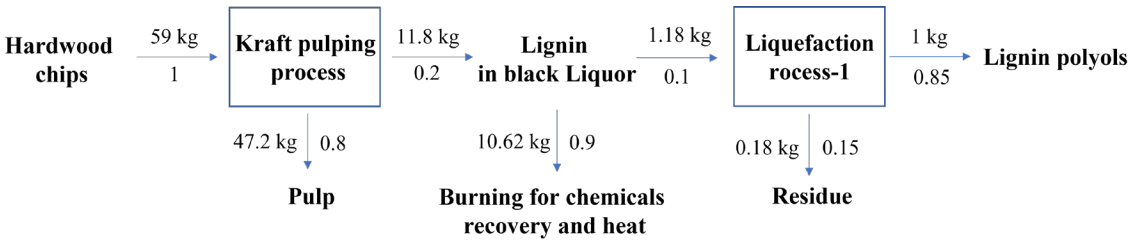

Figure B.2 Lignin mass balance flow from woodchips to lignin polyols produced by liquefaction process-1.

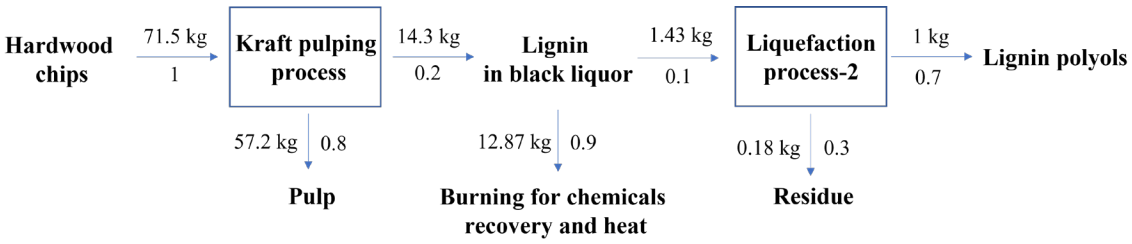

Figure B.3 Lignin mass balance flow from woodchips to lignin polyols produced by liquefaction process-2.

The inputs for the production of 1 kg lignin polyols with the liquefaction process-1 and 2 are listed in Table B.7 and B.8. These inputs were calculated based on the mass allocation factors. Since the lignin recovery rate of the liquefaction process-1 was higher than that of the liquefaction process-2, the process-1 needed less amount of wood chips, chemicals and water used in the Kraft pulping process, and methanol than the process-2, while the higher pH value resulted in more acetic acid needed in the process-1 compared with the process-2. Besides that, the amounts of wood waste combusted in industrial boiler were negative values due to the recycling of residue after the liquefaction processes. The heat from steam was for the pulping processes and liquefaction processes, and the electricity was for the vacuum filtration of the liquid phase and the solid phase after the liquefaction processes.[16]

Table B.7 Inputs for the production of 1 kg lignin polyols with the liquefaction process-1.

Material Inputs or Outputs (negative values)	Amount
Wood chips, wet, measured as dry mass {CH}| wood chips production, hardwood, at sawmill | APOS, U	1.003 kg
Sodium hydroxide, without water, in 50% solution state {GLO}| market for | APOS, S	0.1199 kg
Sodium sulfide {GLO}| market for | APOS, U	0.03924 kg
Water, decarbonised, at user {GLO}| market for | APOS, U	0.8829 kg
Acetic acid, without water, in 98% solution state {GLO}| market for | APOS, U	1.648 kg
Methanol {GLO}| market for | APOS, S	1.666 kg
Wood waste, unspecified, combusted in industrial boiler/US	-0.18 kg

Process Energy Inputs	Amount
Heat, from steam, in chemical industry {RER}| market for heat, from steam, in chemical industry | APOS, U (This is for the Kraft pulping process)	1.264 MJ
Heat, from steam, in chemical industry {RER}| market for heat, from steam, in chemical industry | APOS, U (This is for the liquefaction process)	41.292 MJ
Electricity, low voltage {NPCC, US only}| market for | APOS, U	1.079 MJ

Table B.8 Inputs for the production of 1 kg lignin polyols with the liquefaction process-2.

Material Inputs or Outputs (negative values)	Amount
Wood chips, wet, measured as dry mass {CH}| wood chips production, hardwood, at sawmill | APOS, U	1.2155 kg
Sodium hydroxide, without water, in 50% solution state {GLO}| market for | APOS, S	0.1417 kg
Sodium sulfide {GLO}| market for | APOS, U	0.04687 kg
Water, decarbonised, at user {GLO}| market for | APOS, U	1.099 kg
Acetic acid, without water, in 98% solution state {GLO}| market for | APOS, U	0.03689 kg
Methanol {GLO}| market for | APOS, S	1.844 kg
Wood waste, unspecified, combusted in industrial boiler/US	-0.42 kg
Process Energy Inputs	**Amount**
Heat, from steam, in chemical industry {RER}| market for heat, from steam, in chemical	1.574 MJ

industry | APOS, U (This is for the Kraft pulping process)	
Heat, from steam, in chemical industry {RER}| market for heat, from steam, in chemical industry | APOS, U (This is for the liquefaction process)	11.549 MJ
Electricity, low voltage {NPCC, US only}| market for | APOS, U	1.195 MJ

B.9 Results and Discussion

The greenhouse gas emissions of process-1, 2, and fossil-based polyol are shown in Figure B.4. Although the lignin recovery rate of process-1 (85%) was higher than that of the process-2 (70%), the CO_2 produced by the process-1 (8.9 kg CO_2/kg lignin) was more than that by process-2 (3.2 kg CO_2/kg lignin). Such GHG emissions were lower than that of the acetic acid solvent lignin (10.9 kg CO_2/kg lignin) and ethanol solvent lignin (4.7 kg CO_2/kg lignin) produced by the Aqueous Lignin Purification with Hot Agents (ALPHA) process.[9] For the process-1, the heat, methanol, and acetic acid used the liquefaction process were the major contributors to the CO_2 emissions, while the heat and methanol used in the liquefaction process contributed to the most of CO_2 emissions of process-2. Such a difference was related to higher consumption of acetic acid in the process-1 than the process-2. Moreover, if using 1 kg lignin to replace 1 kg fossil-based polyols to prepare flexible PU foams, the process-2 lignin may be preferable since it theoretically generates less CO_2 emissions (3.2 kg CO_2/kg lignin) than fossil-based polyols (3.4 kg CO_2/kg polyol).

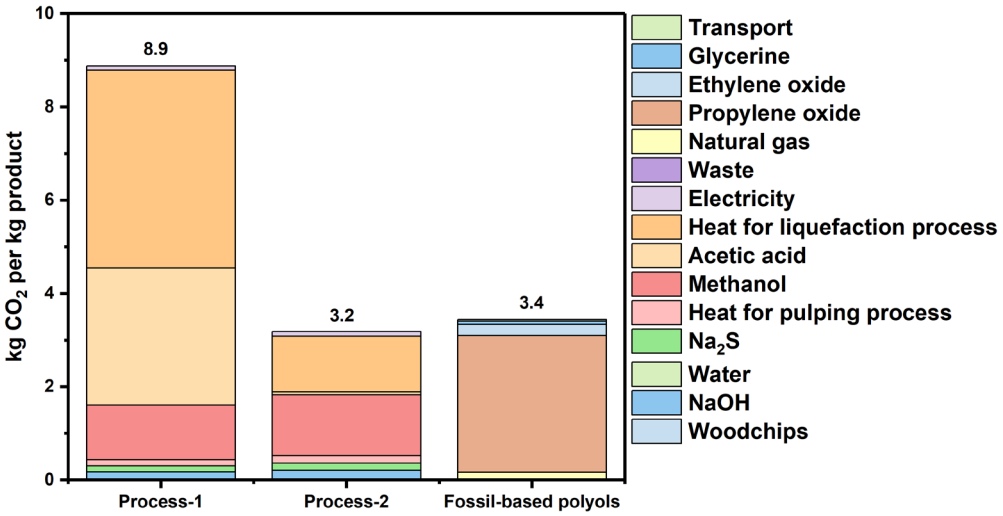

Figure B.4 Greenhouse gas emissions of process-1, process-2, and fossil-based polyol.

Figure B.5 shows the energy consumption of process-1, 2, and fossil-based polyol. It was found that to produce 1 kg lignin, the process-2 theoretically consumes less energy (102.9 MJ) than the process-1 (224.4 MJ), and the chemicals, heat, electricity, and woodchips are the major energy consuming processes. When producing 1 kg lignin to substitute 1 kg fossil-based polyols for the production of flexible PU foams, the process-2 is preferred because its energy consumption (100.6 MJ/kg lignin) is similar to that of fossil-based polyols (91.6 MJ/kg polyol).

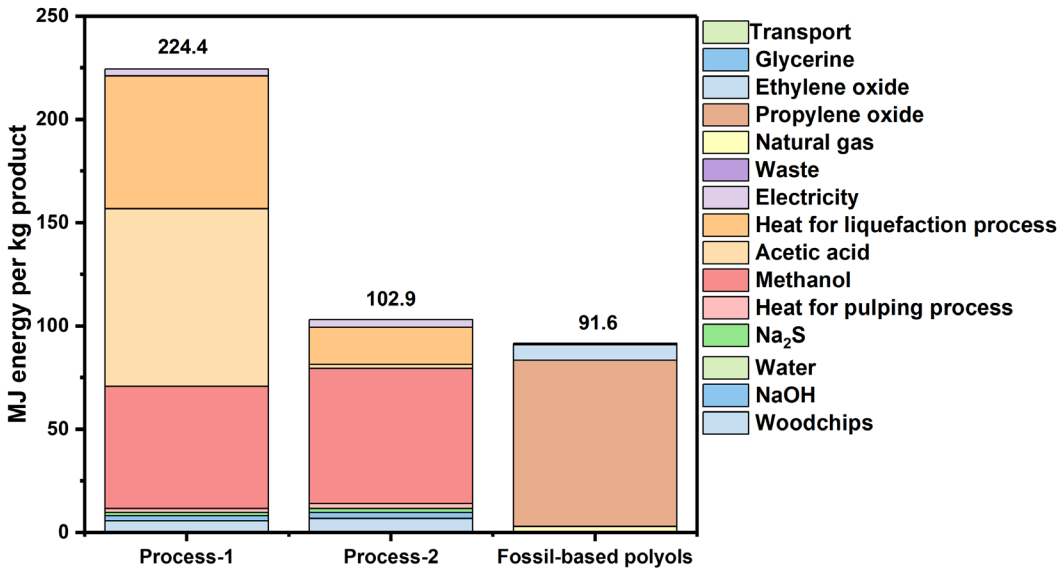

Figure B.5 Energy consumption of process-1, process-2, and fossil-based polyol.

B.10 Conclusions

Overall, the process-2 with the lowest lignin recovery rate (70%) has less greenhouse gas emissions and energy consumption than the process-1 with the highest lignin recovery rate (85%). The major contributors to those environmental impacts are methanol, acetic acid, and heat used in the liquefaction processes. From the environmental point of view, the process-2 is more suitable for the replacement of fossil-based polyols. To further reduce the environmental burden caused by the new lignin recovery processes, it is necessary to seek for an effective solvent system that can recover more lignin from the Kraft black liquor with less solvents.

B.11 References

1. Barros-Timmons, A., Polyurethane Foams: Past, Present, and Future. *Materials (Basel, Switzerland) 11* (10), 1841.

2. Wu, J.-W.; Sung, W.-F.; Chu, H.-S., Thermal conductivity of polyurethane foams. *International journal of heat and mass transfer* **1999,** *42* (12), 2211-2217.

3. Bowen, H. J. M., Absorption by polyurethane foams; new method of separation. *Journal of The Chemical Society A: Inorganic, Physical, Theoretical* **1970**, 1082-1085.

4. Campanella, A.; Bonnaillie, L. M.; Wool, R. P., Polyurethane foams from soyoil-based polyols. *Journal of Applied Polymer Science* **2009,** *112*, 2567-2578.

5. Yang, W.; Dong, Q.; Liu, S.; Xie, H.; Liu, L.; Li, J. In *Recycling and Disposal Methods for Polyurethane Foam Wastes*, Elsevier B.V., 2012; pp 167-175.

6. Li, Y.; Ragauskas, A. J., Kraft Lignin-based Rigid Polyurethane Foam. *Journal of Wood Chemistry and Technology* **2012,** *32* (3), 210-224.

7. Haridevan, H.; Evans, D.; Ragauskas, A. J.; Martin, D. J.; Annamalai, P. K., Valorisation of technical lignin in rigid polyurethane foam: a critical evaluation on trends, guidelines and future perspectives. *Green Chemistry* **2021,** *23*.

8. Mahmood, N.; Yuan, Z.; Schmidt, J.; Xu, C. C., Depolymerization of lignins and their applications for the preparation of polyols and rigid polyurethane foams: A review. *Renewable and Sustainable Energy Reviews* **2016,** *60*, 317-329.

9. Kulas, D. G.; Thies, M. C.; Shonnard, D. R., Techno-Economic Analysis and Life Cycle Assessment of Waste Lignin Fractionation and Valorization Using the ALPHA Process. *ACS Sustainable Chemistry & Engineering* **2021,** *9* (15), 5388-5395.

10. Manzardo, A.; Marson, A.; Roso, M.; Boaretti, C.; Lorenzetti, A., Life Cycle Assessment Framework To Support the Design of Biobased Rigid Polyurethane Foams. *ACS Omega* **2019,** *4* (9).

11. Tran, H.; Vakkilainnen, E. K., The kraft chemical recovery process. *Tappi Kraft Pulping Short Course* **2008**, 1-8.

12. Jiménez-González, C.; Kim, S.; Overcash, M. R., Methodology for developing gate-to-gate Life Cycle Inventory information. *International Journal of Life Cycle Assessment* **2000,** *5* (3), 153-159.

13. Fengel, D.; Wegener, G., *Wood: chemistry, ultrastructure, reactions*. Walter de Gruyter: 2011.

14. Drake, M., A review of the traditional pulping methods and the recent improvements in the pulping processes. *Biomass Conversion and Biorefinery* **2021**, 1-12.

15. Ela, R.; Spahn, L.; Safaie, N.; Ferrier, R. C.; Ong, R. G., Understanding the Effect of Precipitation Process Variables on Hardwood Lignin Characteristics and Recovery from Black Liquor. *ACS Sustainable Chemistry And Engineering* **2020,** *8* (37), 13997-14005.

16. Huttunen, M.; Nygren, L.; Kinnarinen, T.; Ekberg, B.; Lindh, T.; Ahola, J.; Karvonen, V.; Häkkinen, A., Specific energy consumption of vacuum filtration: Experimental evaluation using a pilot-scale horizontal belt filter. *Drying Technology* **2019**, 1-16.

C Copyright documentation

ACS Chemistry for Life®

Solution proposed to your case.

Short Description: Request for the permissions of a published article
Priority: 3 - Moderate

If you feel your case is not completely resolved, please select the button below and select "Reject Solution" from the portal.

Leave a comment as to what is still causing the issue to your case.

Reopen Case

Comments:

Additional comments

12-02-2022 11:32:43 AM EST - Jawwad Saeed
Dear Peng,

Your permission requested is granted and there is no fee for this reuse.

In your planned reuse, you must cite the ACS article as the source, add this direct link: <https://pubs.acs.org/doi/10.1021/acsomega.2c01206>, and include a notice to the readers that further permission related to the material excerpted should be directed to the ACS.

Please do not hesitate to contact me if you need any further assistance.

Regards,
Jawwad Saeed
ACS Customer Services & Information
https://help.acs.org

49 Spadina Ave. Suite 200
Toronto ON M5V 2J1 Canada
www.biorender.com

Confirmation of Publication and Licensing Rights

December 14th, 2022
Science Suite Inc.

Subscription:	*Individual*
Agreement number:	*XZ24RKVQD5*
Journal name:	*Dissertation*

To whom this may concern,

This document is to confirm that Peng Quan has been granted a license to use the BioRender content, including icons, templates and other original artwork, appearing in the attached completed graphic pursuant to BioRender's Academic License Terms. This license permits BioRender content to be sublicensed for use in journal publications.

All rights and ownership of BioRender content are reserved by BioRender. All completed graphics must be accompanied by the following citation: "Created with BioRender.com".

BioRender content included in the completed graphic is not licensed for any commercial uses beyond publication in a journal. For any commercial use of this figure, users may, if allowed, recreate it in BioRender under an Industry BioRender Plan.

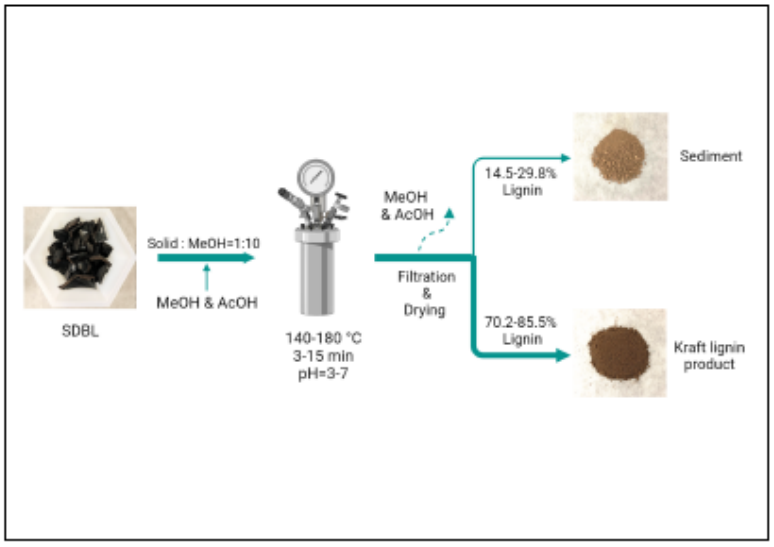

For any questions regarding this document, or other questions about publishing with BioRender refer to our BioRender Publication Guide, or contact BioRender Support at support@biorender.com.

49 Spadina Ave. Suite 200
Toronto ON M5V 2J1 Canada
www.biorender.com

Confirmation of Publication and Licensing Rights

December 9th, 2022
Science Suite Inc.

Subscription:	*Individual*
Agreement number:	*OG24QVGBSI*
Journal name:	*Dissertation*

To whom this may concern,

This document is to confirm that Peng Quan has been granted a license to use the BioRender content, including icons, templates and other original artwork, appearing in the attached completed graphic pursuant to BioRender's Academic License Terms. This license permits BioRender content to be sublicensed for use in journal publications.

All rights and ownership of BioRender content are reserved by BioRender. All completed graphics must be accompanied by the following citation: "Created with BioRender.com".

BioRender content included in the completed graphic is not licensed for any commercial uses beyond publication in a journal. For any commercial use of this figure, users may, if allowed, recreate it in BioRender under an Industry BioRender Plan.

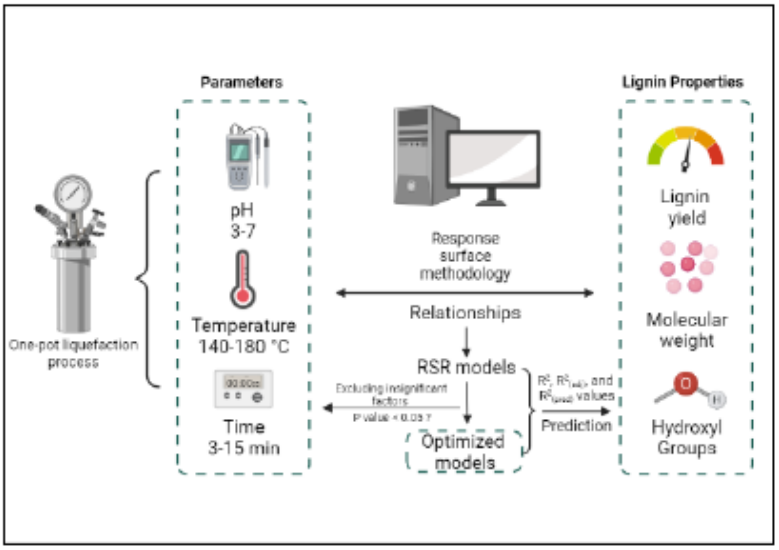

For any questions regarding this document, or other questions about publishing with BioRender refer to our BioRender Publication Guide, or contact BioRender Support at support@biorender.com.

49 Spadina Ave. Suite 200
Toronto ON M5V 2J1 Canada
www.biorender.com

Confirmation of Publication and Licensing Rights

December 9th, 2022
Science Suite Inc.

Subscription:	*Individual*
Agreement number:	*AQ24QVHTO3*
Journal name:	*Dissertation*

To whom this may concern,

This document is to confirm that Peng Quan has been granted a license to use the BioRender content, including icons, templates and other original artwork, appearing in the attached completed graphic pursuant to BioRender's Academic License Terms. This license permits BioRender content to be sublicensed for use in journal publications.

All rights and ownership of BioRender content are reserved by BioRender. All completed graphics must be accompanied by the following citation: "Created with BioRender.com".

BioRender content included in the completed graphic is not licensed for any commercial uses beyond publication in a journal. For any commercial use of this figure, users may, if allowed, recreate it in BioRender under an Industry BioRender Plan.

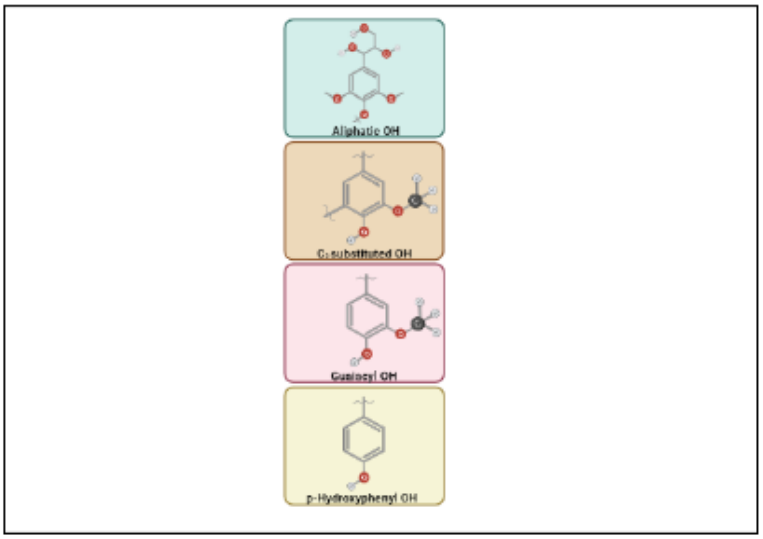

For any questions regarding this document, or other questions about publishing with BioRender refer to our BioRender Publication Guide, or contact BioRender Support at support@biorender.com.

49 Spadina Ave. Suite 200
Toronto ON M5V 2J1 Canada
www.biorender.com

Confirmation of Publication and Licensing Rights

December 14th, 2022
Science Suite Inc.

Subscription:	*Individual*
Agreement number:	*YF24RKWEIE*
Journal name:	*Dissertation*

To whom this may concern,

This document is to confirm that Peng Quan has been granted a license to use the BioRender content, including icons, templates and other original artwork, appearing in the attached completed graphic pursuant to BioRender's Academic License Terms. This license permits BioRender content to be sublicensed for use in journal publications.

All rights and ownership of BioRender content are reserved by BioRender. All completed graphics must be accompanied by the following citation: "Created with BioRender.com".

BioRender content included in the completed graphic is not licensed for any commercial uses beyond publication in a journal. For any commercial use of this figure, users may, if allowed, recreate it in BioRender under an Industry BioRender Plan.

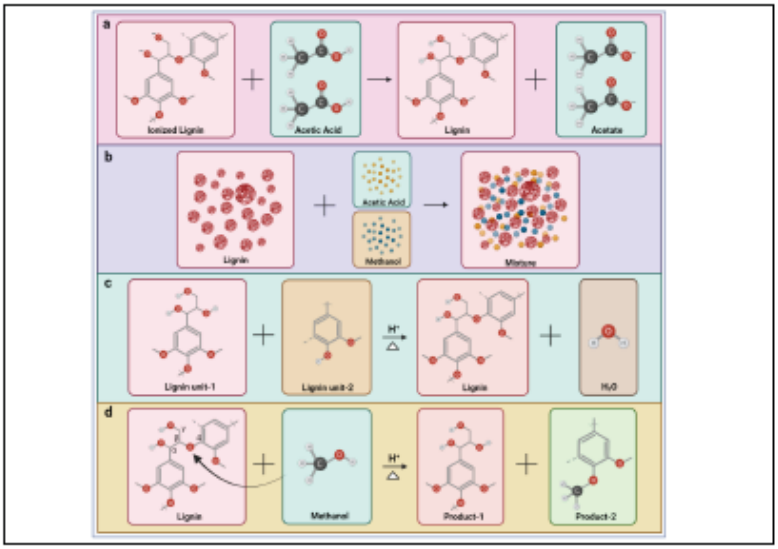

For any questions regarding this document, or other questions about publishing with BioRender refer to our BioRender Publication Guide, or contact BioRender Support at support@biorender.com.